



Universidade do Minho
Escola de Engenharia

Inês Maia Silva Rodrigo Gonçalves

**Titanium surface modification by laser
to enhance the anti-biofilm effect of
dental implants**

Dissertação de Mestrado

Ciclo de Estudos Integrados Conducentes ao
Grau de Mestre em Engenharia Biomédica

Trabalho realizado sob orientação de:

Professor Óscar Carvalho

Professor Júlio Souza

Março 2019

DIREITOS DE AUTOR E CONDIÇÕES DE UTILIZAÇÃO DO TRABALHO POR TERCEIROS

Este é um trabalho académico que pode ser utilizado por terceiros desde que respeitadas as regras e boas práticas internacionalmente aceites, no que concerne aos direitos de autor e direitos conexos.

Assim, o presente trabalho pode ser utilizado nos termos previstos na licença abaixo indicada.

Caso o utilizador necessite de permissão para poder fazer um uso do trabalho em condições não previstas no licenciamento indicado, deverá contactar o autor, através do RepositóriUM da Universidade do Minho.

ACKNOWLEDGMENTS

This work has been an enriching journey in both academic and personal level. Nonetheless it would not be possible without the help of many people to whom I would like to express my deepest gratitude.

Firstly, I would like to express my gratitude to Professor Filipe Silva for the opportunity of joining the quest to do what has not yet been done, and for his passionate and ever inspiring speeches. I also would like to thank all the people from the lab, for sharing their knowledge with me. A special *kiitos* to Laura for helping me with the wettability and roughness measurements techniques. Also, a big thanks to both of my supervisors, Óscar and Júlio. To Óscar for always being present and supportive throughout the work, for teaching me the techniques required for the experimentation and for being an example that engineering is a state of mind. To Júlio for bringing focus to the course the work was taken, for the prompt reviews of the written work and for providing the contacts for my time in Belgium.

I would also like to show my gratitude to Professor Wim Teughels for allowing me the opportunity to work in the *Labo Orale Biologie* of the *Katholieke Universiteit Leuven*. A big thanks to Esteban, Martine and Tim for receiving me so well and for helping with all the procedures. Also, a big thanks to the guys from BIOMAT, namely Ben, for helping me with the SEM, and Evelinetje, for bringing very good ice cream.

To my friends, Mariana, Tiago, Edgar, Daniel, Susana, Simas, Sandra, Margarida and Rita, a big thanks for all the phone calls, joyful moments and for being the great people that you are. Also, a big thanks to the 日本語 “cod-fish” class and めぐみ先生 for blessing my week with very interesting moments.

Finally, a big thanks to João, for supporting me throughout this journey, in all the good and bad moments. Also, the most heartfelt thanks to my family, for always supporting me and encouraging me to keep moving forward and go to distance. Without you I would never have reached this far so, once again, thank you so much.

This work is supported by Fundação para a Ciência e Tecnologia (FCT) with the reference project UID/EEA/04436/2019, by FEDER funds through the COMPETE 2020 – Programa Operacional Competitividade e Internacionalização (POCI) with the reference project POCI-01-0145-FEDER-006941 and POCI-01-0145-FEDER-030498 and the project with reference NORTE-01-0145-FEDER-000018-HAMaBICo.

Co-financed by:



STATEMENT OF INTEGRITY

I hereby declare having conducted this academic work with integrity. I confirm that I have not used plagiarism or any form of undue use of information or falsification of results along the process leading to its elaboration.

I further declare that I have fully acknowledged the Code of Ethical Conduct of the University of Minho.

ABSTRACT

Peri-implant diseases are one the main causes of dental implant failure. Throughout the years, new strategies for dental implants fabrication have been developed in order to prevent such infections to occur. In one hand, the increase of the surface roughness and hydrophilicity can promote a better connection of the bone cells with the implant. Consequently, the healing time is shortened. On the other hand, those alterations also promote bacteria to adhere and proliferate. Therefore, another strategy is to incorporate organic or inorganic elements with antibacterial properties onto the surface of implants.

The intend of this work was to develop and test surfaces that generate a dipole repellent for the bacteria when immersed in an aqueous solution. Two approaches were developed for that purpose. In one approach a pattern of different titanium dioxide thickness was created on the titanium surface, using a Q-Switched Nd:YAG laser system operating at 1064 nm. The other strategy was to incorporate silver particles on a laser textured titanium surface. The incorporation of the silver was performed by laser sintering and through hot-pressing. The antibacterial properties of the samples with different oxide thickness and the samples with hot-pressed silver were tested against 14 bacterial strains. The surface characteristics of the samples were also evaluated by optical and scanning electronical microscopy, the wettability and roughness were also measured, and the oxides were characterized by Energy Dispersive X-ray Spectroscopy.

The tests performed on the samples showed that the surfaces were hydrophilic and moderately rough. The oxide present in the samples with different oxide thickness was mostly in the rutile form. Those samples also showed no signs of antibacterial effects when compared to polished samples. The samples with silver, on the other hand, showed a reduction of *Porphyromonas gingivalis* and *Prevotella intermedia* strains. A reduction of the biofilm was also noticed on the surface of those samples.

Keywords: Dental implants; Antibacterial; Silver; Titanium oxide; Laser surface texturing; Laser sintering; Hot-pressing sintering

RESUMO

As doenças periimplantares são uma das principais causas de falhas em implantes. Ao longo dos anos, novas estratégias têm sido desenvolvidas com o intuito de prevenir a ocorrência de infecções. Por um lado, o aumento da rugosidade e hidrofílicidade das superfícies dos implantes promove uma melhor ligação entre as células ósseas e os implantes. Por conseguinte, o tempo de recuperação é reduzido. Por outro lado, essas características também promovem a adesão e proliferação de bactérias. Consequentemente, outras estratégias desenvolvidas incluem a incorporação de elementos antibacterianos orgânicos ou inorgânicos na superfície dos implantes.

Com este trabalho pretendeu-se desenvolver e testar superfícies que gerem dipolos repelentes para bactérias, quando imersas em soluções aquosas. Duas abordagens foram desenvolvidas. Uma das abordagens correspondeu a criar um padrão com diferentes espessuras de dióxido de titânio através da utilização de um sistema laser Q-Switched Nd:YAG que opera a 1064 nm. Outra estratégia correspondeu à incorporação de partículas de prata numa superfície de titânio previamente texturizada por laser. A incorporação da prata foi efectuada através de laser e de prensagem a quente. As propriedades antibacterianas das amostras produzidas foram testadas numa cultura com 14 diferentes estirpes bacterianas. As características das superfícies foram também examinadas por microscopia óptica e electrónica, a molhabilidade e rugosidade foram também medidas, e os óxidos caracterizados por Espectroscopia de Raios-X por Dispersão de Energia.

Os testes realizados revelaram que as superfícies apresentavam características hidrofílicas e eram moderadamente rugosas. O óxido presente nas amostras com diferentes espessuras de óxido encontrava-se maioritariamente na forma *rutile*. Estas também não revelaram propriedades antibacterianas comparativamente a uma superfície polida. Por outro lado, as amostras com prata mostraram-se eficazes a reduzir a adesão das estirpes de *Porphyromonas gingivalis* e *Prevotella intermedia*. Também se revelaram inibidoras da formação de biofilme na sua superfície.

Palavras-chave: Implantes dentários; Antibacteriano; Prata; Óxido de titânio; Texturização a laser; Sinterização a laser; Sinterização por prensagem a quente

TABLE OF CONTENTS

ACKNOWLEDGMENTS	III
STATEMENT OF INTEGRITY	IV
ABSTRACT	V
RESUMO	VI
TABLE OF CONTENTS	VII
LIST OF FIGURES	IX
LIST OF TABLES.....	XII
CHAPTER 1 – INTRODUCTION	1
1. Motivation.....	2
2. Objectives and Contribution of the Work	3
3. General Organization	4
CHAPTER 2 – STATE OF THE ART	5
1. Titanium and Dental Implants.....	6
2. Bacterial adhesion mechanisms.....	9
2.1. Etiology and prevalence of peri-implant diseases	11
3. Current Treatments and Strategies for Peri-implantitis	12
3.1. Surface topography modifications	13
3.1.1. Surface factors.....	14
3.1.1.1. Wettability.....	14
3.1.2. Laser Surface Modification.....	16
3.2. Incorporation of Antibacterial Agents.....	19
3.2.1. Antibacterial properties of Silver (Ag).....	19
3.2.2. Other antibacterial agents	21
3.2.3. Methods of incorporation of antibacterial agents.....	23
3.2.3.1. Powder technology	24
3.2.3.2. Laser Technology – Selective Laser Sintering.....	26
CHAPTER 3 – EXPERIMENTAL PROCEDURE.....	27
1. Experimental Methods.....	28
2. Preparation of specimens	29
3. Laser Texturing.....	31
3.1. Group 1 preparation.....	31
3.1.1. Laser Sintering	35
3.1.2. Hot-Pressing	36

3.2. Group 2 preparation.....	36
4. Physicochemical Analyses	39
4.1. Microscopy and X-ray Powder Diffraction (XRD)	39
4.2. Wettability.....	40
4.3. Roughness	41
5. Biofilm Assays.....	42
5.1. Biofilm growth.....	42
5.2. Quantitative Polymerase Chain Reaction (qPCR).....	45
CHAPTER 4 – RESULTS AND DISCUSSION.....	46
1. Surface characterization.....	47
1.1. Microscopic analyses.....	47
1.2. Pattern for silver incorporation.....	47
1.3. Silver Sintering by laser	48
1.4. Silver Sintering by Hot-Pressing	54
1.5. Titanium Dioxide with Different Thickness – Nd:YAG laser 3	54
1.7. X-Ray Diffraction (XRD)	58
1.8. Wettability.....	59
1.9. Roughness	60
2. Microbiological tests	61
2.1. Effect of titanium discs on bacterial biofilm	61
2.2. Effect of titanium discs on bacterial proliferation	61
3. Discussion.....	63
CHAPTER 5 – FINAL REMARKS	67
1. Conclusions	68
2. Future Work	69
BIBLIOGRAPHY.....	70
APPENDIX	81

LIST OF FIGURES

Figure 2.1 – Atomic structure representation. Adapted from [22].	6
Figure 2.2 – Crystal conformations of titanium dioxide. Adapted from [23].	7
Figure 2.3 – A) Anatase; B) Rutile; C) Brookite; D) TiO ₂ (B). Adapted from [24].	7
Figure 2.4 – Modern shapes of the implant body. A) Cylindrical unthreaded press-fit; B) Cylindrical screw; C) Cylindrical tapered screw. Adapted from [27].	8
Figure 2.5 – Representation of the three main components of endosteal implants. Adapted from [28].	9
Figure 2.6 – Illustration of multispecies biofilm formation. Adapted from [32].	11
Figure 2.7 – Representation of the free energy per unit area of the liquid-gas, solid-gas and solid-liquid interfaces in an A) hydrophilic and B) hydrophobic surface. Adapted from [49].	15
Figure 2.8 – Example of surface laser texturing. Adapted from [59].	18
Figure 2.9 – Proposed silver antibacterial mechanisms. A) Silver uptake by the bacteria; B) Inhibition of protein synthesis by interaction with ribosomes; C) Binding to thiol (-SH) groups of respiratory enzymes; D) Disturbance of electron transport; E) Formation of ROS species; F) Interaction with DNA; G) Formation of pits in the cellular wall. Adapted from [90].	21
Figure 2.10 – Different strategies for antibacterial agents incorporation. Adapted from [10].	24
Figure 3.1 – Flow chart representation of the experimental work.	28
Figure 3.2 – Schematic representation of a 24 well plate used for microbiological assays.	30
Figure 3.3 – Schematic cross-sectional illustration of the projected grid patterns.	31
Figure 3.4 – Different patterns performed on the titanium surface by laser. A) Coarse pattern; B) Wider pattern.	32
Figure 3.5 – Titanium grade V disc with coarse pattern for silver sintering tests.	32
Figure 3.6 – Incorporation of silver tests. A) Laser patterning of the samples; B) Deposition of silver solution on the surface; C) Result of using silver solution; D) Silver powder pressed on the sample; E) Result of pressing silver powder on the sample.	34
Figure 3.7 – Nd:YAG laser 3 (YZD 600 2A, Bende, China).	35
Figure 3.8 – Representation of hot-pressing main components. Adapted from [121].	36
Figure 3.9 – Nd:YAG laser 2 (LM-D 60 7500W, SISMA, Italy).	37
Figure 3.10 – Titanium samples sputter-coated with gold.	39
Figure 3.11 – Optical goniometer (OCA 15 plus, Dataphysics, Germany).	40

Figure 3.12 – Wettability measurement of a titanium sample. A) Placement of water drop on the surface and B) analysis through the corresponding software.....	41
Figure 3.13 – Mechanic profilometer (SurfTest SJ 201, Mitutoyo, Tokyo, Japan).	42
Figure 3.14 – Bioreactor (BIOSTAT® B, Germany).....	43
Figure 3.15 – Schematic representation of the initial steps for biological assays. 1) Placement of the samples on the 24 well plates; 2) Addition of bacterial culture, BHI-2 and chlorhexidine to the respective well; 3) Incubation of the samples in anaerobic environment.	44
Figure 4.1 – SEM images of the titanium surface with different patterns. A) and C) Coarse pattern; B) and D) Wider pattern.	48
Figure 4.2 – SEM images of the titanium test surface covered with A) silver powder and B) silver solution treated by different laser conditions.	49
Figure 4.3 – SEM images of titanium surfaces.	50
Figure 4.4 – SEM images of titanium samples covered with silver after laser sintering.	51
Figure 4.5 – Optical micrographs of the titanium surfaces covered with silver layers after laser sintering.	52
Figure 4.6 – Optical micrographs of coarse pattern titanium samples covered with silver layers after laser sintering.	53
Figure 4.7 – Optical micrographs of titanium surface after laser sintering.	53
Figure 4.8 – SEM images of the titanium surface covered with silver layers after hot-pressing. The silver is in light gray and the titanium in dark gray.....	54
Figure 4.9 – Optical micrographs of titanium oxide pattern after laser irradiation.	55
Figure 4.10 – Optical micrographs of the thick titanium dioxide pattern.	56
Figure 4.11 – Optical micro graphs of titanium oxide pattern after laser irradiation.	57
Figure 4.12 – Optical micrographs of the thick titanium dioxide pattern.....	58
Figure 4.13 – X-Ray diffraction spectra of the samples with a pattern of thick titanium dioxide.	59
Figure 4.14 – Mean values of water contact angle measurements.....	60
Figure 4.15 – Mean roughness values of each tested surface.....	60
Figure 4.16 – Effect of surface treatment with silver and different oxide thickness on complex multi-species biofilms (mean ± standard deviation, n=3). Negative control refers to polished titanium samples and positive control refers to polished titanium samples with and addition of chlorhexidine. (A) and (B) represent the concentration of <i>P. gingivalis</i> (Pg) and <i>P. intermedia</i> (Pi)	

after 24h and 72h of culture in anaerobic conditions in contact with titanium samples. Data are expressed as $\text{Log}_{10}\text{Geq/mL}$ 61

Figure 4.17 – Sample surface by SEM after being incubated with bacteria in anaerobic conditions for 24 hours. **A)** Titanium samples with sintered silver; **B)** Titanium samples with thick oxide pattern; **C)** Polished titanium samples; **D)** Polished titanium samples with chlorhexidine solution. 62

Figure 4.18 – Sample surface by SEM after being incubated with bacteria in anaerobic conditions for 72 hours. **A)** Titanium samples with sintered silver; **B)** Titanium samples with thick oxide pattern; **C)** Polished titanium samples; **D)** Polished titanium samples with chlorhexidine solution. 63

LIST OF TABLES

Table 2.1 – Mechanical properties of different titanium grades and oral tissues.[19]	8
Table 2.2 – Main assessments and outcomes of the incorporation of metallic particles for antibacterial purposes.....	22
Table 3.1 – 24 well plates incubation schedule.....	30
Table 3.2 – Laser parameters for titanium patterning.	32
Table 3.3 – Laser parameters for silver sintering.	35
Table 3.4 – Laser 3 parameters for surface patterning tests of Ti samples.	37
Table 3.5 – Laser 2 parameters for surface patterning tests of Ti samples.	38
Table 3.6 – Specific characteristics of the Nd:YAG lasers.	38
Table 4.1 – Nd:YAG laser parameters for the silver sintering.....	54
Table 4.2 – Nd:YAG laser parameters for titanium oxide pattern.....	56
Table 4.3 – Laser parameters for surface treatment of Ti samples.	57

LIST OF ABBREVIATIONS AND SYMBOLS

ASTM – American Society for Testing and Materials
At % – Atomic Percentage
ATCC – American Type Culture Collection
ATP – Adenosine Triphosphate
BHI-2 – Brain Heart Infusion 2
CFU – Colony-Forming Unit
CHX – Chlorhexidine
CIST – Cumulative Interceptive Supportive Therapy
cpTi – Commercially Pure titanium
CW – Continuous Wave
DSM – Deutsche Sammlung von Mikroorganismen
DLVO – Derjaguin, Landau, Verwey, Overbeek
DNA – Deoxyribonucleic Acid
EWOP – European Workshop on Periodontology
HA – Hyaluronic Acid
HAp – Hydroxyapatite
IBAD – Ion-beam assisted deposition
Nd:YAG – Neodymium-doped Yttrium Aluminum Garnet
OM – Optical microscopy
PBS – Phosphate-buffered saline
PEO – Plasma Electrolytic Oxidation
Pg – *Porphyromonas gingivalis*
Pi – *Prevotella intermedia*
PIII – Plasma Immersion Ion Implantation
qPCR – Quantitative Polymerase Chain Reaction
Ra – Arithmetic Mean Surface Roughness
ROS – Reactive Oxygen Species
Rt – Maximum height peak to valley
RT-qPCR – Reverse Transcription qPCR
Rz – Average Maximum Peak to Valley
Sa – Arithmetical Mean Height
SEM – Scanning Electron Microscopy

SLC – Sisma Laser Controller

SLM – Selective Laser Melting

spp – *species pluralis*

Ti6Al4V – Titanium–6 Aluminum–4 Vanadium

UV – Ultraviolet

Wt % – Weight percentage

XDLVO – Extended DLVO

XRD – X-Ray Diffraction

YAG – Yttrium-Aluminum-Garnet

Chapter 1 – INTRODUCTION

Chapter I deals with the background, objectives and hypotheses of the present work, as well as its overall contribution. A brief description of the contents of each chapter is also described in the end of this chapter.

1. Motivation

The oral cavity is a quite important part of the human body since disturbances on its functions lead to a reduction of the quality of life. A significant percentage of the population suffers from oral diseases including tooth loss, even with the increase of health conditions through the years [1,2]. Consequently, strategies to replace the missing teeth have been increasingly sought and developed. The purpose of a dental implant is to replace a missing tooth by mimicking its structure and function. Therefore, an implant allows the patient to properly masticate and speak [3]. The placement of an implant is only considered successfully established in the oral cavity when it is fully osseointegrated. That means that the implant must be connected to the adjacent bone only by bone tissue and without the presence of any other type of tissue [3–5]. The success of dental implants is quite elevated. Nevertheless, there are still some conditions that can cause failure of osseointegration. Bacterial accumulation on the implantation site can induce an inflammatory response that can eventually lead to the implant failure.

The inflammatory peri-implant diseases can be defined as peri-implant mucositis or peri-implantitis. During the 1st European Workshop on Periodontology (EWOP), peri-implant mucositis was defined as a reversible inflammatory reaction in the soft tissues surrounding a functioning implant, while peri-implantitis as an inflammatory reaction associated with loss of supporting bone around a functioning implant.[5,6] Infection of the tissues surrounding the implant implies an increase of the hospitalization time, of the cost of medical expenses and of the discomfort of the patient. Antibiotic treatment is usually required which can lead to the increase of multi resistant bacteria. The microbial flora that usually dwell in the oral cavity is composed mainly by aerobic, gram-positive bacteria. Peri-implantitis are commonly associated with a shift to anaerobic, gram-negative bacteria, as occurs in periodontal diseases.[3,7] Determined conditions or habits can increase the susceptibility of a patient to develop peri-implant diseases. Poor diet, lack of oral hygiene habits or smoking as well as auto-immune diseases and history of periodontal diseases are examples of some of those conditions.[4,8,9] Despite having some antibacterial properties, titanium surfaces are prone to bacterial contamination which can

lead to an inflammatory response, that is, to inflammatory peri-implant diseases [10].

Current treatments present some disadvantages as they can be uncomfortable to the patient. The fact that they are not completely effective increases the probability of the development of antibiotic-resistant bacteria. Consequently, some new strategies were laid out to avoid implant failure. One approach is through the modification of the implant surface topography. This strategy usually aims to improve the osseointegration, which can also contribute to diminish the probability of bacterial infection [11]. Other strategy is the functionalization of the titanium surface by the incorporation of antibacterial agents. This latter strategy is more versatile due to the number of possible antibacterial compounds and techniques for incorporation that can be used [12]. Some of the most common treatments are sandblasting, acid etching, plasma nitriding, titanium plasma-spraying and anodic oxidation. Sandblast and acid etching are commonly used sequentially on the same surface. [13–15] The antibacterial agents incorporated on the surface can be inorganic, like gold (Au), silver (Ag), copper (Cu), zinc (Zn) and hydroxyapatite (HAp), or organic like the antibiotics vancomycin, tobramycin and gentamicin or other compounds as chitosan and hyaluronic acid (HA).[10,16]

2. Objectives and Contribution of the Work

The development of antibacterial surfaces is a current challenge for the manufacture of dental implants. To achieve the desired topography for the implant, many methods for surface modifications can be utilized. The usage of laser technology has shown to be an interesting option since it allows to better control the patterns created on the surface. It is also a technique that allows a fast preparation of the surface whilst avoiding contaminations that usually occur using other methods. The present work aims to develop and characterize different methods of modify titanium surfaces to produce implants with antibacterial properties. Two hypothesis for the attainment of the antibacterial effect were investigated. One through the addition of an inorganic element to the titanium surface and other through the variation of the titanium dioxide

thickness. The inorganic agent utilized was silver and both surfaces were treated with laser techniques. Consequently, new ways to use different Q-switched Nd:YAG lasers in the surface treatment of dental implants were explored. The antibacterial properties of the developed surfaces were also tested with a wide number of bacteria, giving a closer perspective to a real situation.

3. General Organization

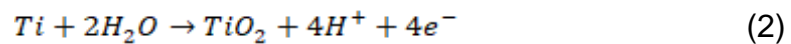
This document is divided in a total of five chapters that depict the research made throughout the past year to complete this project. Chapter I introduces the dental implants and the problem of peri-implantitis which is the motivation for this work. Hereinafter the aims that were expected to be accomplished and the contribution of the work are also described. Chapter II presents the usage of titanium in dental implants and describes how peri-implantitis can affect the success of implants application. The current developments that have been made to produce antibacterial titanium surfaces are also described. Firstly, surface alteration approaches and secondly, the incorporation of antibacterial components are reviewed. Chapter III shows the materials used and tests that were made in order to develop and characterize the titanium surfaces. Initially a brief description of the utilized materials is presented, followed by a description of the equipment and techniques utilized to alter the samples. Hereinafter, the equipment and techniques utilized to characterize the surfaces are also presented. Lastly, the microbiological assays that were performed are described as well. Chapter IV exposes the results obtained in the course of the present work and the conclusions obtained from them. Firstly, the microscopical observations made to find the adequate parameters to alter the samples are showed. Subsequently, the characterization of the final samples and the obtained results of the microbiological assays are presented. Lastly, a discussion of the previously presented results is made. Chapter V resumes the main conclusions obtained with the present work and presents a group of suggestions for future works.

Chapter 2 – STATE OF THE ART

Chapter II deals with issues related to the biofilm accumulation around dental implants and the main strategies to decrease biofilm adhesion and proliferation.

1. Titanium and Dental Implants

Titanium and titanium alloys show physicochemical properties required for a dental implant [17,18]. The tensile and flexural strength of the titanium alloys (see Table 2.1) is higher than that recorded for other alternative materials for dental implants [17]. The chemical reactivity of titanium is high when in contact with the room environment or oral cavity. Therefore, a titanium thin oxide film ranging from 0.1 up to 20 nm is formed on the surface after processing or finishing, according to the equations (1) and (2) [17,19]. The thin titanium oxide layer is responsible for the chemical stability and corrosion resistance of titanium and its alloys, contributing for their overall biocompatibility [19].



In the solid state, commercially pure titanium (cp Ti) shows two main crystalline structures that are illustrated in Figure 2.1. A hexagonal close-packed atomic structure takes place in cpTi until 882 °C, named alpha phase. Above that temperature and below the melting point at 1665 °C, cpTi acquires a body-centered cubic conformation, known as beta phase.[19] Titanium dioxide (TiO₂) can be found in one of four different conformations in nature. The most common are anatase and rutile, but it can also appear in brookite or TiO₂ (B) forms. In the first two the atoms adopt a tetragonal conformation while in the last forms the atoms are displayed in a rhombohedral and monoclinic conformation respectively. [20,21] Illustrations of those conformations are presented in Figure 2.2 and Figure 2.3.

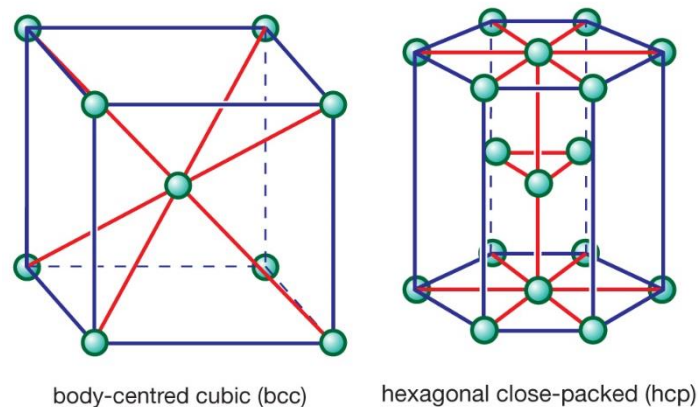


Figure 2.1 – Atomic structure representation. Adapted from [22].

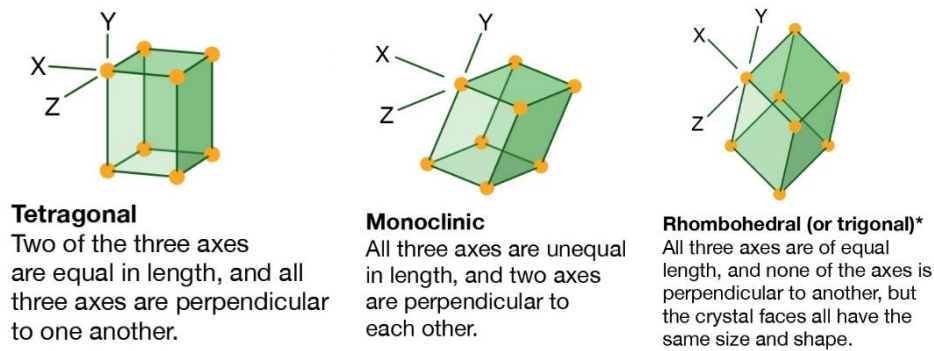


Figure 2.2 – Crystal conformations of titanium dioxide. Adapted from [23].

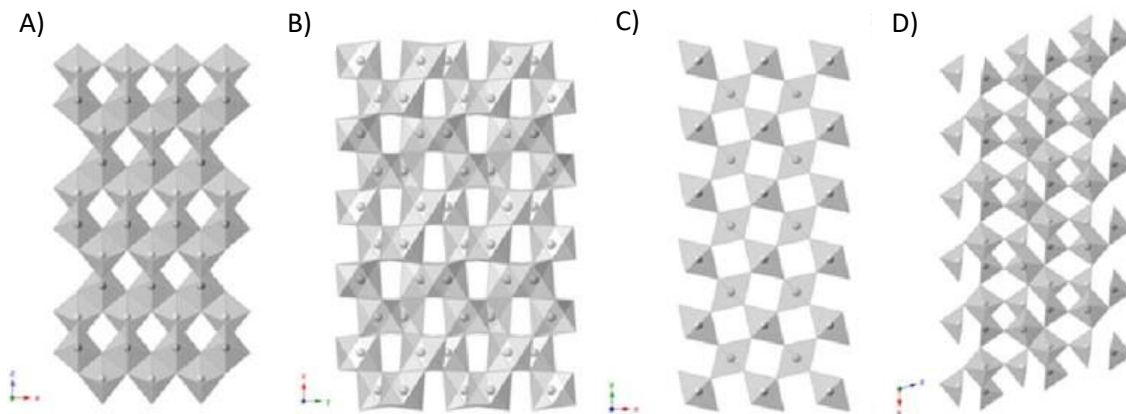


Figure 2.3 – **A)** Anatase; **B)** Rutile; **C)** Brookite; **D)** TiO₂ (B). Adapted from [24].

Since Ti is the ninth most common element, the price is attractive for manufacturing [19,25]. It is also safe to be used in patients in need of magnetic resonance imaging and therefore dental implants can be clearly inspected by radiographic imaging, as titanium is a non-ferromagnetic metal [17].

The American Society for Testing and Materials (ASTM) defined six different types of titanium to be used for dental implants. They are denominated by grades ranging from I to VI according to the Ti content. The first four grades correspond to commercially pure or unalloyed titanium while grades V and VI are composed of Ti, Al and V chemical elements. The differences among the grades are in mechanical and physical properties, as presented in Table 2.1.[19]

Table 2.1 – Mechanical properties of different titanium grades and oral tissues.
[19]

Material	Modulus (GPa)	Ultimate Tensile Strength (MPa)	Yield Strength (MPa)	Elongation (%)	Density (g/cc)
cp grade I Ti	102	240	170	24	4.5
cp grade II Ti	102	345	275	20	4.5
cp grade III Ti	102	450	380	18	4.5
cp grade IV Ti	104	550	483	15	4.5
Ti-6Al-4V grade V	113	930	860	10	4.4
Cortical Bone	18	140	n/a	1	0.7
Dentin	18.3	52	n/a	0	2.2
Enamel	84	10	n/a	0	3

Dental implant systems can be manufactured as a single-unit or two-pieces titanium structural components. In the case of two-pieces the osseointegrated is named implant fixture and the coronal part is named abutment which support the prosthetic structure. Schematics of implant fixture and abutment can be seen in Figure 2.4 and Figure 2.5.[3,26] The implant size often varies between 3 to 6 mm in diameter and 7 to 20 mm in length, depending on the patient mandibular bone size [5].

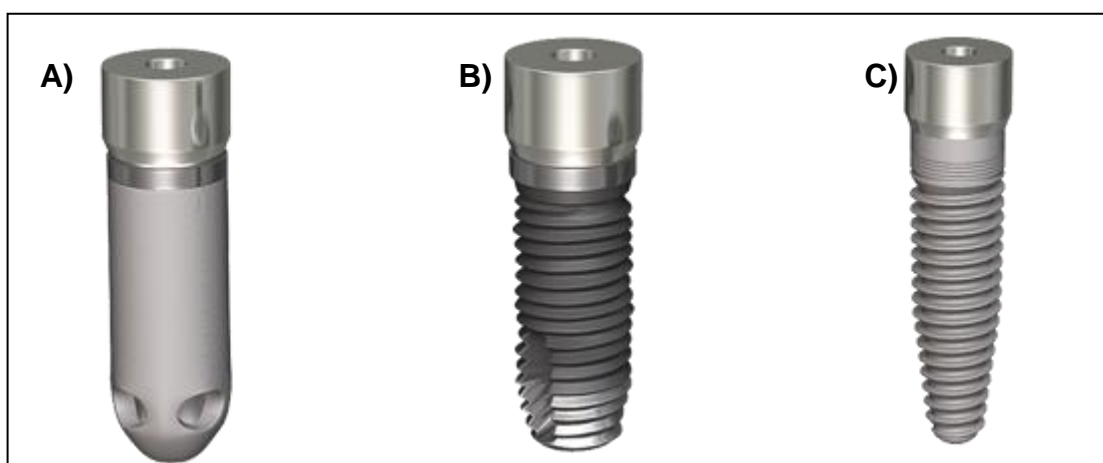


Figure 2.4 – Modern shapes of the implant body. A) Cylindrical unthreaded press-fit; B) Cylindrical screw; C) Cylindrical tapered screw. Adapted from [27].

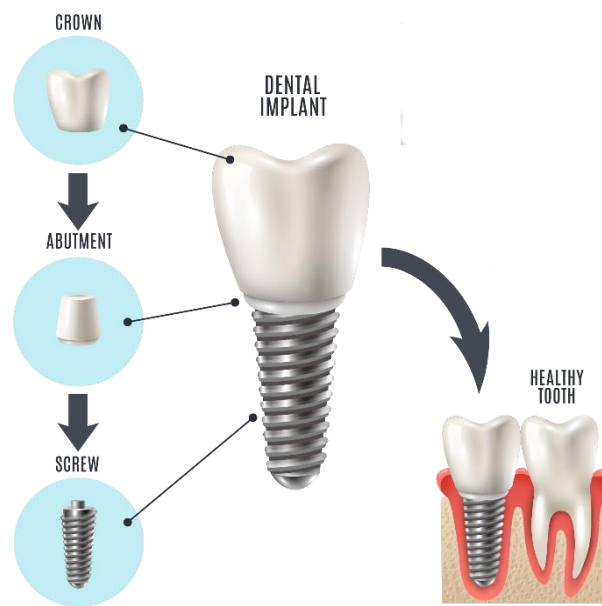


Figure 2.5 – Representation of the three main components of endosteal implants. Adapted from [28].

2. Bacterial adhesion mechanisms

In orthopedics and implant dentistry, efforts have been made to understand the mechanisms of bacterial adhesion and to develop materials that prevent the adherence or kill the adherent bacteria. The concept known as “race for the surface” was stated to enhance the development of structural materials to decrease the biofilm accumulation on implant surfaces [14].

The planktonic oral bacteria are not directly responsible for the inflammation process in the oral cavity. Only when they adhere to the surface and start proliferating and interacting with other bacteria. An inflammatory response can be induced when the bacteria adhere to the surfaces and initiates a biofilm growth process. The bacterial change from planktonic to sessile can be stimulated by a number of environmental factors such as osmolarity, pH, carbon, iron availability, oxygen tension, temperature, and presence of nutrients [29].

Currently the bacterial adhesion is described as a process that can be divided in four stages [30]. The first one corresponds to the initial transport of the bacterium to the surface and can occur by many ways as Brownian motion, sedimentation of the bacterium in the solution, liquid flow or the bacterium own active movement [29]. Characteristics of the surface as the surface topography

and energy have a great impact on the occurrence of subsequent interactions[10]. The primary bacteria colonies formed on the implant-supported prostheses are usually aerobic, gram-positive, and are called early colonizers. Early colonizers are represented by *Streptococcus oralis* (*S. oralis*), *Streptococcus gordonii* (*S. gordonii*), and *Actinomyces naeslundii* (*A. naeslundii*). The second stage corresponds to the first interaction between the bacterium and the surface that will lead to the attachment or repulsion of bacteria. This interaction can be described by two different models, the thermodynamic and the DLVO (Derjaguin, Landau, Verwey, Overbeek) theory [31]. On the later, Lifshitz-Van der Waals and electrostatic forces are considered dominants between the bacteria and the implant. This assumption assumes both the surfaces to be chemically inert, which is not the case. Short-range Lewis acid–base was proposed to be added in a new theory designated as extended DLVO (XDLVO) theory. Since the interactions on this stage are weak, the bacterial adhesion is also reversible.[29] In the third stage more specific interactions (covalent, ionic, or hydrogen bonding) between the bacteria and the surface take place. Those interactions are usually between proteins on the implant surface and specific ligands that are present in bacterial appendages like pili, fimbriae, and fibrillae. Afterwards, most organisms create a protective slime layer, the glycocalyx, against humoral and cellular immune components.[29] In the last stage the biofilm starts to develop since the bacteria are firmly attached to the surface. These microorganisms not only grow and multiply, but also allow other kinds of pathological organisms to adhere in a process called coaggregation [32]. This process is mediated by specific molecules and a genetically controlled chemical communication, designated by quorum sensing [32,33]. Consequently, all the coaggregated bacteria act as a community and can proliferate in a more effective way. Each bacterial strain can coaggregate with a certain number of other strains. The bacteria *S. gordonii* and *S. oralis* usually coaggregate with each other and with other *Streptococcus* strains. *Fusobacterium nucleatum* strains are the ones that coaggregate with a greater number of different strains.[34] Some bacteria can only develop when associated with other, so their presence in the biofilm is dependent of the adhesion of those bacteria [30]. Those bacteria are called secondary colonizers and are, in majority, anaerobic and pathogenic.[33,35] Such relationship also

grants protection against external factors as the host immune system or the surrounding environmental shear stresses [5,30,33]. A schematic representation of the biofilm formation is presented in Figure 2.6. Coaggregated bacteria can also exchange drug resistant genes which increases the development of multidrug resistant bacteria [5]. The activity of some strains is also enhanced due to those associations. For instance, *P. gingivalis* supports the *F. nucleatum* growth while the amino acids exposed by *F. nucleatum* increase the efficacy of the *P. gingivalis* proteases. [7]. Bacterial proliferation can also have a negative impact on the long-term performance of the implant itself since it leads to an increase of the acidity of the medium which, in turn, contributes to the increase of the corrosion rate of the titanium implant [36].

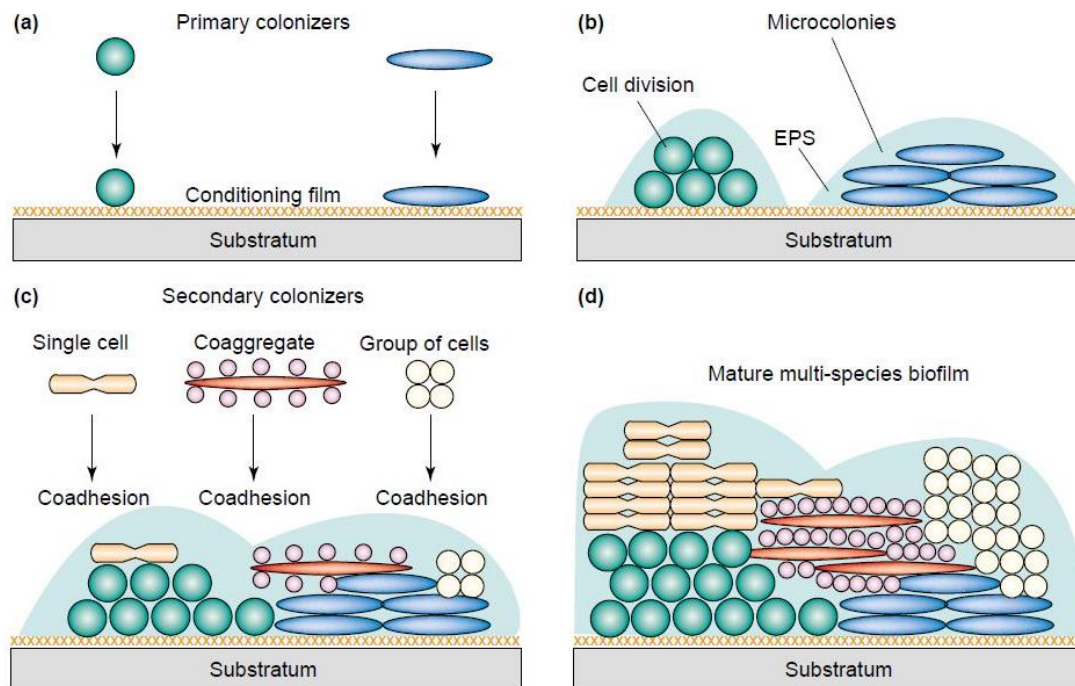


Figure 2.6 – Illustration of multispecies biofilm formation. Adapted from [32].

2.1. Etiology and prevalence of peri-implant diseases

A pathobiont is considered an oral species with capacity to induce periodontal diseases under certain specific environmental and /or metabolic conditions. The pathobionts for periodontal diseases can vary from case to case, however microbial complexes started to be associated to those conditions. The ‘red complex’ composed by *Tannerella forsythia*, *P. gingivalis* and *Treponema denticola* and the ‘orange complex’ composed by *Fusobacterium spp*, *Prevotella*

spp, *Parvimonas micra*, *Eubacterium spp* and *Streptococcus constellatus*. [9,35,37,38] Some of those bacteria are also associated with peri-implantitis, namely *P. gingivalis*, *Prevotella intermedia* (*P. intermedia*), *F. nucleatum*, and *Aggregatibacter actinomycetemcomitans* (*A. actinomycetemcomitans*). Some studies indicate *P. gingivalis* is one of the most important bacteria for the development of peri-implantitis since even in small amount it can cause dysbiosis of the periodontal biofilm, leading to inflammatory responses of the surrounding tissues. [35] Edentulous patients that were treated for periodontitis are susceptible to have higher percentage of peri-implantitis related pathobionts. [39]

About two million implants are estimated to be placed each year and the numbers tend to rise due to the ageing of the population [5]. Consequently, reports of implant failures are a major concern. A study reports that early implant failures can range between 0.76% to 7.47%, whereas late failures are between 2.1% to 11.3% [40]. Follow-up carried out over a period of 5 to 11 years for patients with dental implants reported an occurrence of mucositis in 40 to 90% of the implants from 80% of the subjects while 20% were affected with peri-implantitis. [4] In another study, the incidence of peri-implantitis ranged from 0 to 6.47% over a 5-year period and from 5.8 to 16.9% over 10 years after the placement of the implant [41]. Other studies reported an occurrence of mucositis in more than 50% subjects while peri-implantitis occurred in 28% to 77% of the subjects [6,8,42]. Peri-implant diseases could ultimately lead to the total loss of the implant. This problem was also reported in some studies and its prevalence ranged from 0 up to 13.6%. Disparities are found between different studies relative to the prevalence of the inflammatory peri-implant [42].

3. Current Treatments and Strategies for Peri-implantitis

Patients that present signs of peri-implantitis are treated according to a protocol designated Cumulative Interceptive Supportive Therapy (CIST) that involve the steps: 1) mechanical debridement, like scaling or root planning, to eliminate bacteria from the inflammation site; 2) antiseptic treatment to disinfect the implant surface; 3) antibiotic prescription to decrease the number of bacteria in the surrounding peri-implant tissues; 4) local surgery and placement of

biomaterials to enhance the bone repair around the implant. [4,5] One method to disinfect the surface of titanium implants is through the application of ultraviolet (UV) light. The UV light excites the titanium dioxide molecules, generating pairs of electrons and holes. This leads to the generation of reactive species with hydroxyl radicals and superoxide ions. Those radicals have bactericidal properties since they are able to disturb vital bacterial functions or even the bacterial membrane stability. [43,44] A period of 80 min treatment can eliminate 75 to 95% of bacteria, depending on how well the deeper parts of the implant can be excited by UV.[5] Laser techniques are also currently used to irradiate osseointegrated implant sites and eliminate bacteria since it is a minimally invasive treatment. This treatment can nonetheless damage the surrounding tissues due to the heat they provoke.[45–47]

The referred treatments present some disadvantages as they can be uncomfortable to the patient and the fact that they are not completely effective increases the probability of the development of antibiotic-resistant bacteria. Consequently, some new strategies were laid out to avoid implant failure. The surface physicochemical modification of implants aims to improve the osseointegration and therefore can also contribute to decrease the probability of bacterial infection [11]. The functionalization of the titanium surface by the incorporation of antibacterial agents can involve a large number of possible antibacterial compounds and techniques [12].

3.1. Surface topography modifications

Some of the most common surface topography treatments are gritblasting, acid etching, plasma nitriding, titanium plasma-spraying, and anodic oxidation. [13–15] Plasma-spraying comprises the heating of metal powders at high temperatures to achieve a plasma state [15]. The particles then fall and solidify on the test surface. Sandblast and acid etching are commonly used sequentially on the same surface. Gritblasting is performed with abrasive metallic oxide particles, like Al_2O_3 , TiO_2 or SiO_2 [15]. The size of the particles ranging from 30 up to 250 μm is chosen depending on the desired roughness (0.5 up to 2 μm) [48]. The acid etching is usually carried out with both sulfuric and hydrochloric acid or nitric and hydrofluoric acids [15,48]. Anodization of titanium is performed at a high current density or potential (e.g. 200 A/m^2 or 20-100 V) when the test

surface is immersed in sulfuric acid, hydrofluoric acid, nitric acid or phosphoric acidic solutions [15].

3.1.1. Surface factors

The composition of the implant surface can influence the bacterial adhesion. Some materials, like Au, Ti, Co, Va and Al, have a certain degree of antibacterial behavior [10]. Among those materials, Ti reveals the highest degree of antibacterial effect followed by Au [10]. Nevertheless, in some cases, it is not enough to prevent the bacterial adhesion and proliferation. The roughness and the wettability of the surface have also a role on both osseointegration and bacterial adhesion.

The average roughness (Ra) of a surface can be measured by arithmetic deviation of a linear profile. For a surface to be considered smooth in implant dentistry, the Ra roughness value must be below 0.5 μm . For higher values the surface is considered minimally rough (0.5 – 1 μm), moderately rough (1 – 2 μm) or rough (> 2 μm). Surfaces with rough topography have larger contact area for interaction with blood platelets, proteins, and osteoblasts [14]. Moderately rough surfaces showed more promising results for osseointegration than other surfaces although rough surfaces also increased the attachment of bacteria.[4,43] Ra roughness lower than 0.2 μm does not contribute to biofilm development [10].

3.1.1.1. Wettability

Hydrophilic surfaces are associated with high surface energy that is classified by the contact angle between a water drop and the substrate below 90° while the hydrophobic are related to low surface energy that is measured by a water contact angle higher than 90°.[4] Bacteria with hydrophilic characteristics tend to prefer hydrophilic surfaces while hydrophobic bacteria prefer hydrophobic surfaces [29]. Nevertheless, bacteria tend to adhere on hydrophobic surfaces. Strong hydrophilic surfaces lead to the formation of a monolayer of water molecules which disrupts the protein adsorption. Consequently, the bacterial adhesion is also disturbed.[5]

Surfaces can be more or less repellent to fluids depending on each material properties. When a drop of a liquid is placed on a surface, tension

forces will occur on the air-liquid and solid-liquid interfaces. If the forces between the solid and liquid are adhesives, the drop tend to spread over the surface. On the other hand, if the forces are cohesive, the drop will acquire a spherical conformation, minimizing the contact with the surface. Thus, the wettability of a material can be classified depending on the angle that a liquid's drop forms when placed on its surface. Hydrophilic surfaces attract fluids, so the angle is below 90° while hydrophobic surfaces repel fluids, so the contact angle is over 90° . In cases where the angle is close to 0° or to 180° the surfaces are called super hydrophilic or super hydrophobic, respectively.[49]

The contact angle (θ) can also be defined mathematically according to Young's equation,

$$\gamma_{lg} \cos \theta = \gamma_{sg} - \gamma_{sl} \quad (3)$$

where γ_{lg} , γ_{sg} and γ_{sl} represent the free energy per unit area of the liquid-gas, solid-gas and solid-liquid interfaces respectively [50]. For hydrophilic surfaces, γ_{sg} should be greater than γ_{sl} while in hydrophobic surfaces it should be smaller, as presented in Figure 2.7.

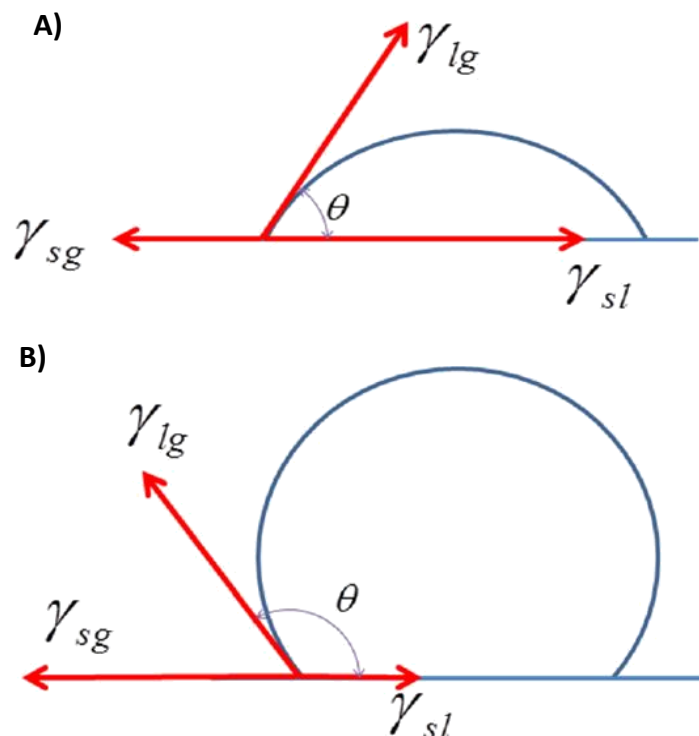


Figure 2.7 – Representation of the free energy per unit area of the liquid-gas, solid-gas and solid-liquid interfaces in an **A)** hydrophilic and **B)** hydrophobic surface. Adapted from [49].

Despite being commonly used, the Young's model does not take into account the influence of the roughness of the surface. Consequently, other models were proposed for wettability measurements. The Wenzel's model for small roughness and the Cassie-Baxter model for increasing roughness [49].

3.1.2. Laser Surface Modification

Lasers have many applications in a variety of fields, from medical treatments, to cutting or engraving metals and ceramics [51]. Their function is to convert electrical energy into a high energy density beam of light [52,53]. The beam is generated through the excitation of electrons in a medium that results in the emission of photons. Depending on the medium, lasers are characterized as solid, liquid or gas.[52]

Nd:YAG lasers use as medium a crystal of Yttrium Aluminum-Garnet (YAG) with the chemical composition $Y_3Al_5O_{12}$. The crystal is also doped with neodymium ions (Nd^{3+}), a rare-earth, in a concentration of about 1 at. %. [52–54] The YAG laser can work in a continuous wave (CW) mode or pulsed mode. In CW the beam is emitted continuously while in the pulsed mode the beam is emitted periodically. To minimize energy losses in the pulsed mode a technique designated Q-switching is used.[52,55] The most common emission wavelength is 1064 nm [53,54]. Nevertheless, with the utilization of crystals of lithium iodate ($LiIO_3$) and lithium triborate (LiB_3O_5), the frequency of the light beam can be multiplied and generate harmonics with 532, 355 and 266 nm of wavelength [53,54]. The YAG usually requires a cooling system since the process to generate the light beam induces the heating of the equipment. The cooling system can use water, air or a combination of both [52]. The laser beam can induce melting, vaporization or sublimation on metals, ceramics and polymers materials [56,57]. Consequently, the power, wavelength and pulse duration must be optimized depending on the properties of each material to be treated [49,52].

Characteristics as beam shape, beam quality, spot size, peak power and fluence (or laser energy per unit area) are used to describe the light beam of pulsed lasers. In order to do so, some parameters must be known, either by

measurement or given by the manufacturer. The energy per pulse (E_{pulse}) and the peak power per pulse (P_{peak}) can be calculated with the given laser average power (P_{Av}), repetition rate (R_{rate}) and pulse duration (t_{pulse}), as presented in equations (4) and (5). The fluence (F) can be obtained by dividing the energy by the effective focal spot area (A), as presented in Equation (6).

$$E_{pulse} = \frac{P_{Av}}{R_{rate}} \quad [J] \quad (4)$$

$$P_{peak} = \frac{E_{pulse}}{t_{pulse}} \quad [W] \quad (5)$$

$$F = \frac{E}{A} \quad [J/cm^2] \quad (6)$$

Several studies proposed and tested the modification of implants surface by laser ablation. This type of treatment allows a precise control over small and large areas, leading to the improvement of the wettability and roughness of the implants. [12,58,59] An example of a laser texture treated surface is presented in Figure 2.8. An *in vitro* study reported an increase of the adhesiveness and proliferation of osteoblast-like cells on laser treated titanium surfaces. Nevertheless, there was no increase of the cells' differentiation.[60,61] *In vivo* experiments performed in commercially available implants showed improvements at the osseointegration level of surfaces with micro- and nano-features [62–64]. For instance, implants with laser treatment, inserted in rabbit femur and tibia, showed a significant increase of the contact with bone (bone to implant contact - BIC), when compared with regular implants [62]. In another study, a similar procedure was used and an increase of the removal torque of the laser treated implants was reported [63]. Other study that used a sheep model also recorded a higher BIC for laser treated implants than that on machined implants [64].

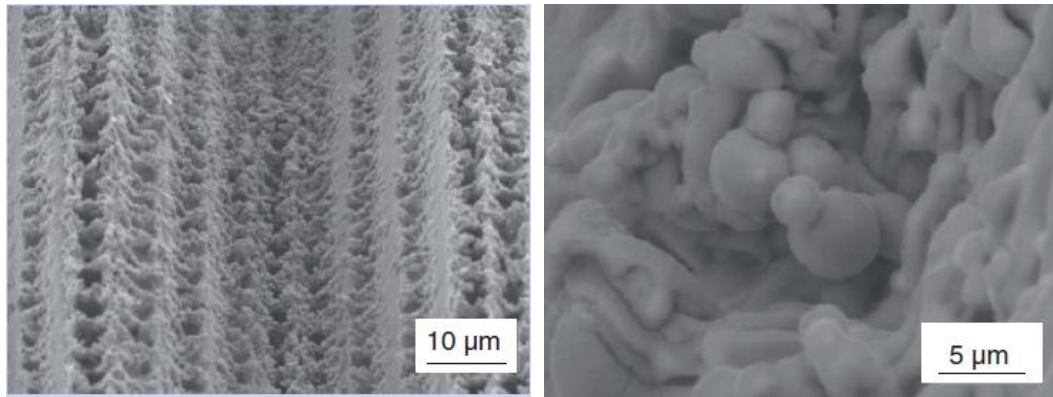


Figure 2.8 – Example of surface laser texturing. Adapted from [59].

One study reported the reduction of *Porphyromonas gingivalis* biofilm formation on laser treated cp Ti grade IV when compared to gritblasted and machined surfaces [65]. Other studies reported the reduction of *Staphylococcus aureus*, *Pseudomonas aeruginosa* and *Porphyromonas gingivalis* biofilm on laser treated samples when compared to gritblasted implant specimens [66]. Another study also reported a decrease of *Streptococcus mutans* and *Streptococcus sanguinis* on laser treated implants when compared to polished ones [67]. The reduction of *Staphylococcus aureus* biofilm on the surface of laser treated cp Ti grade II and Ti6Al4V was also reported [68]. Most studies refer the increase of the hydrophilicity and the generation of a stable oxide layer the probable cause for the increase of cellular adhesion and proliferation, or the reduction of bacterial biofilm observed on laser treated samples.

Some studies also combined the laser ablation treatment with the incorporation of inorganic elements on the surface. Coating laser ablated surfaces with hydroxyapatite (HA) by chemical deposition, was reported to shorten the implant healing time [69,70]. Laser ablation was also used to synthesize and deposit Ag-based nanoparticles on a cp Ti surface. A decrease of *Lactobacillus salivarius* biofilm was reported. [71]

Currently some of the commercially available implants have micro- and nano-features on the upper part of the implant and abutment to stimulate osseointegration [5]. However, the exposure of rough surfaces at the bone crest level can increase the probability of biofilm accumulation and implant failure by peri-implantitis.

3.2. Incorporation of Antibacterial Agents

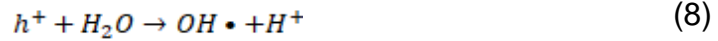
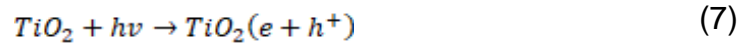
One strategy to prevent the development of biofilms on the surface of dental implants is the incorporation of other materials with bactericidal properties. The incorporation of other metals on the titanium-based surface leads to the formation of galvanic electrochemical reactions that affect the attachment and proliferation of bacteria [47–61]. Some examples of metals incorporated on titanium and the main outcome against some bacteria are displayed on Table 2.2.

3.2.1. Antibacterial properties of Silver (Ag)

Antibacterial properties of Ag have been exploited in many fields, from food storing and water purification systems, to wound dressing for scarring improvement. [87] The incorporation of Ag nanoparticles on the titanium surfaces promotes antibacterial properties to the implant without developing bacterial resistance [44]. Many mechanisms were proposed to explain the Ag antibacterial effect, as illustrated in Figure 2.9. For instance, Ag ions bond to the bacterial membrane, upsetting the ion balance of the cell [10,88]. This interaction leads to an increase of Ag intake, transforming the bacteria into a reservoir of Ag ions. Some studies propose that Ag destroys cross-linking bonds between proteins of the cell walls. Consequently, pits are formed on the wall which leads to the leakage of cytoplasm and disruption of the bacteria [87]. Silver ions and nanoparticles also interact with sulphur containing groups of membrane proteins that have an important role in the production of adenosine triphosphate (ATP) [81,83,86]. Therefore, the permeability of the bacteria increases, and the proton motive force decreased, resulting in the death of the bacteria [86]. Silver can interact with the bacterial DNA as well, halting division and metabolism processes [10,87].

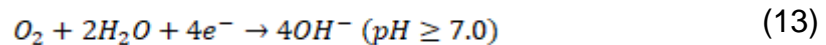
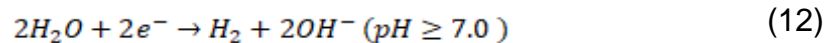
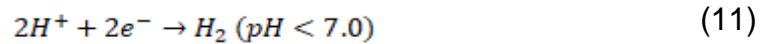
Another antibacterial method that is associated to the incorporation of other metals on the titanium surface is the generation of reactive oxygen species (ROS) [72,74,79,85]. Noble metals, like Au and Ag, have a higher electrochemical potential for electrons, or Fermi level, than Ti. As such, electrons tend to accumulate on the noble metal side and leaving holes on Ti-based surfaces. Electron/hole pairs (e^-/h^+) not only interact with the bacteria but

also contribute to the formation of the ROS, by reacting with water (H₂O) or with hydroxide ions (OH⁻), as shown in the equations (7)-(10) [79].



Reactive oxidative species are normally produced intracellularly due to the aerobic metabolism of some bacteria. The increased generation of ROS promoted by the metal surface leads to an imbalance that also causes the leakage of the bacteria cytoplasm and the disruption of the membrane [72].

The micro-galvanic interactions between Ti and implanted Ag particles can also promote the occurrence of reactions that consume protons, as the ones represented by equations (11) – (14) [73]. Therefore, some regions near the implanted metal will be depleted of protons which will cause a deregulation of the electronic imbalance. Ionic transportation on the bacterial membrane will be disrupted by the imbalance which will lead to the ATP production decrease [73], pore formation, and cell lysis [80], killing the bacterial cells.



Silver can be added alone on the implant surface or incorporated with other metals, polymers or glass-ceramics [87,89]. Despite being an effective strategy against pathogens, it is still currently controversial if the Ag content has cytotoxic effects on the host.

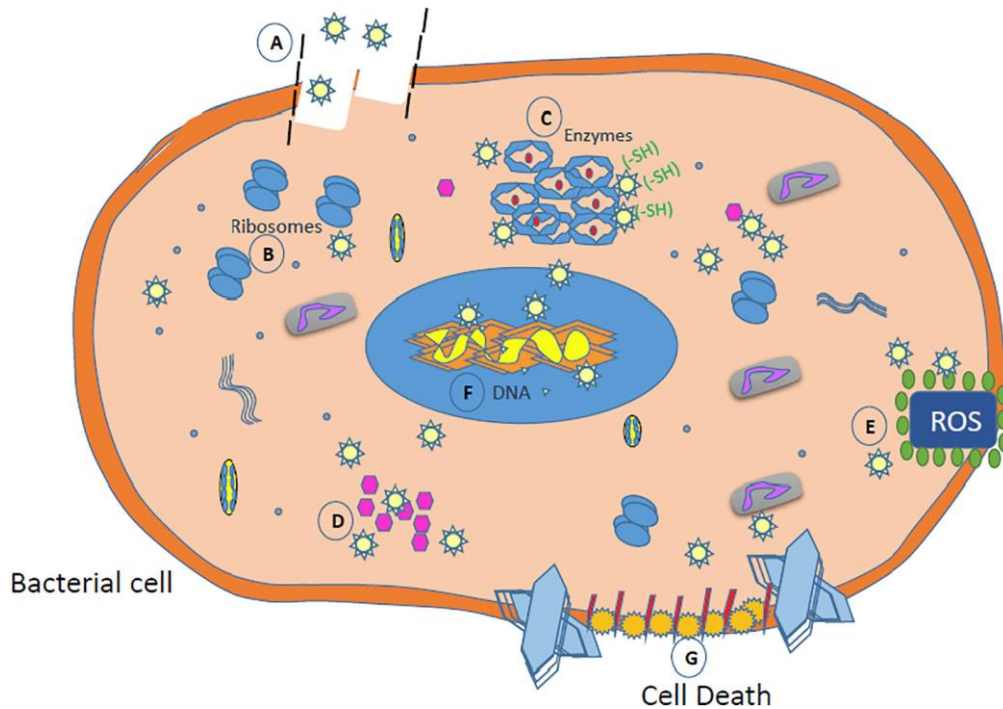


Figure 2.9 – Proposed silver antibacterial mechanisms. **A)** Silver uptake by the bacteria; **B)** Inhibition of protein synthesis by interaction with ribosomes; **C)** Binding to thiol (-SH) groups of respiratory enzymes; **D)** Disturbance of electron transport; **E)** Formation of ROS species; **F)** Interaction with DNA; **G)** Formation of pits in the cellular wall. Adapted from [90].

3.2.2. Other antibacterial agents

Antibacterial activity was also reported in other metals. The incorporation of 5 wt.% of copper (Cu) on a titanium surface has showed antibacterial activity of around 90%. Copper ions are released into the medium and interact with the membrane of the bacteria, disturbing the electron flow. This leads to a cytoplasm leakage and can also cause the oxidation of the nucleus [75]. Implantation of zinc (Zn) has also showed antibacterial effects on gram-positive and gram-negative bacteria [74,76,77]. In a physiological environment, Zn ions are released from the titanium surface and penetrate the bacteria, accumulating on the cytosol [74,76,77]. Since this process requires the consumption of ATP, the energy available for the bacteria gradually decreases [76]. In one study, both Zn and Ag were co-implanted on a titanium surface. In a physiological liquid, micro-galvanic couples of Ag and Zn are formed, with Zn as the anode and Ag as the cathode. Consequently, electrons are transferred to Ag and Zn^{2+} ions are released, in accordance to the equation: [77]



Similar effects were noticed using Au as the implanted metal on the titanium surface. A Schottky barrier is formed and Fermi level alignment occurs on the contact zones among Au particles and bacteria, leading to the transfer of electrons from microbial membranes to Au nanoparticles [82]. The constant electron loss contributes to cell lysis and cytoplasm leakage, killing the bacteria [79]. Other elements that were also tested include fluorine, iodine, bismuth, boron, cerium, carbon, glass, iron, nitrogen, and cobalt [10,48,89,91]. The incorporation of elements which are already present in the human body lessens the probability of cytotoxicity. Nonetheless, some non-essential compounds have higher antibacterial effects at a very low dosage [92].

The incorporation of antibiotics, like gentamicin and vancomycin, or antiseptics, like chlorhexidine, was also studied [10,48,89]. Those compounds are incorporated on degradable molecules and slowly released from the surface. Consequently, that approach is only effective in short-term release [5,89]. Combinations of the previously referred elements with hydroxyapatite (HAp) to also increase the osseointegration is another strategic approach [91]. The long-term antibacterial effect is also a problem of such strategy since HAp can be absorbed into the bone tissue [48].

Table 2.2 – Main assessments and outcomes of the incorporation of metallic particles for antibacterial purposes.

<i>Materials</i>	<i>Synthesis Method</i>	<i>Microbiological Assessment</i>	<i>Bacteria</i>	<i>Main Outcome</i>	<i>Reference</i>
<i>Ti - Ag-NPs</i>	Plasma immersion ion implantation (0.5, 1h, 1.5h, 2h, 3h)	CFU counting Live/dead staining	<i>S. aureus</i> ; <i>E. coli</i>	Antibacterial effect on 90% to 98% of <i>S. aureus</i> and on 95% to 99% of <i>E. coli</i> strains after 24 h of culture	[72,73,80]
<i>Ti-Ag</i>	Powder metallurgy	CFU counting	<i>S. aureus</i>	Samples with more Ag (3-5 wt.%) showed antibacterial rate of 98 to 99.99%	[86]
<i>Ti-Ag-N</i> ; <i>Ti-N-Ag</i> ; <i>Ti-Ag+N</i>	Plasma immersion ion implantation	CFU counting	<i>S. aureus</i> ; <i>E. coli</i>	Antibacterial effect on 95 to 98% of <i>S. aureus</i> and on 100% of <i>E. coli</i> strains	[81]
<i>Ti-Zn/Ag</i>	Plasma immersion ion implantation	CFU counting Live/Dead staining	<i>S. aureus</i> ; <i>E. coli</i>	Reduction of 45% to 99% of <i>S. aureus</i> and of 39% to 99% of <i>E. coli</i> strains	[77,78]

<i>Materials</i>	<i>Synthesis Method</i>	<i>Microbiological Assessment</i>	<i>Bacteria</i>	<i>Main Outcome</i>	<i>Reference</i>
<i>Ti-Zn</i>	Plasma electrolytic oxidation	CFU counting	<i>S. aureus</i> ; <i>E. coli</i>	Reduction of 96 to 99.8% of <i>S. aureus</i> and of 40 to 100% of <i>E. coli</i> strains	[85]
<i>Ti-Zn</i>	Plasma immersion ion implantation	CFU counting	<i>S. aureus</i> ; <i>E. coli</i>	Reduction of 24.67% of <i>S. aureus</i> and of 31.49% of <i>E. coli</i> strains	[76]
<i>Ti-Zn/Mg</i>	Plasma immersion ion implantation	CFU counting	<i>P. gingivalis</i> , <i>F. nucleatum</i> and <i>S. mutans</i>	Inhibitory rate of 40–50% against all the tested pathogens	[74]
<i>Ti-Cu</i>	Powder metallurgy	CFU counting	<i>S. aureus</i>	Antibacterial rates of 90.33% and 92.57%	[75]
<i>TiO₂ Nanotubes Gold</i>	Gold immobilized onto TiO ₂ using 3-aminopropyltrimethoxysilane as coupling agent	CFU counting	<i>S. aureus</i> ; <i>E. coli</i>	Antibacterial effect on 50% of <i>S. aureus</i> and on 45% of <i>E. coli</i> strains	[79]
<i>TiO₂ Nanotubes Gold</i>	Magnetron sputtering	CFU counting	<i>S. aureus</i> ; <i>E. coli</i>	Cell lysis and cytoplasm leakage of bacterial cells on Au-modified TiO ₂	[82]

3.2.3. Methods of incorporation of antibacterial agents

The incorporation of inorganic materials on titanium can be achieved by various techniques that can be included on three different approaches, as illustrated in Figure 2.10. One method is the incorporation of the elements on Ti without the formation of coating. Techniques included on this approach are ion implantation, plasma immersion ion implantation (PIII), oxidation, and alloying of the components with Ti. [5,10] Another strategy is the formation of a thin titanium dioxide layer followed by the incorporation of the antibacterial elements on that layer. The dioxide layer and the doping can be achieved by ion-beam assisted deposition (IBAD), plasma electrolytic oxidation (PEO), anodic spark deposition, and sputtering. [10,91]

Similar to the previous approach, another method is to deposit a thick layer on the Ti surface. The layer can be composed of titanium dioxide or another compound like Hap and then chemically modified. [10] Techniques like thermal spray, electrochemical deposition, sol-gel dip coating, IBAD, sputtering,

layer-by-layer, and plasma electrolytic process (PEP) are used for that purpose. [10,44,91]

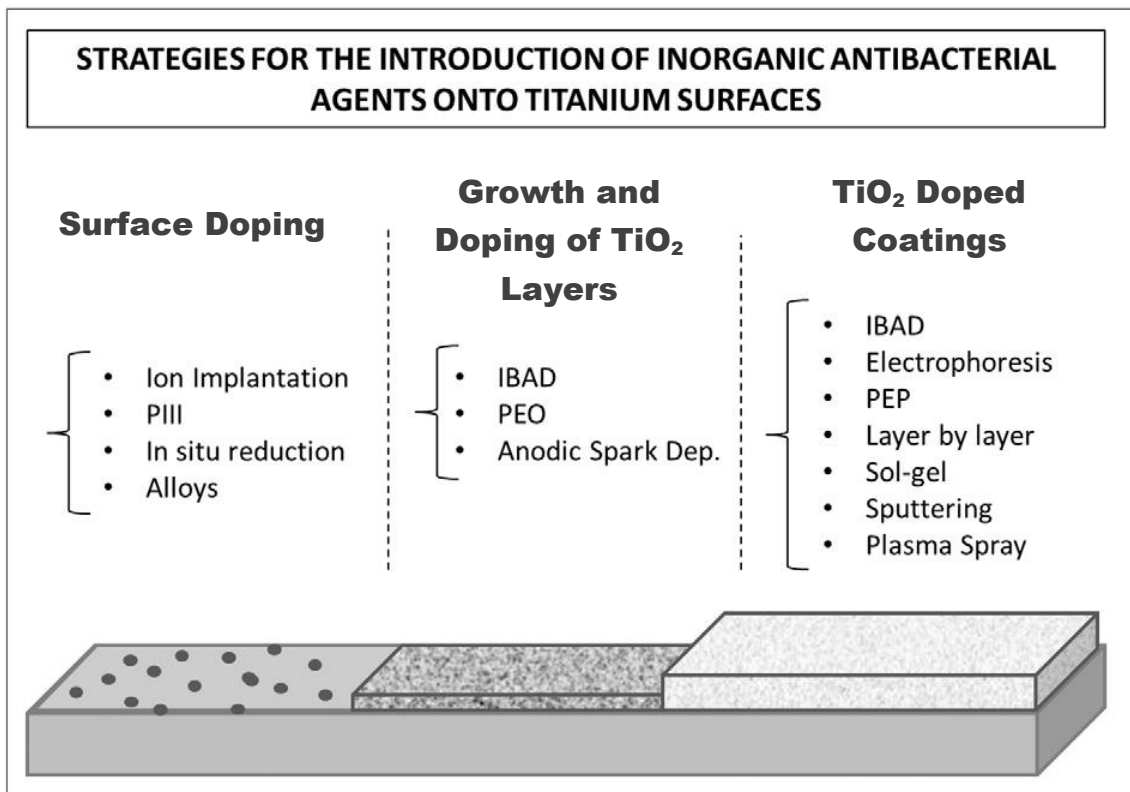


Figure 2.10 – Different strategies for antibacterial agents incorporation. Adapted from [10].

3.2.3.1. Powder technology

Hot-pressing is a technique used to turn ceramic or metal powders into a compact piece. This process combines the compaction of a powder or powders using uniaxial pressure, with the simultaneous heating for sintering [93–102]. The powder is inserted into a die and then heated and compressed for a certain period of time that can range from several minutes to hours [93,103]. The die is usually cylindrical with a closed end. On the open end a plunger is inserted to apply the pressure on the powders inside the die. Both parts are usually made of graphite.[97,101] The components are represented in Figure 3.8.

The temperatures used are moderate to high usually not rising above 2500°C and pressure values typically vary between 10 to 70 MPa [99,101,102]. The heating can be done through an induction furnace or with the assistance of

an applied electric field [100]. The second method is the most commonly utilized and requires passing a low voltage, high density current through the material.

The press can be hydraulic, pneumatic or mechanic. The first two presses are preferred when the pressing time is long. Due to the temperature and pressure, the powders suffer plastic deformation that causes the collapse of the pores and voids in between the particles.[94,100,104,105] The pressure exerted is uniaxial which implies very small lateral deformation. Nevertheless, some radial pressure is always present and is essential for the effectiveness of the process. The differential stress between the axial and radial directions, generates shear stress that improves the particle bonding.[102]

Since the process occurs at high temperatures, it is likely for the materials to oxidize. To better control the environment of the process, the chamber where the die is placed can be in vacuum or filled with an inert gas. The die to be used must not only sustain the needed forces but must not interact with the material as well.[94,104,105]

The hot-pressing procedure starts with the introduction of the powder or powders on the die. The die is then heated to a determined temperature and the cavity of the mold is pressurized. While the powder is being compacted the temperature rise to the maximum. The conditions of temperature and pressure are maintained for the intended time and then the die is cooled slowly and under pressure. The cooling process must be at a temperature that the oxidation of the material would not occur.[106]

Sintering by hot-pressing is, therefore, a method to manufacture titanium alloys containing other metals with antibacterial properties. For instance, two studies assessed the antibacterial properties of a Ti-Cu alloy [107,108]. A high antibacterial rate (up to 99.9 %) against *S. aureus* and *E. coli* and moderate antibacterial rate against *P. gingivalis* were noticed for content of around 5 wt.% Cu [107,108]. In other study, powder metallurgy, casting, and heat treatment method were used to prepare Ti-Ag alloys. Ti-Ag alloys revealed a antibacterial effect against *Staphylococcus aureus* without cytotoxic effect. [109]

3.2.3.2. Laser Technology – Selective Laser Sintering

Laser machines are used not only to change the surface topography, but also to incorporate other elements on the implant. A Ti-based structure can be manufactured by direct metal laser sintering from powder while adding other elements in multilayers [110]. In a previous study, titanium surfaces were successfully coated with carbide [111], calcium-phosphorus (Ca-P) [112], HAp [113,114] and fluorapatite ($\text{Ca}_5(\text{PO}_4)_3\text{F}$) [115]. Improvement of the biocompatibility of the surfaces was reported on those studies. Another research group reported a higher proliferation of osteoblasts on a cp Ti implant produced by Selective Laser Melting (SLM). [116] Copper-bearing Ti6Al4V alloys produced by SLM were reported as non-cytotoxic for the proliferation of gingival fibroblasts or osteoblasts.[117,118]

A previous study assessed the antibacterial effect of TiCu alloys with different percentage of Cu produced by SLM. Ti alloys containing 4 or 6 wt% Cu exhibited antibacterial properties against the *E. coli* and *S. aureus*. Cytocompatibility of the samples was also reported in contact with bone marrow stromal cells. [119] In another study, titanium alloy surfaces were coated with a silver-hydroxyapatite (Ag-HAp) composite. The samples showed antibacterial effects against the *Staphylococcus aureus*. [120]

Chapter 3 – EXPERIMENTAL PROCEDURE

Chapter III includes a brief description of the processing methods, equipment, and tests used in this study.

1. Experimental Methods

The experimental work started with the preparation of the samples followed by the modification of the surfaces using the laser approach. Silver was also sintered on titanium test surfaces by laser or hot pressing. Surfaces were inspected by microscopic, wettability, and roughness analyses. A schematic representation of the experimental process is presented in Figure 3.1.

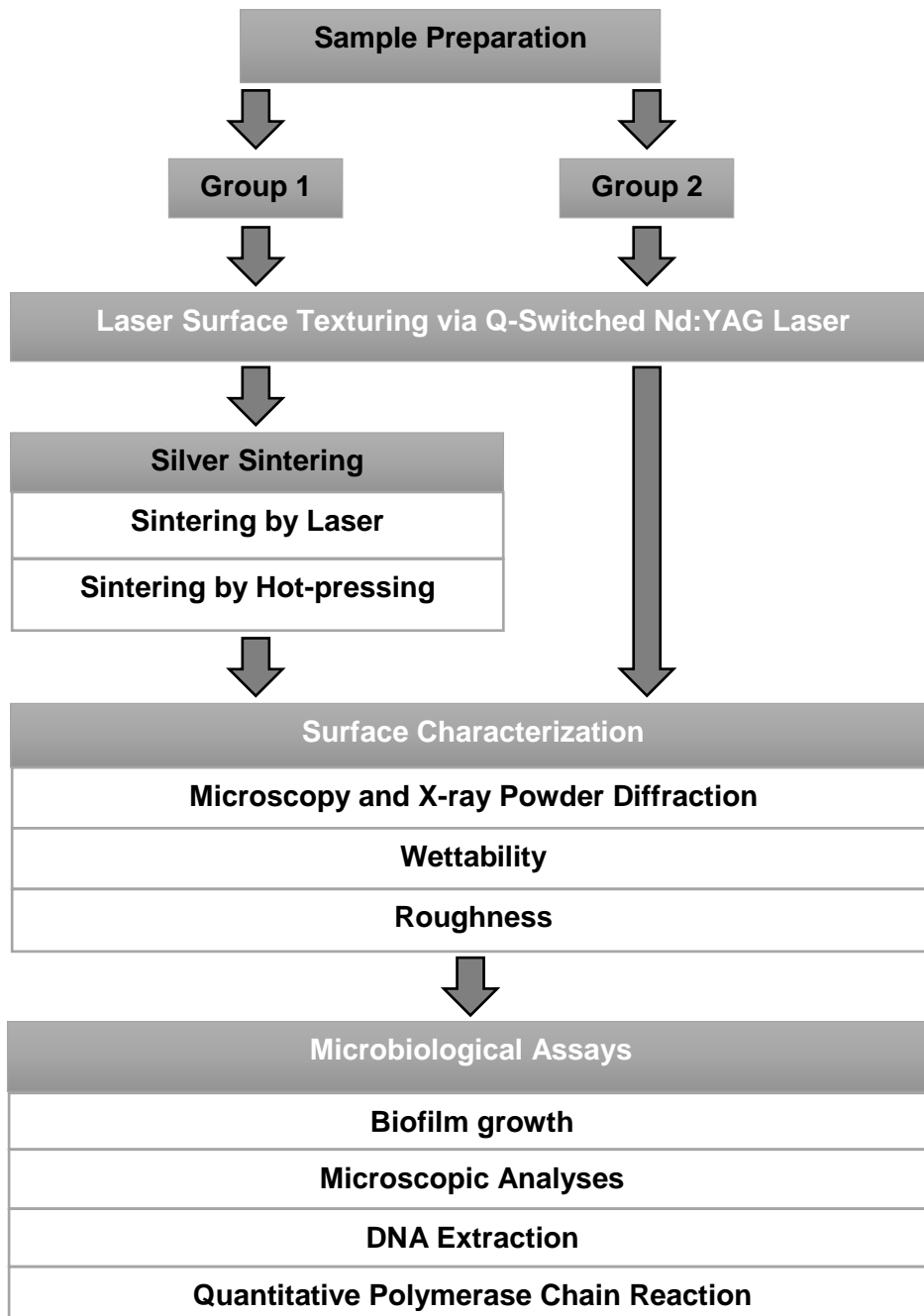


Figure 3.1 – Flow chart representation of the experimental work.

2. Preparation of specimens

Cylindrical samples with 2 mm in height were cut from commercially pure grade IV Titanium rods with 8.25 mm in diameter and from titanium alloy grade V rods with 6 mm and 30 mm in diameter. Titanium cylinder surfaces were wet ground on SiC abrasive papers down to 4000 mesh and then ultrasonically cleaned in isopropyl alcohol for 10 min and in distilled water for 5 min. The samples were then stored in desiccator for 24 h prior to the laser modification.

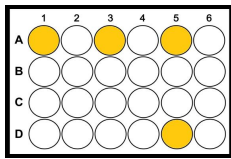
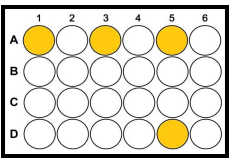
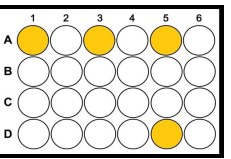
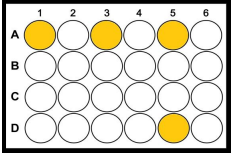
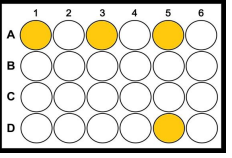
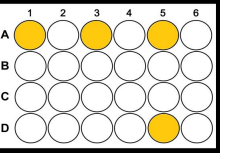
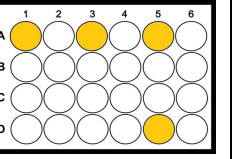
The discs were divided into two groups. The first group (G1) was used to test the incorporation of silver (Ag) on the surface of the discs. Prior to the sintering of Ag, the surface of the samples was textured by Nd:YAG laser. The incorporation of Ag was also tested using a solution of Ag powder and isopropyl alcohol and the Ag powder alone. The sintering was tested using a Nd:YAG laser and a hot-pressing equipment. A final group of samples was prepared with the Ag powder being sintered by hot-pressing, for the physicochemical tests and microbiological assays. The second group (G2) was used to test the formation of a pattern of Ti oxide with different thickness. For the tests two different Nd:YAG lasers were used. A final group of samples patterned by one of the lasers was prepared for the physicochemical tests and microbiological assays. An additional group solely comprising polished samples was also prepared to be used as a control for the physicochemical tests and microbiological assays.

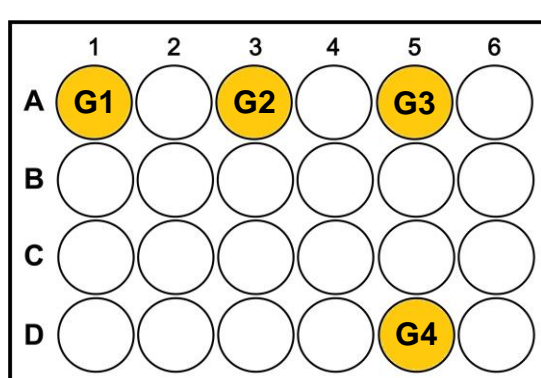
Prior to the microscopy analyses and the roughness evaluation, the samples were ultrasonically cleaned in isopropyl alcohol for 5 min and left to dry in the desiccator for 24 h. For wettability measurements, the samples were ultrasonically cleaned, first with a detergent solution (1:10 of RBS solution in ultrapure water) for 5 min and secondly with isopropyl alcohol for 5 min.

For the microbiological assays the samples were initially sterilized with ethylene oxide gas. Two 24 well plates were prepared in three consecutive days and incubated one plate for 24 h and the other for 72 h (Table 3.1). The plates contained four different samples, as presented in Figure 3.2. One sample of each group 1 and 2 was placed on a different well. Two polished samples were also placed in another two wells to serve as positive and negative control. Each well was filled with bioreactor culture and brain heart infusion (BHI) broth. To

the positive control, the antiseptic chlorhexidine was also added. Two new plates were also prepared for microscopy analyses.

Table 3.1 – 24 well plates incubation schedule.

Incubation Start Day Incubation Time	Day 1	Day 2	Day 3	Day 4
	24h			
72h				
	DNA Extraction			SEM



G1 – G1 discs + 900 µl BHI-2 + 100 µl Bioreactor culture

G2 – G2 discs + 900 µl BHI-2 + 100 µl Bioreactor culture

G3 – Polished discs + 900 µl BHI-2 + 100 µl Bioreactor culture

G4 – Polished discs + 500 µl BHI-2 + 100 µl Bioreactor culture + 400 µl Chlorhexidine

Figure 3.2 – Schematic representation of a 24 well plate used for microbiological assays.

3. Laser Texturing

3.1. Group 1 preparation

The patterning of the samples was performed with a Q-switched diode-pumped Nd:YAG laser 1 (OEM plus 6W, SISMA, Italy) with 1064 nm of working wavelength and a maximum power of 6 W. The laser beam was emitted through a galvanometer scanning head (2-axis subsystem Focusshifter, model MS-10 [Y] D1 V2, from RAYLASE) that controls the focus and movement of the beam on the surface. The general parameters for the patterning and the layout sketches are defined in a computer-control unit through a built-in marking control software designated as Sisma Laser Controller (SLC). Other characteristics of the laser are presented in Table 3.6.

Two patterns were tested on the titanium samples. Both patterns comprised series of sets of horizontal and vertical lines spaced out differently. Within a group of the patterns the sets of lines are farther apart which originates a coarse pattern, with wider titanium protrusions and smaller space between them. The lines of the second pattern, on the other hand, are close to each other, originating a pattern with thinner protrusions and a wider space between them. The design of both patterns is shown in Figure 3.4. The patterns have 8 mm of diameter and the wider pattern had a groove spacing of 0 μm and a groove width of 40 μm . The laser parameters to each condition are described on Table 3.2 . In Figure 3.5 an example of a 30 mm disc with the coarse pattern is presented.

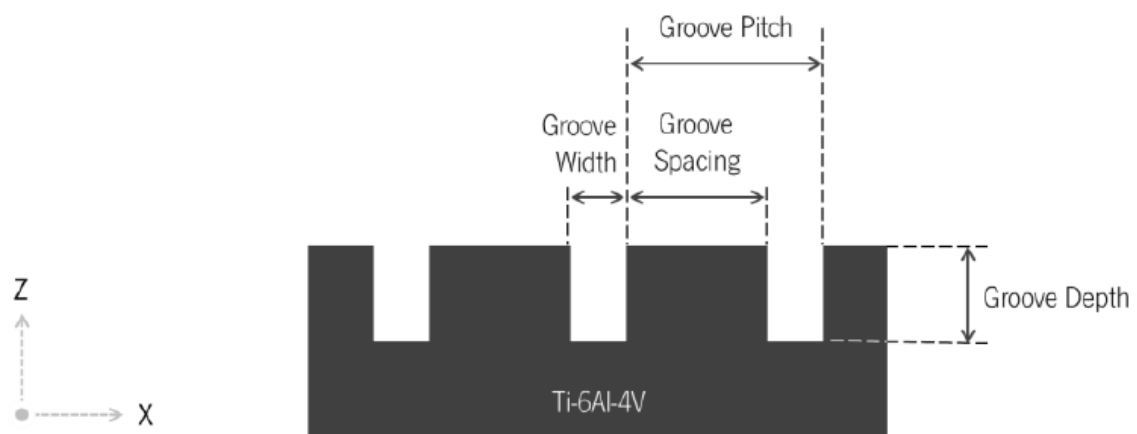


Figure 3.3 – Schematic cross-sectional illustration of the projected grid patterns.

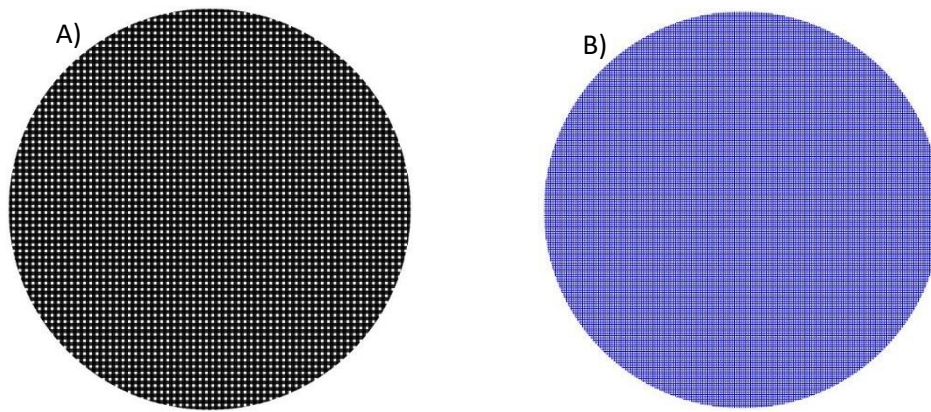


Figure 3.4 – Different patterns performed on the titanium surface by laser. **A)** Coarse pattern; **B)** Wider pattern.

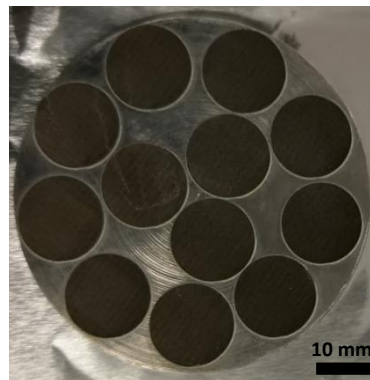


Figure 3.5 – Titanium grade V disc with coarse pattern for silver sintering tests.

Table 3.2 – Laser parameters for titanium patterning.

	Power (%)	Velocity (ms)	Number of Passes	Wobbel	Wobbel Frequency (Hz)	Fill Spacing (mm)
Coarse Pattern	100	200	10	0.008	550	0.5
Wider Pattern	20	400	10	-	-	0.5

The silver used in the preparation of the samples was a power with particles of approximately 1.61 μm in diameter. The incorporation on the titanium surface was initially tested with the titanium alloy of 30 mm in diameter. Ten drops of a solution composed of 25 ml of isopropyl and 0.48 g Ag powder were added on the top of the titanium sample while spinning. The resulting surface is displayed in Figure 3.6 C. The sample was then treated with a Nd:YAG laser in different regions, each one with different parameters. Nevertheless, the silver was irregularly spread over the surface and the tested conditions used mostly melted the titanium surface.

To compare the usage of the Ag solution with the usage of only the powder, two 6 mm diameter titanium alloy samples were patterned with the previously described coarse pattern. Afterwards, ten drops of the Ag solution were added on the surface of one of the samples, while on the other sample 0.2 g of Ag powder was pressed at approximately 30 bar for 10 seconds. The excess of silver on the surfaces was removed with SiC abrasive paper of 4000 mesh. As the previous test, the samples were then treated by laser, with different conditions being used in different areas of the surface.

Pressing the silver powder onto the surface allowed a more evenly spread of the Ag over the Ti surface. Therefore, that method was the one used on the experiments onward. The press machine and the pressing die are shown in Figure 3.6 D. For the experiments carried out using the titanium samples of 30 mm in diameter 1 g of silver powder was used. One example of a sample with pressed silver on the surface is displayed in Figure 3.6 E.

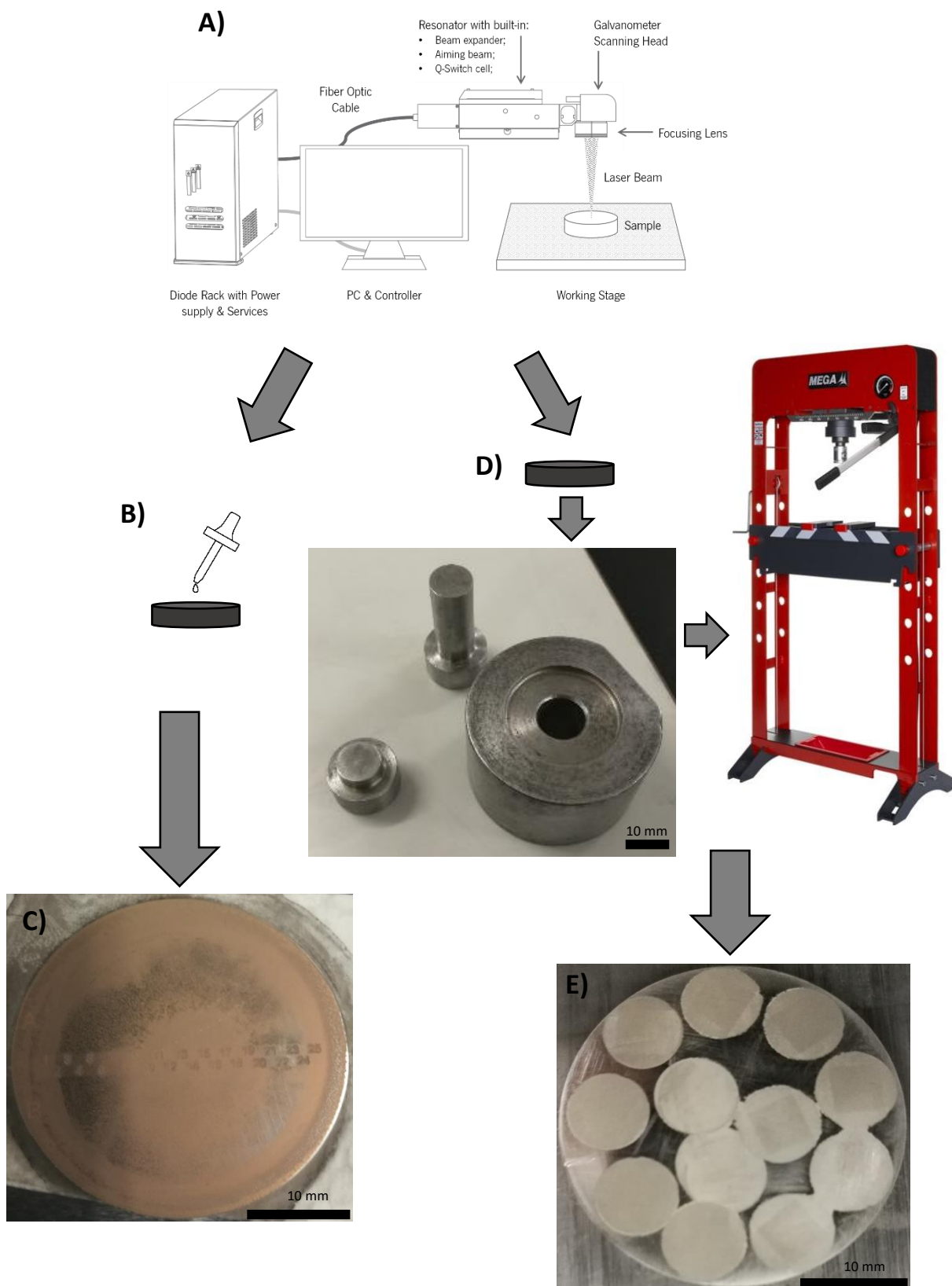


Figure 3.6 – Incorporation of silver tests. **A)** Laser patterning of the samples; **B)** Deposition of silver solution on the surface; **C)** Result of using silver solution; **D)** Silver powder pressed on the sample; **E)** Result of pressing silver powder on the sample.

3.1.1. Laser Sintering

The silver sintering was tested with the Nd:YAG laser 3 (YZD 600 2A, Bende, China) with 1064 nm of working wavelength and a maximum power of 200 W. The laser is presented in Figure 3.7 and the associated detailed information was presented on the previous chapter. The beam pathway as well as the time and distance of each pulse was defined through the software EzCAD. Other parameters, like the current and frequency of the pulse, were defined on a touch screen incorporated on the laser hardware. Different sets of parameters were tested. The final parameters are shown in Table 3.3.

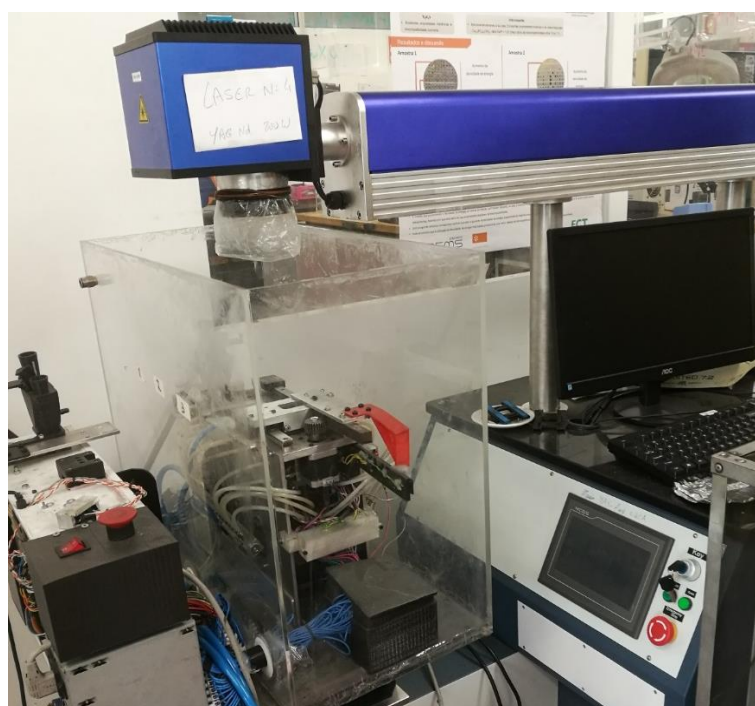


Figure 3.7 – Nd:YAG laser 3 (YZD 600 2A, Bende, China).

Table 3.3 – Laser parameters for silver sintering.

<i>Parameters</i>	<i>Point time (ms)</i>	<i>Point distance (mm)</i>	<i>Line distance (mm)</i>	<i>Loop distance (mm)</i>	<i>Current (A)</i>	<i>Frequency (Hz)</i>	<i>Light (mm)</i>	<i>Pulse (ms)</i>
	10	0.025	0.025	0.5	1 to 2	200	0.1	0.1 to 1.5

3.1.2. Hot-Pressing

Lastly, the sintering was tested using hot-pressing techniques since it is a way of applying heat and pressure at the same time. Silver powder was sintered on the surface of the titanium samples by means of pressure-assisted sintering process (hot pressing), in vacuum (10^{-2} mBar), using a high frequency induction furnace shown in Figure 3.8. The titanium discs were placed on the graphite mold with 1 mg of silver powder on the previously patterned surface. The samples were pressed and heated up to 950 °C with a heating rate of 95 °C/min and to a pressure of 18 MPa. Then the pressure and temperature were maintained for one minute. Afterward, the samples were cooled, till room temperature, inside the mold and in vacuum.

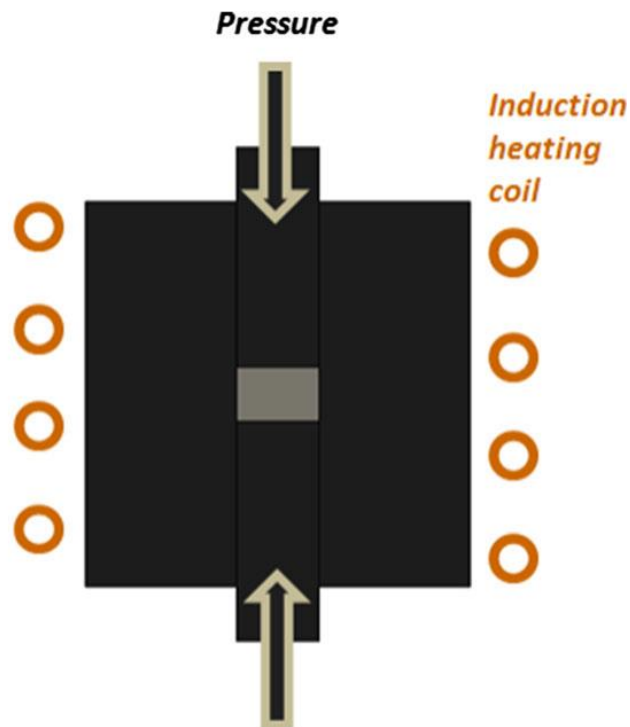


Figure 3.8 – Representation of hot-pressing main components. Adapted from [121].

3.2. Group 2 preparation

The patterning of the samples was tested with two different Nd:YAG lasers. One of the lasers was the same used for silver sintering. The different range of parameters tested is presented in Table 3.4. Other set of samples were treated with the Nd:YAG laser 2 (LM-D 60 7500W, SISMA, Italy) with 1064 nm of

working wavelength and a maximum power of 7500 W. This equipment (Figure 3.9) has an incorporated touchscreen that serves as a control unit to define the general parameters to be used. The laser is also equipped with a camera that allows a real-time monitoring of the samples. The beam is triggered manually through a pedal. Since there is no relative movement of the beam, the samples must instead be manually placed in different positions, in order to treat different areas of the surface. The different parameters used on the tests are presented in Table 3.5. Detailed characteristics of both lasers are presented on Table 3.6. The samples used for the subsequent tests were patterned with the Nd:YAG laser 2.

Table 3.4 – Laser 3 parameters for surface patterning tests of Ti samples.

Parameters	Point time (ms)	Point distance (mm)	Line distance (mm)	Loop distance (mm)	Current (A)	Frequency (Hz)	Light (mm)	Pulse (ms)
	10 to 450	0.025	0.02 to 0.7	0.5	1 to 10	200	0.1	0.1 to 1.0



Figure 3.9 – Nd:YAG laser 2 (LM-D 60 7500W, SISMA, Italy)

Table 3.5 – Laser 2 parameters for surface patterning tests of Ti samples.

Power (%)	Point Time (ms)	Frequency (Hz)	Diameter (mm)	Passes	Pulse Type
2 to 10	0.1 to 1.0	2 to 10	0.3 to 0.9	1 to 5	20 section pulse shape mode; single pulse; 3 section mode

Table 3.6 – Specific characteristics of the Nd:YAG lasers.

Parameters	Nd:YAG laser 1	Nd:YAG laser 2	Nd:YAG laser 3
Spot diameter (μm)	3	200 – 2000	0.2 – 3.0
Wavelength (nm)	1064	1064	1064
Maximum Power (W)	6	7500	200
Maximum Speed (mm/s)	2000	-	-
Repetition Rate Range (Hz)	20000	0 – 50	-
Pulse Width (ns)	35	300000 - 30000000	0.3 – 20
Max Pulse Energy (mJ)	0.3	90J	70000
Beam quality factor, $M^2 <$	1.8	-	-
Colling System	Forced-aired Cooling	Water/Air	Forced-aired Cooling and chiller
Power Supply	230V, $\pm 10\%$, 50/60Hz	230 V 50/60 Hz 1Ph	220V, 50HZ,60A

4. Physicochemical Analyses

The surface of the samples was analyzed by optical and electronic microscopy and therefore both wettability and roughness were measured. Prior to the physicochemical analyses, the samples were ultrasonically washed in isopropyl for 5 min and left to dry overnight on the desiccator.

4.1. Microscopy and X-ray Powder Diffraction (XRD)

Morphologic aspects and the surfaces of the samples were analyzed by scanning electron microscopy (SEM), (TM3030, Hitachi, Japan) at 15 kV by back-scattering and secondary electron mode, and by optical microscopy (OM), (Leica DM 2500M, Leica Microsystems, Germany). The magnifications used were up to x1000 for the former, and up to x10 for the latter. Samples of G2 were analyzed by XRD using a diffractometer in a Bragg-Brentano θ - 2θ configuration and a Cu K α radiation with a wavelength (λ) of 1.540 Å. The data were collected in the 2θ range of 20° – 80° using step scan mode with step width of 0.04°

For microscopic analyses of the biofilms, discs covered with biofilms were washed two times in phosphate-buffered saline (PBS) and fixed in glutaraldehyde 2% for 5 min. Then, discs were washed three times in PBS, and dehydrated through a series of graded ethanol solutions (50, 70, 80, 90, 100%). Samples covered with biofilms were sputter-coated with gold (Figure 3.10) and analyzed by SEM.[122]



Figure 3.10 – Titanium samples sputter-coated with gold.

4.2. Wettability

Water contact angle measurements were performed using the sessile drop method (2 μl distilled water droplet) using a video-based drop shape analyzer. Contact angles were measured using an optical goniometer (OCA 15 plus, Dataphysics, Germany) that is displayed in Figure 3.11. The droplet profile was analyzed using the corresponding software (SCA 20, Dataphysics, Germany). Three measurements were carried out on each one of three samples ($n = 9$).[123] The measurement of one of the titanium samples is illustrated in Figure 3.12.

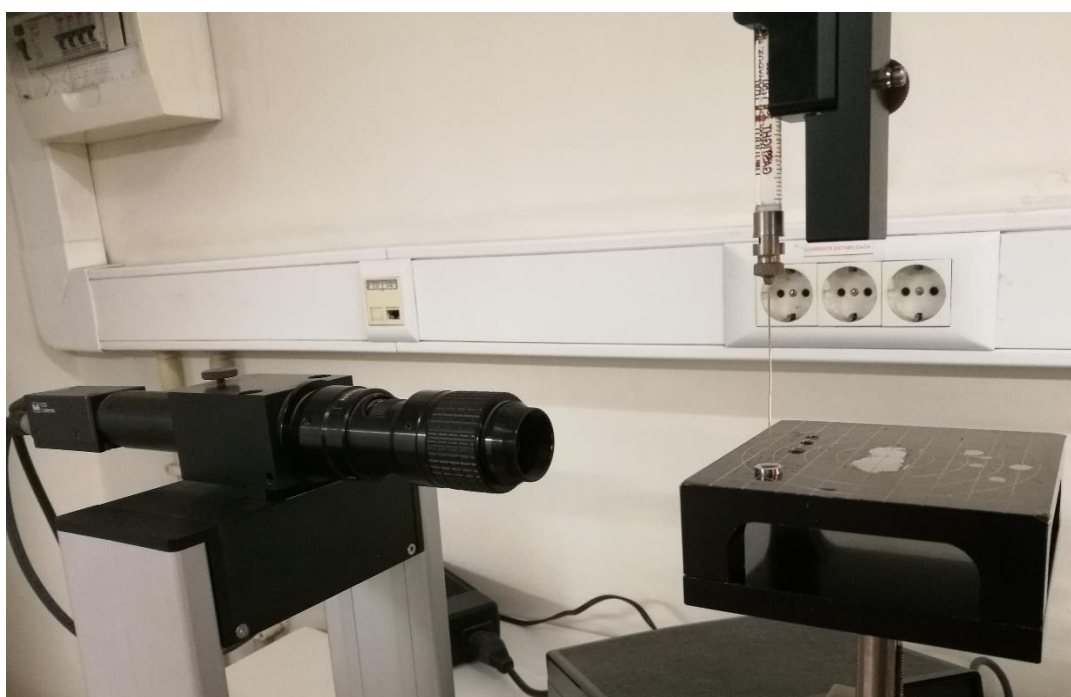


Figure 3.11 – Optical goniometer (OCA 15 plus, Dataphysics, Germany).

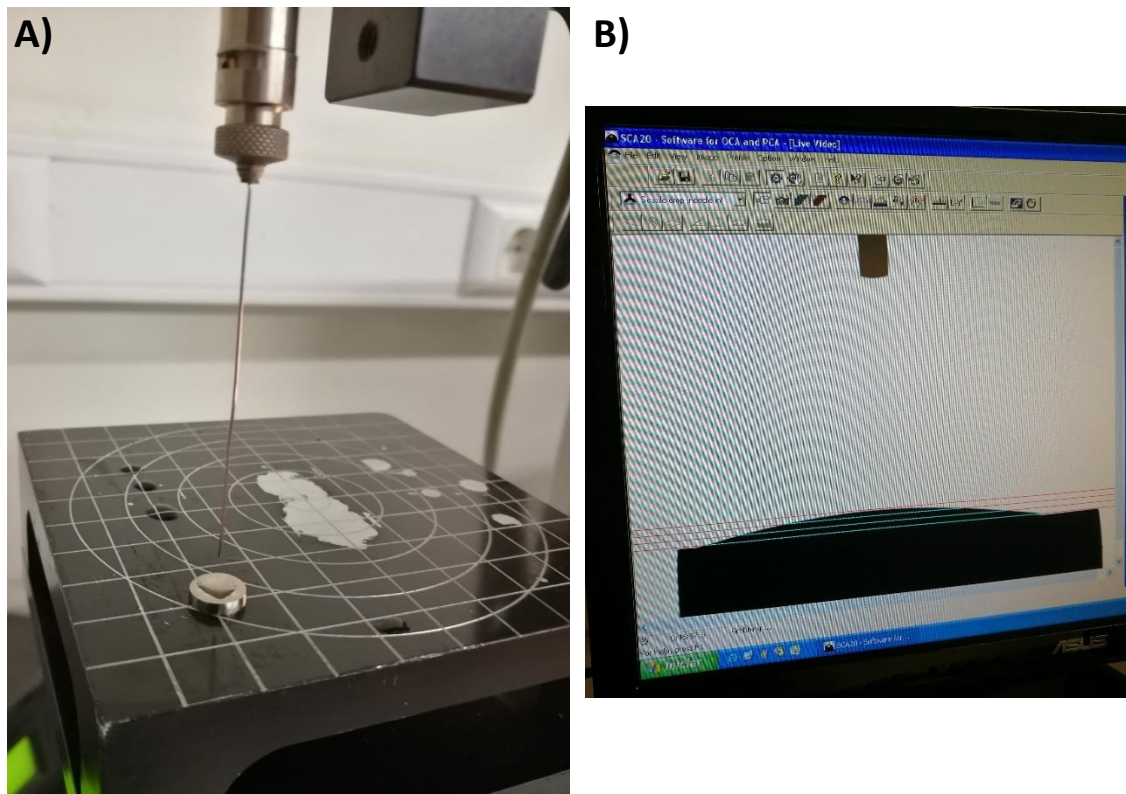


Figure 3.12 – Wettability measurement of a titanium sample. **A)** Placement of water drop on the surface and **B)** analysis through the corresponding software.

4.3. Roughness

Roughness mean values of the disc samples were obtained regarding the following parameters: Ra (arithmetic mean value between the peak and valley height values in the effective roughness profile), Rq (root mean square average of the roughness profile ordinates) and Rz (arithmetic mean value of the single roughness depths of consecutive sampling lengths). The values were measured according to the ISO 1997 standard using a mechanic profilometer (Surftest SJ 201, Mitutoyo, Tokyo, Japan), that is presented in Figure 3.13. The equipment is composed by a sharp diamond stylus with 2 μm of diameter and 70° of opening angle. The roughness values were recorded at three different areas on each material ($n = 9$). The measurement length was 0.7 mm and cut off at 0.25 mm for 3 s.



Figure 3.13 – Mechanic profilometer (Surftest SJ 201, Mitutoyo, Tokyo, Japan).

5. Biofilm Assays

5.1. Biofilm growth

Titanium discs were tested against a multi-species biofilm, grown in a bioreactor (BIOSTAT® B, Germany), as seen in Figure 3.14. The multi-species biofilms included 14 strains as follow: 2 early colonizer bacterial species (*Streptococcus mitis* DSM 12643 and *Streptococcus gordonii* ATCC 49818), 6 pathogen bacterial species (*Aggregatibacter actinomycetemcomitans* ATCC 43718, *Fusobacterium nucleatum* ATCC 20482, *Porphyromonas gingivalis* ATCC 33277, *Prevotella intermedia* ATCC 25611, *Streptococcus mutans* ATCC 20523, *Streptococcus sobrinus* ATCC 20742) and 6 beneficial bacterial species (*Veillonella parvula* DSM 2008, *Actinomyces viscosus* DSM 43327, *Streptococcus salivarius* TOVE-R, *Actinomyces naeslundii* ATCC 51655, *Streptococcus sanguinis* LM14657, *Streptococcus oralis* DSM 20627). 750ml of Brain Heart Infusion 2 (BHI-2) broth were added to the bioreactor vessel together with 5.0 mg/mL of hemin, 1.0 mg/mL of menadione, and 200 μ L of

Antifoam Y-30 (Sigma, St. Louis, USA). The BHI-2 broth was composed of 37 g/L of brain heart infusion (Difco, Detroit, USA), 2.5 g/L of mucin from porcine stomach type III (Sigma-Aldrich, St. Louis, USA), 1 g/L of yeast extract (Oxoid, Basingstoke, UK), 0.1 g/L of cysteine (Calbiochem, San Diego, USA), 2 g/L of sodium bicarbonate and 0.25% (v/v) glutamic acid (Sigma-Aldrich, St Louis, USA). The calibration of pH electrode was performed with 1/10 HCl 1/10 and the 1 molar NaOCl before the sterilization process. One vessel of 2L was prepared with fresh BHI-2, in order to be able to refresh the growth medium over the experiment period. After the sterilization process, the bioreactor was set-up with 300 rpm of stirring on anaerobic condition (80% N₂, 10% H₂ and 10% CO₂) at 37 °C.[122]

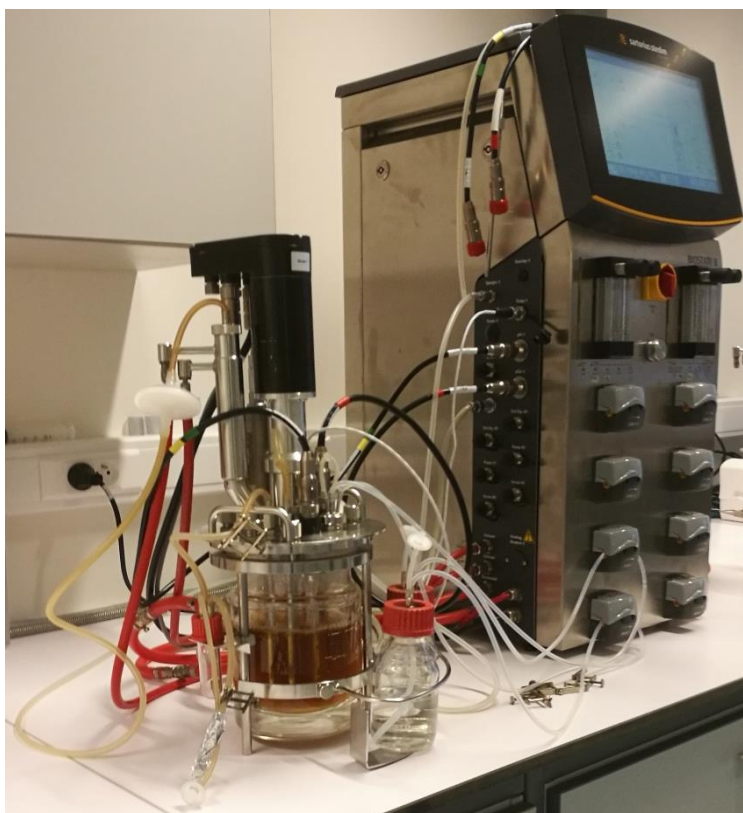


Figure 3.14 – Bioreactor (BIostat® B, Germany).

After 24 h, the absorbance of the bacterial suspension was controlled to achieve the same optical density values prior to incubation in the bioreactor. Stable multi-species biofilm was obtained for 72 h. After this period, Ti discs were placed at the bottom of 24 well plates in three different and consecutive days, as described in the initial section of this chapter. The plates were

incubated at 37 °C under anaerobic conditions over a period of 24 h and 72h biofilm growth.[122,124–128] A schematic resume of the referred steps is presented in Figure 3.15.

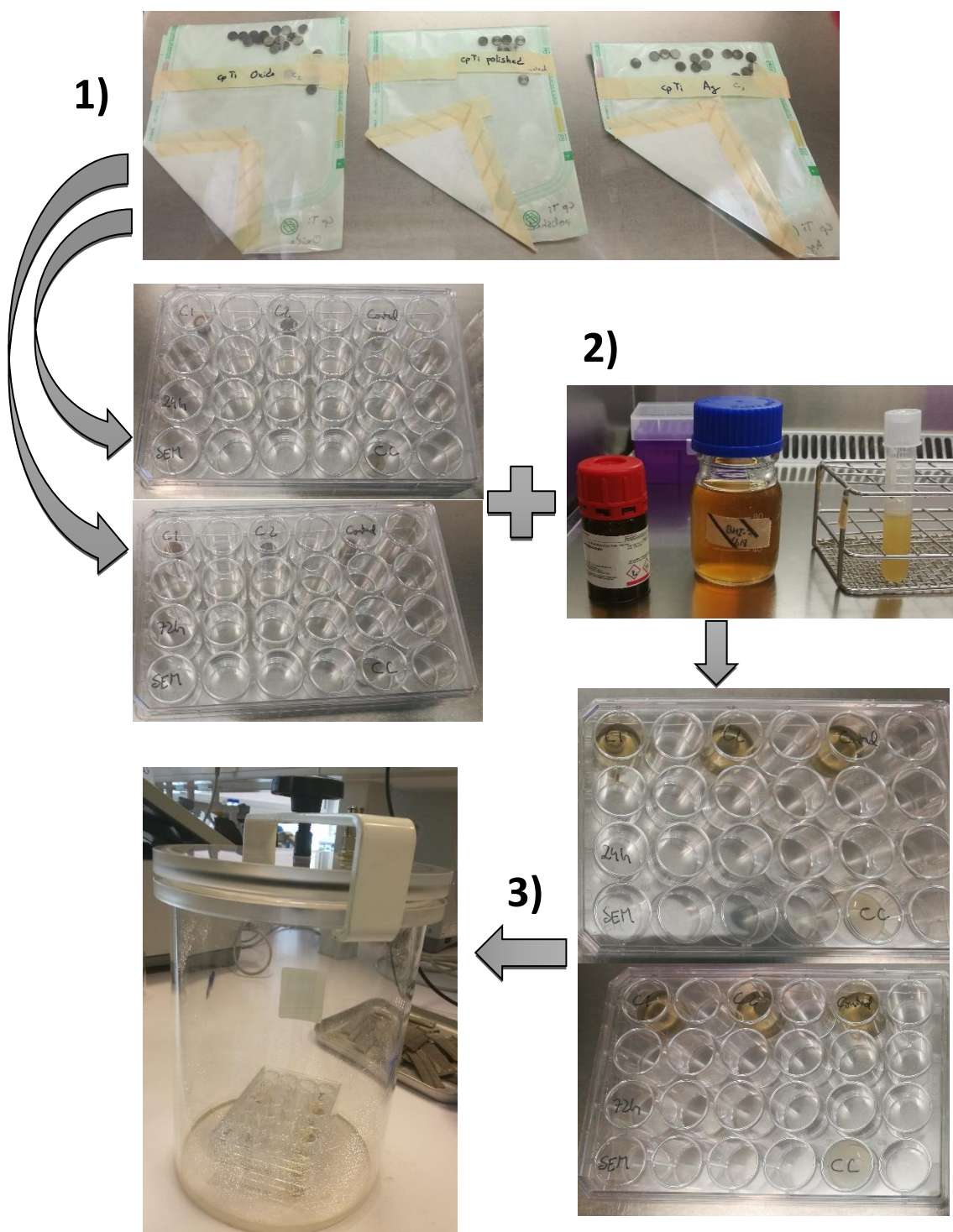


Figure 3.15 – Schematic representation of the initial steps for biological assays. **1)** Placement of the samples on the 24 well plates; **2)** Addition of bacterial culture, BHI-2 and chlorhexidine to the respective well; **3)** Incubation of the samples in anaerobic environment.

5.2. Quantitative Polymerase Chain Reaction (qPCR)

The supernatant from the biofilm culture was carefully removed with pipets, and then the discs were smoothly cleaned with 1 mL PBS to withdraw the weakly attached biofilm. The well attached biofilm was removed with 1.5 mL trypsin and maintained into the incubator for 45 min. The trypsin from each well was added to Eppendorf's to be centrifuged and then the pellets were resuspended in 500 mL PBS. After the dilution, the DNA was extracted from bacterial samples using a QIAamp DNA Mini kit (Qiagen Ltd., Hilden, Germany) in accordance with the manufacturer's instructions. A qPCR assay was performed using a CFX96 Real-Time System (BioRad, Hercules, CA, USA). The TaqMan 5' nuclease assay PCR method was used for detection and quantification of bacterial DNA. TaqMan reactions contained 12.5 μ L of Mastermix (Eurogentec, Seraing, Belgium), 4.5 μ L of sterile H₂O, 1 μ L of each primer and probe, and 5 μ L of template DNA. Primers and probes were used at different concentrations depending on the organism. Assay conditions for all primer/probe sets consisted of an initial 2 minutes at 50 °C, denaturation for 10 minutes at 95 °C, followed by 45 cycles of 95 °C for 15 seconds and 60 °C for 60 seconds. The bacterial counts are expressed as Geq/mL because the concentration was calculated based on plasmid standard curves. [122,127,128]

Chapter 4 – RESULTS AND DISCUSSION

The results of the present study are shown in this chapter followed by a discussion of the findings.

1. Surface characterization

The topographic characteristics of the surface of the samples were inspected by optical and scanning electron microscopy. The wettability of the surfaces was determined by the sessile drop technique and the roughness parameters were measured with a rugosimeter.

1.1. Microscopic analyses

The samples with different oxide thicknesses were evaluated by optical microscopy (OM) while the silver-based specimens were inspected by both OM and scanning electron microscopy (SEM). Such microscopic analyses allowed the selection of adequate parameters for validation.

1.2. Pattern for silver incorporation

The previously described patterns for silver incorporation (Figure 3.4) were inspected by SEM. The obtained images are shown in Figure 4.1. The coarse pattern (A and C) reveals large rectangular columns (105 μm in length and 84 μm in height) with protrusions on the center. The average spacing between the center of two consecutive columns were at 112 x 92.73 μm . The other pattern (B and D) exhibits diamond shape columns connected by thin bridges with a depression on the center. The columns and bridges were separated by circular depressions of approximately 29.44 μm in diameter. The average spacing between the center of two consecutive columns was at 39.87 x 39.09. The top of the columns had 27.13 μm length and 26.20 μm height. No cracks were detected on both patterns. Nevertheless, some regions of the titanium dioxide film exhibited a pillow-shape form due to the laser melting. Those features were mainly noticed on the top of the columns and on the depressions of the wider pattern.

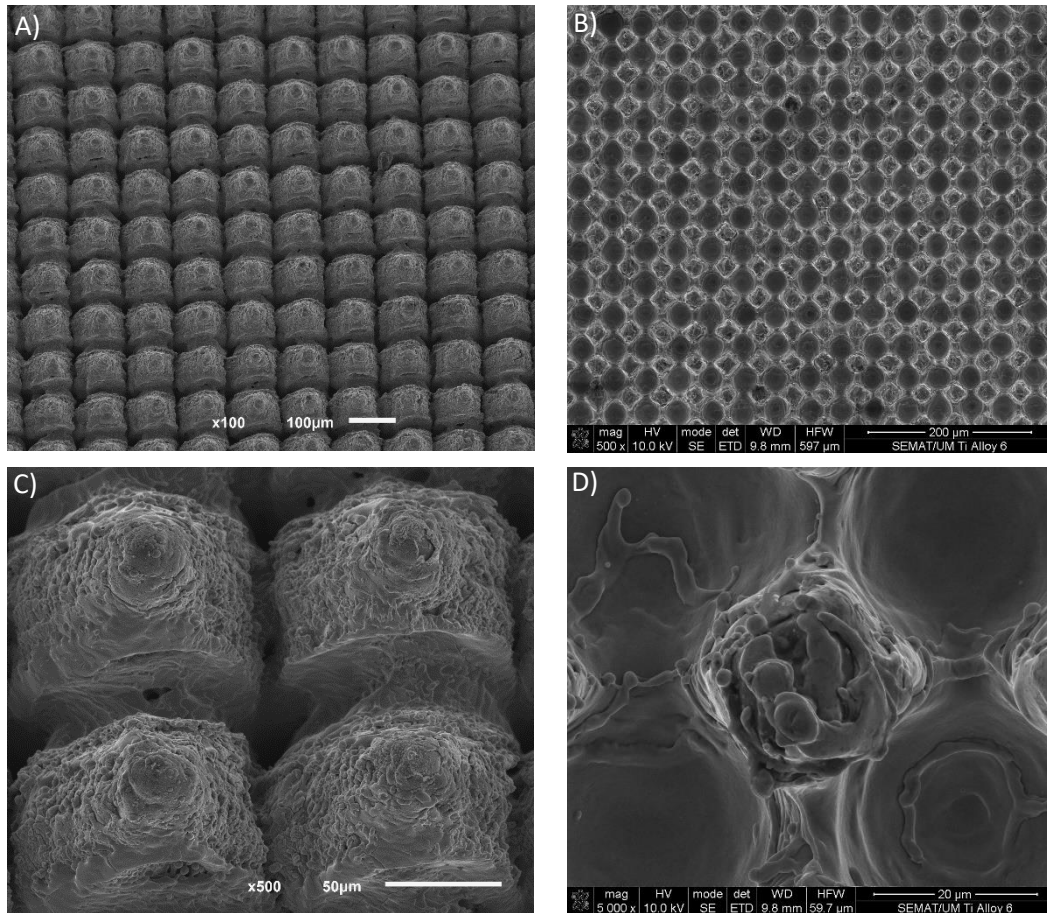


Figure 4.1 – SEM images of the titanium surface with different patterns. **A)** and **C)** Coarse pattern; **B)** and **D)** Wider pattern.

1.3. Silver Sintering by laser

Different laser parameters were tested to achieve the sintering of the silver on the titanium surface. The tested samples were examined by both optical and electronic microscopy. SEM images of the initial test surface patterns are shown in Figure 4.2. Due to the small size of the sample, the different conditions were not clearly distinguishable due to melting of the titanium by the laser irradiation. The use of silver powder instead of the silver in solution was preferred henceforth. Despite the similarity between the results, the surface with silver powder showed better distribution of the silver through the surface and less heat propagation.

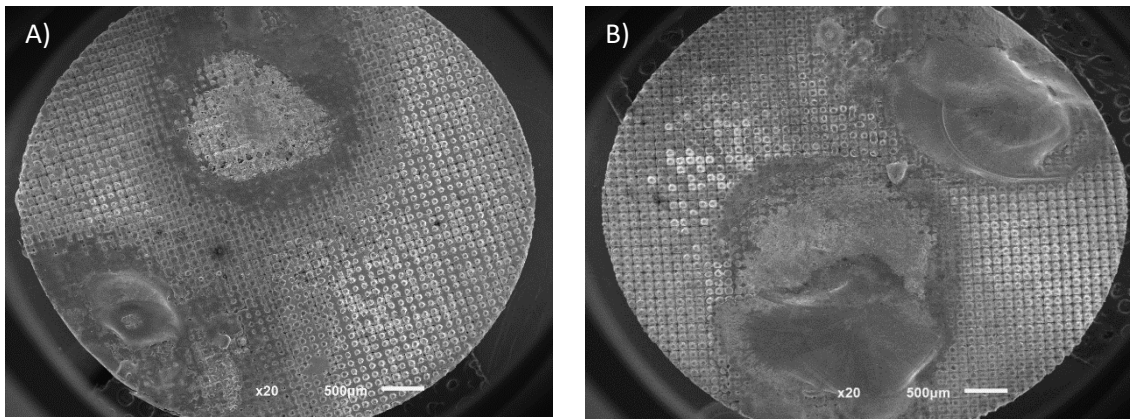
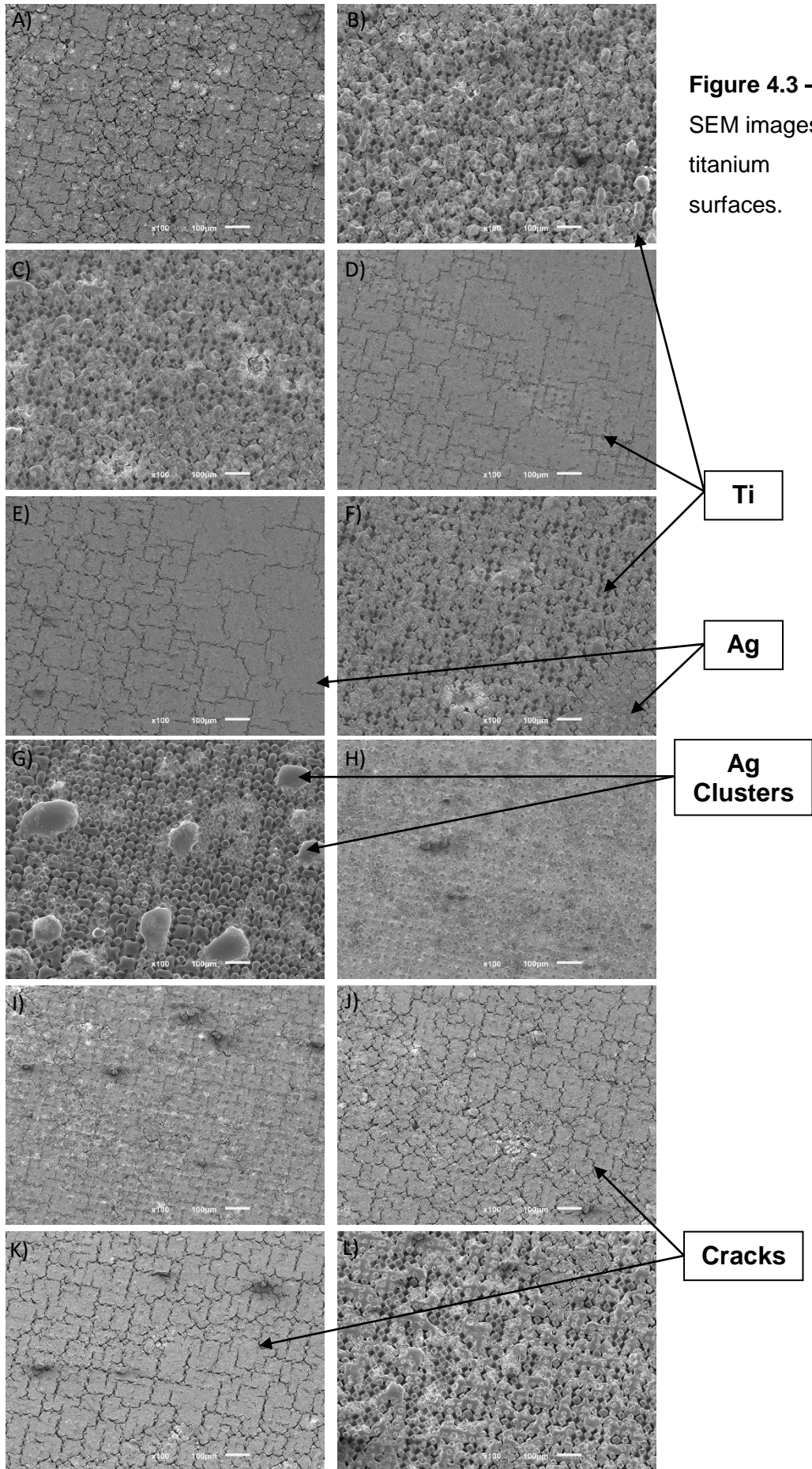
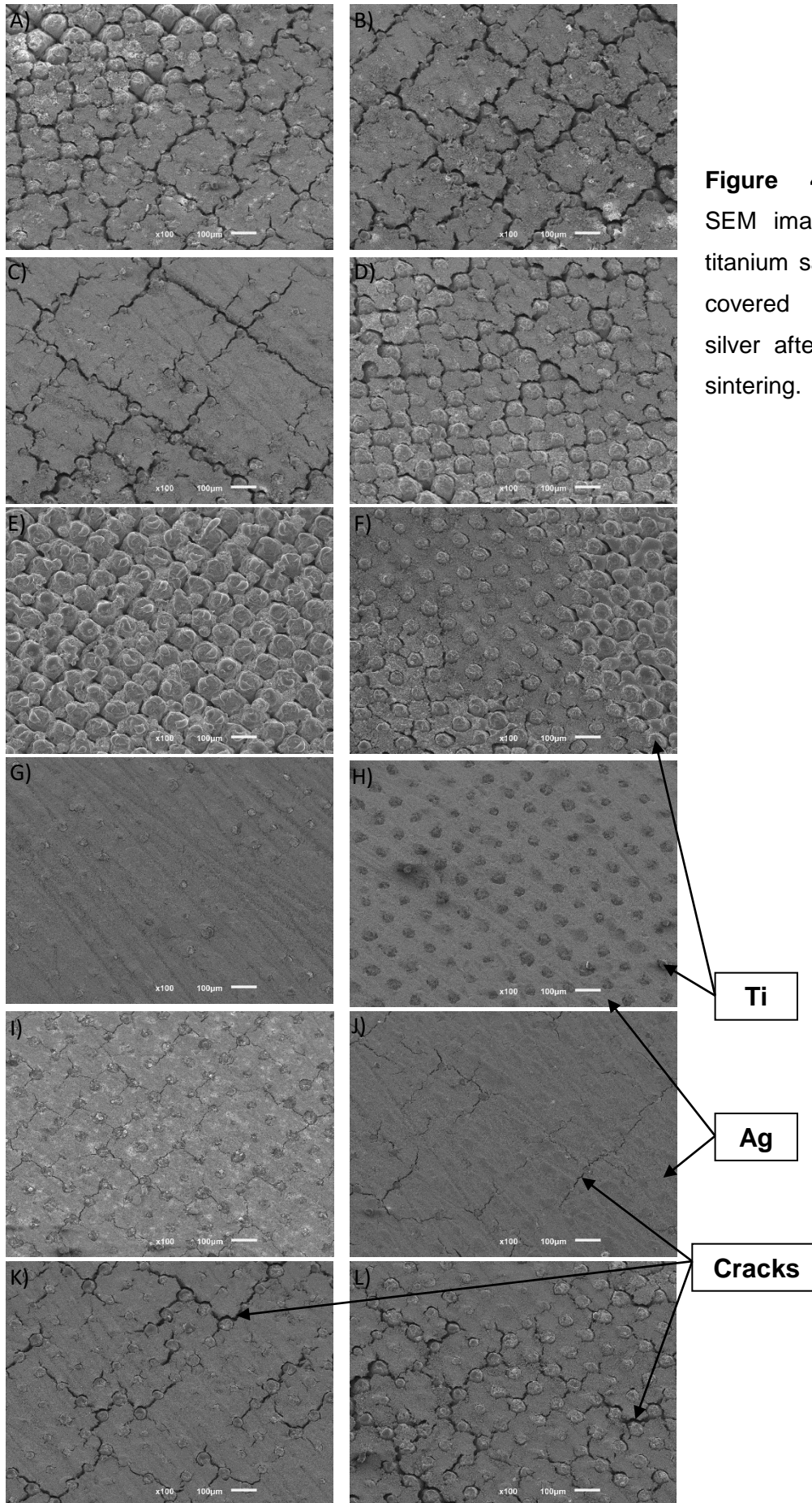


Figure 4.2 – SEM images of the titanium test surface covered with **A)** silver powder and **B)** silver solution treated by different laser conditions.

A broader set of conditions was tested on the titanium samples with each of the patterns. The surface of the samples was then inspected by microscopy as seen in Figure 4.3 (samples with the wider pattern) and in Figure 4.4 (samples with the coarse pattern). On both patterns some conditions lead to the formation of a silver layer with titanium dots, corresponding to the columns of the patterns. Nevertheless, cracks were detected on those layers. Some samples with the wider pattern did not show a uniform layer of silver but rather round shaped clusters. For both patterns, the features of the test samples shown in the Figure 4.3 and Figure 4.4 H were the closest to the expected results.





Another set of conditions was tested based on the previous tests. The samples were inspected by optical microscopy. The corresponding results for the samples with the wider pattern are shown in Figure 4.5 while samples with coarse pattern are shown in Figure 4.6. A continuous layer could not be formed among the columns of the silver pattern. Only the conditions for the sample revealed in Figure 4.6 F correspond to the expected results. Those conditions were repeated on other samples and examined by optical microscopy. The surface of one sample is revealed in different magnification in Figure 4.7. The surface showed a silver layer surrounding the titanium columns free of cracks or breaches and therefore the titanium was not visibly affected by the laser treatment. The laser parameters are summarized in Table 4.1.

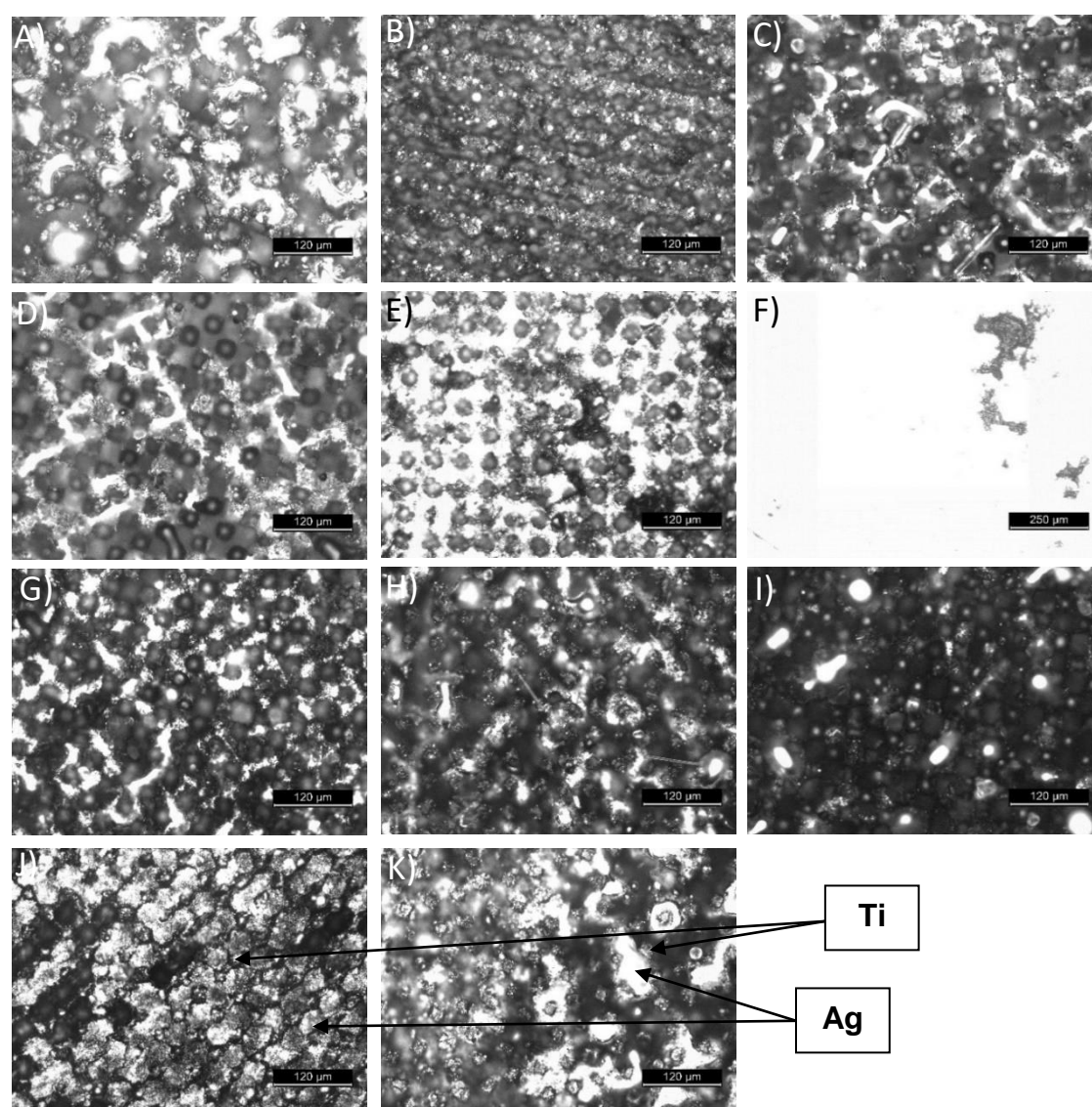


Figure 4.5 – Optical micrographs of the titanium surfaces covered with silver layers after laser sintering.

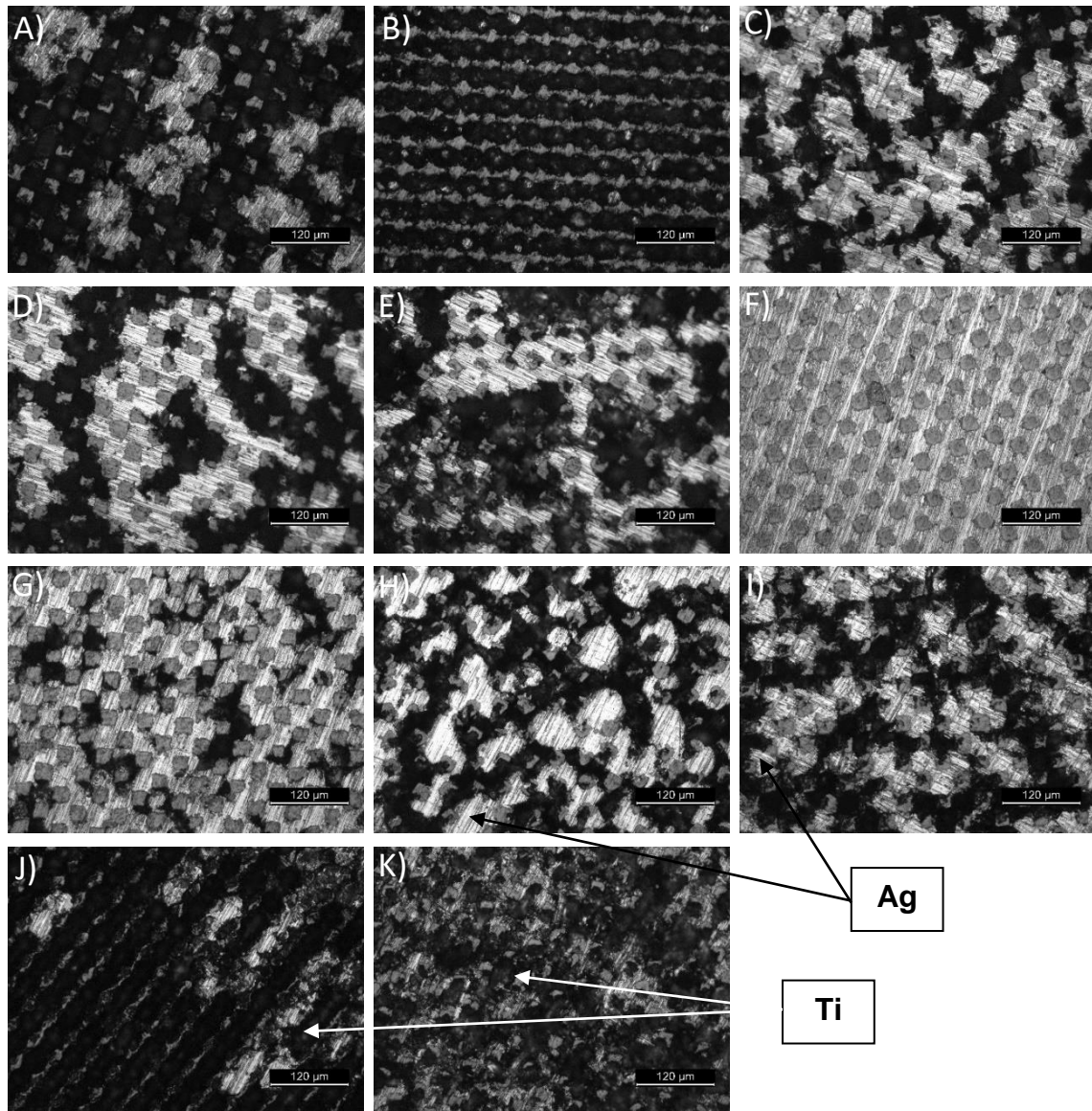


Figure 4.6 – Optical micrographs of coarse pattern titanium samples covered with silver layers after laser sintering.

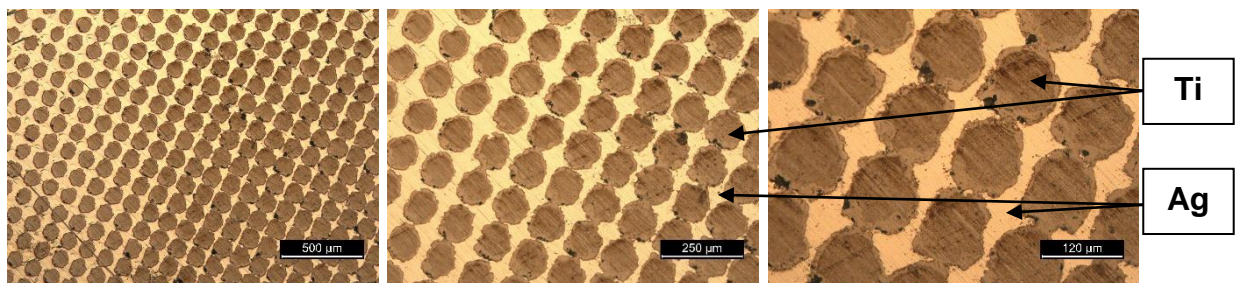


Figure 4.7 – Optical micrographs of titanium surface after laser sintering.

Table 4.1 – Nd:YAG laser parameters for the silver sintering.

Parameters	Current (A)	Pulse	Frequency (Hz)	Point Time (ms)	Light (mm)	Loop Distance (mm)	Line Distance (mm)	Point Distance (mm)
	2	0.8	200	10	0.1	0.5	0.025	0.025

1.4. Silver Sintering by Hot-Pressing

SEM images of the surfaces treated by hot-pressing are shown in Figure 4.8. The surface pattern of the samples was similar to those produced by laser treatment. The grooves of the Ti pattern were filled with silver and no cracks were noted on the surface. Consequently, this method also proved to be effective to incorporate silver on the titanium surface. The hot-pressing method was selected to manufacture samples for the microbiological assays once the sintering atmosphere was well controlled.

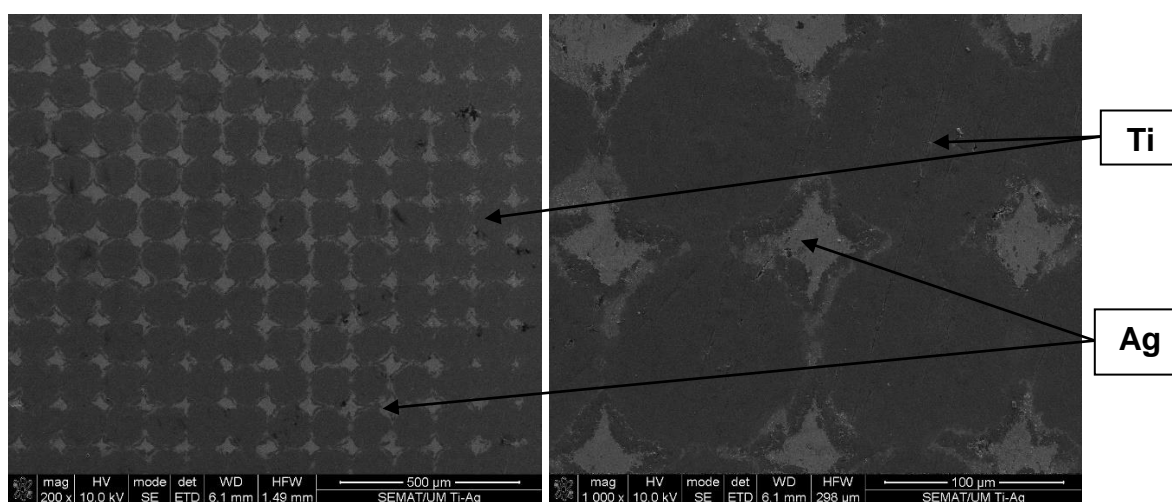


Figure 4.8 – SEM images of the titanium surface covered with silver layers after hot-pressing. The silver is in light gray and the titanium in dark gray.

1.5. Titanium Dioxide with Different Thickness – Nd:YAG laser 3

Titanium discs with 30 mm of diameter were used to test different laser parameters for surface modification. Small lines for each parameter were made and then inspected by optical microscopy. Some of the test results are shown in Figure 4.9.

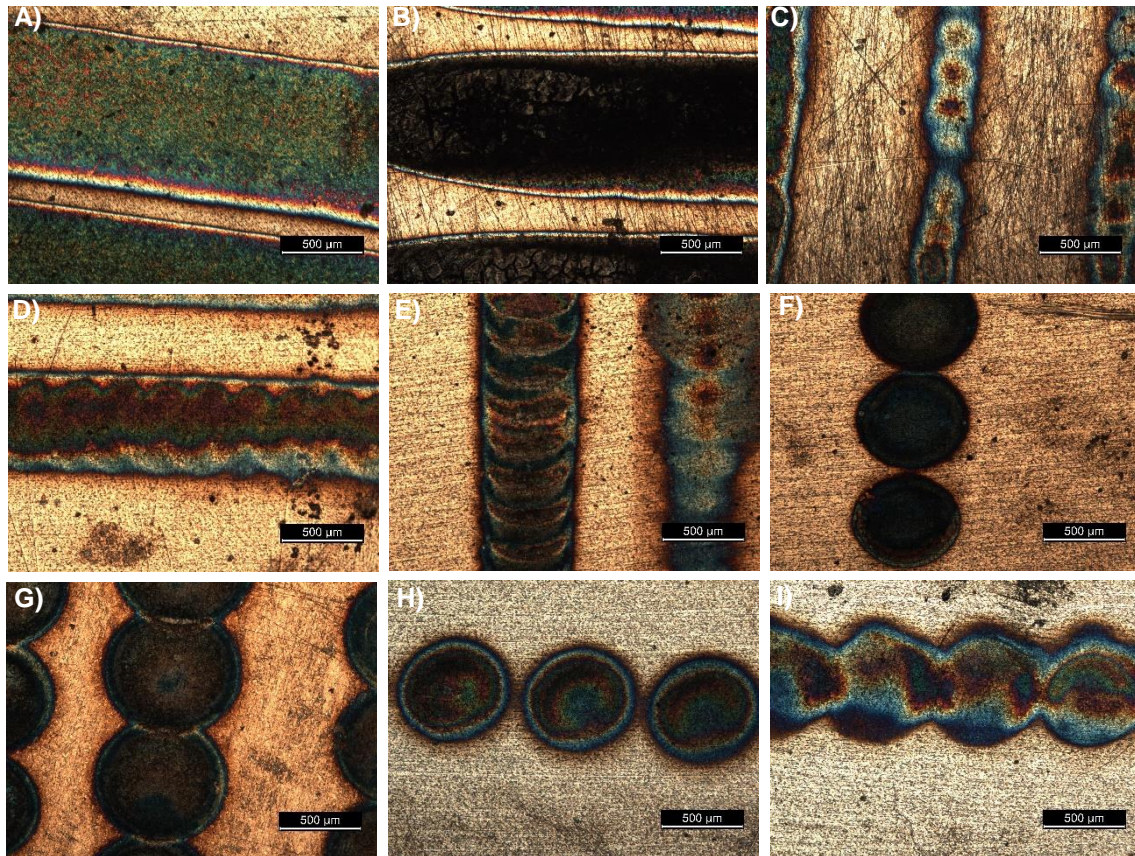
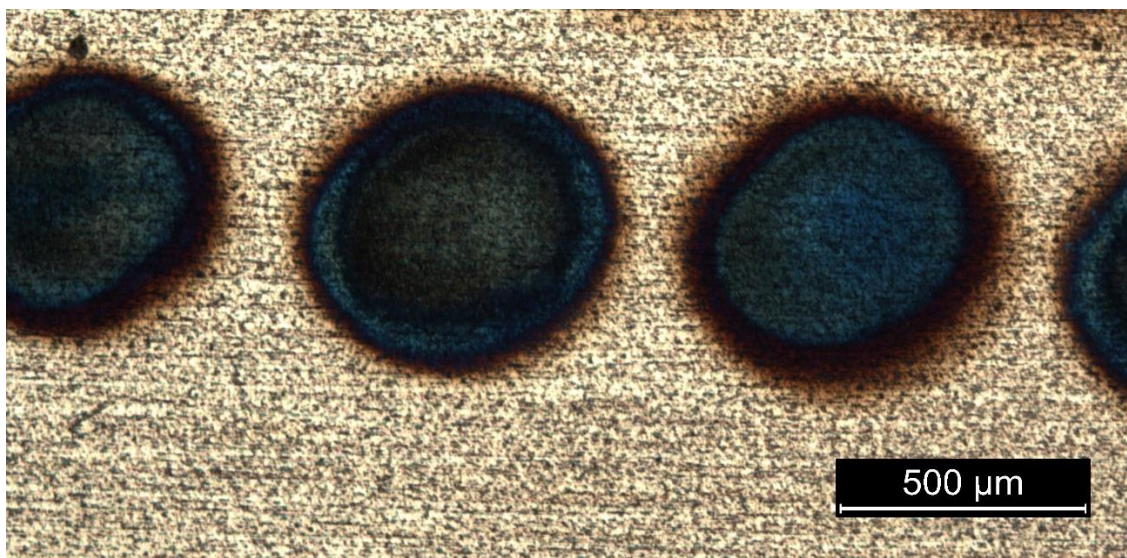


Figure 4.9 – Optical micrographs of titanium oxide pattern after laser irradiation.

Two major characteristics of the laser beam that need to be selected were the beam power and the distance between each pulse. High values of beam power led to excessive titanium melting and the pattern filled with cracks (Figure 4.9 B) while low values of beam power led to faint (Figure 4.9 C) or absent marks. Low spacing, in turn, led each pulse to overlap with the previous. Consequently, the pattern was a line (Figure 4.9 A) or dots with some overlaid areas (Figure 4.9 D, E, G, I). The spacing between the dots of Figure 4.9 H is the intended for the thicker titanium dioxide. The laser parameters and microscopy analyses are shown in Table 4.2 and Figure 4.10, respectively.

Table 4.2 – Nd:YAG laser parameters for titanium oxide pattern.

<i>Parameters</i>	<i>Current (A)</i>	<i>Frequency (Hz)</i>	<i>Light (mm)</i>	<i>Mark Loop</i>	<i>Point distance (mm)</i>	<i>Point time (ms)</i>
	1	200	0.1	2	0.70	60

**Figure 4.10 – Optical micrographs of the thick titanium dioxide pattern.**

1.6. Titanium Dioxide with Different Thickness – Nd:YAG laser 2

A titanium disc of 6 mm in diameter was used to test several conditions of another Nd:YAG laser equipment. The images obtained by optical microscopy of some of the test conditions are shown in Figure 4.11.

The sought laser conditions were the ones which generated the most uniform layer of titanium dioxide. The majority of the tests lead to some degree of surface alteration. Nevertheless, in some cases the energy of the pulse was not evenly distributed, which led to variations of shape and color of TiO₂, as seen in Figure 4.11 B-F. Other conditions led to round shaped TiO₂ marks but also exhibited oxide of different colors (Figure 4.11 A, D, H and I) while groups of surfaces showed only blue oxide but cracks could be noted (Figure 4.11 G).

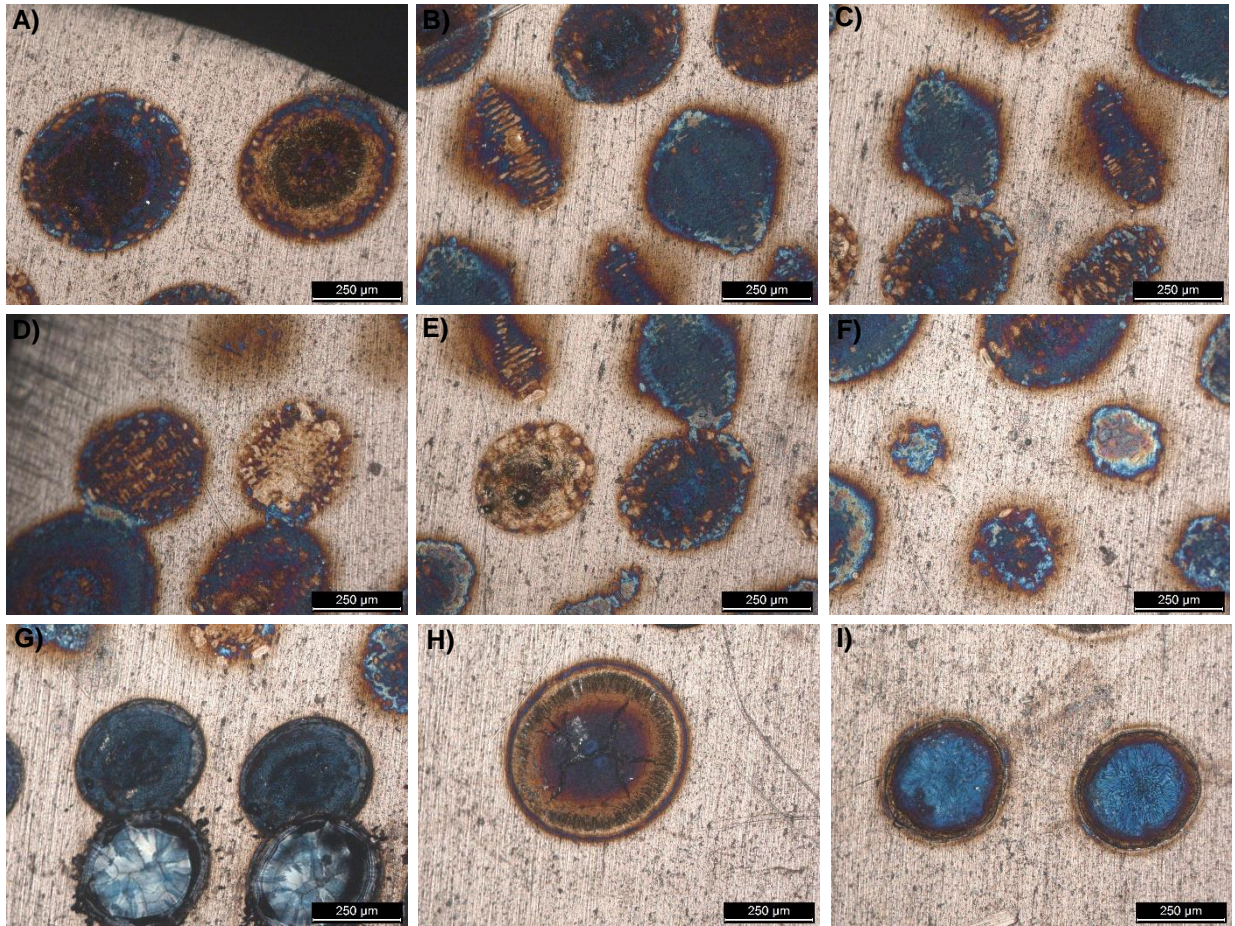


Figure 4.11 – Optical micro graphs of titanium oxide pattern after laser irradiation.

The TiO_2 pattern (Figure 4.12) were performed by following the laser parameters described in Table 4.3. The oxide marks were round shaped and without any visible cracks. The oxide was blue with a fractal-like geometry. On the center of the circle, a depression was noticed. On the other hand, a lighter mark surrounds the seemingly thicker zone. The marks were not aligned along the surface since the sample positioning for each mark was manually carried out.

Table 4.3 – Laser parameters for surface treatment of Ti samples.

Power (%)	Point Time (ms)	Frequency (Hz)	Diameter (mm)	Passes	Pulse Type
3	0.9	5	0.3	1	20 section pulse shape mode

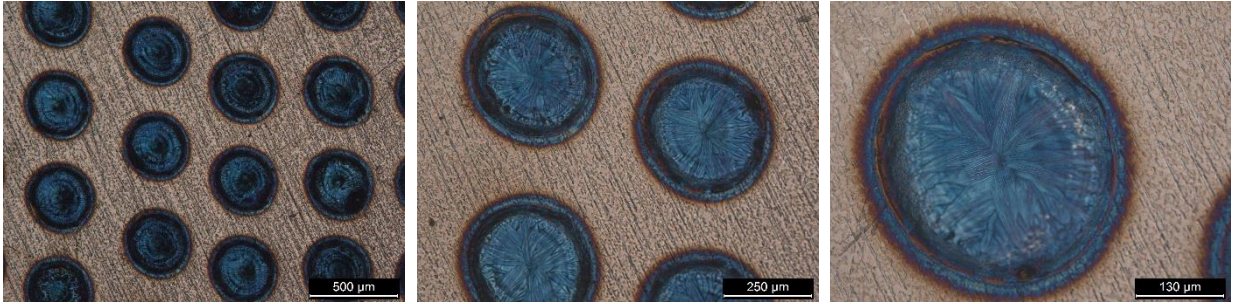


Figure 4.12 – Optical micrographs of the thick titanium dioxide pattern.

1.7. X-Ray Diffraction (XRD)

The XRD spectra is shown in Figure 4.13. The percentage of anatase (X_A) and rutile (X_R) phases was calculated according to the equations (16) and (17), where I_R represents the intensity of the rutile peak at $2\theta = 27.42^\circ$ and I_A represents the intensity of the anatase peak at $2\theta = 25.25^\circ$.

$$X_A = \frac{100}{\left(1 + 1.265 \times \frac{I_R}{I_A}\right)} \quad (16)$$

$$X_R = \frac{100}{\left(1 + 0.8 \times \frac{I_A}{I_R}\right)} \quad (17)$$

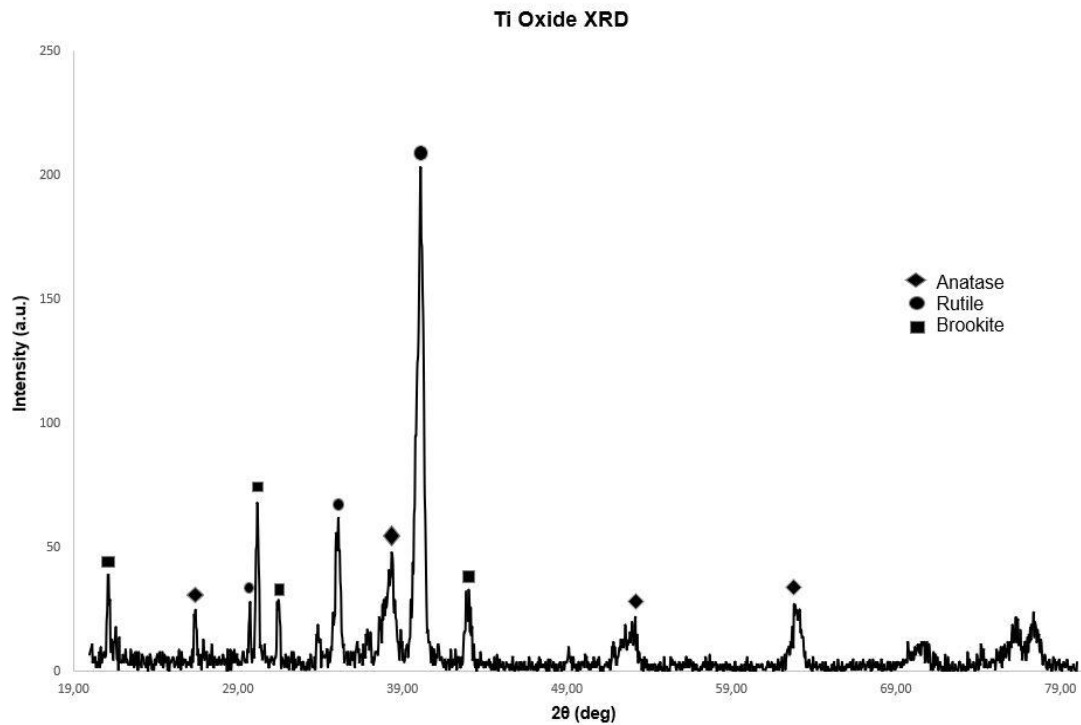


Figure 4.13 – X-Ray diffraction spectra of the samples with a pattern of thick titanium dioxide.

1.8. Wettability

The wettability of the samples was measured by the sessile drop method. The angle between the surface and the water drop was measured at two set points. The first measurement was performed at the moment the drop contacted the surface and the second measurement was recorded after 15 s. The mean values of the measured water contact angle (WCA) are shown in Figure 4.14.

All the samples showed hydrophilic characteristics both the first and last measurements were inferior to 90° . The initial WCA mean values were around 20° and then drop to around 4° . Consequently, all the surfaces can be classified as hydrophilic.

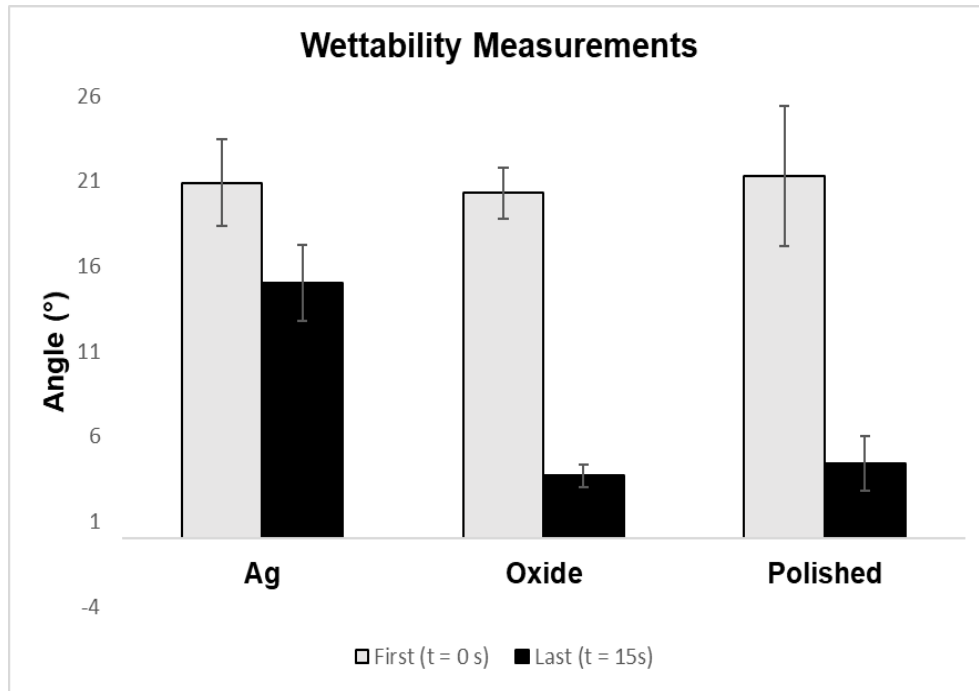


Figure 4.14 – Mean values of water contact angle measurements.

1.9. Roughness

The mean roughness values of those measurements are shown in Figure 4.15. The average roughness (Ra) of all the samples was higher than 0.2 μm . The values for the Ti-Ag samples were lower than those for the other samples.

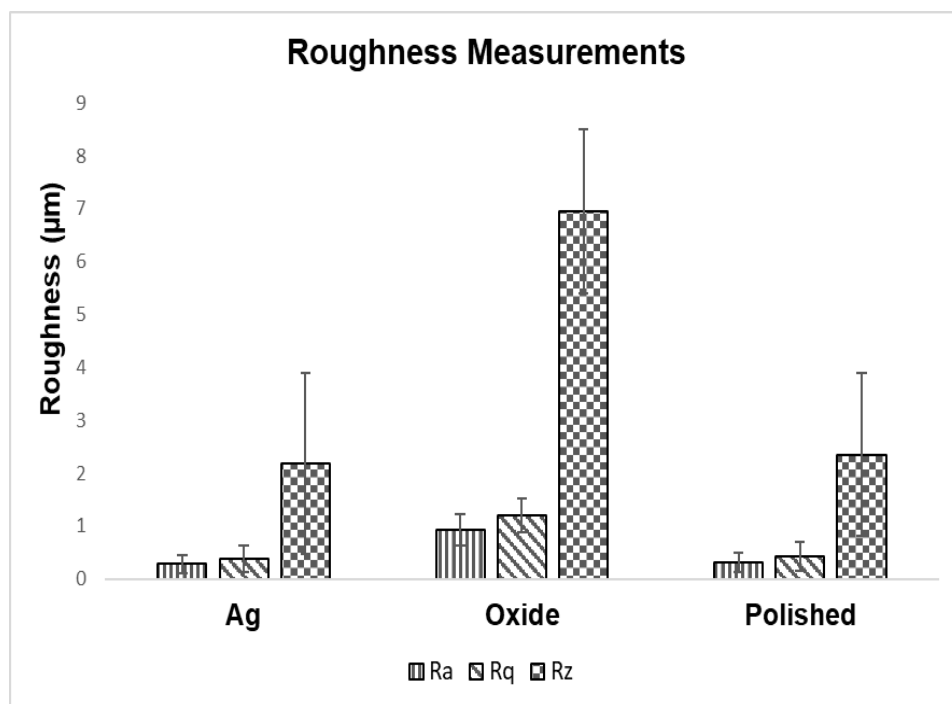


Figure 4.15 – Mean roughness values of each tested surface.

2. Microbiological tests

Microbiological assays were performed on the prepared samples to access their antibacterial properties.

2.1. Effect of titanium discs on bacterial biofilm

The influence of the titanium surfaces on bacterial adhesion was analyzed with qPCR and the results are presented in Figure 4.16. There was a significant reduction of the amount of *P. gingivalis* and *P. intermedia* on the titanium samples coated with silver in comparison with both positive and negative control. The effect was observed in both 24h culture and 72h culture and was more prominent on *P. intermedia*. The samples with different oxide thickness showed a similar values of bacteria as the negative control samples.

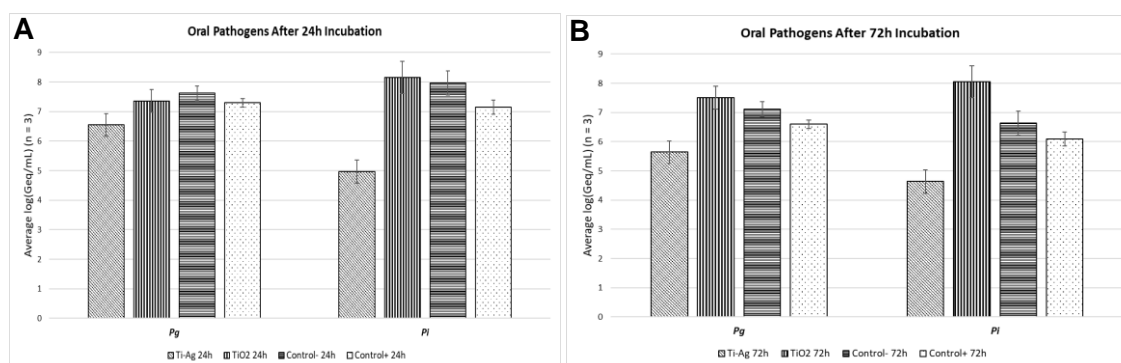


Figure 4.16 – Effect of surface treatment with silver and different oxide thickness on complex multi-species biofilms (mean \pm standard deviation, $n=3$). Negative control refers to polished titanium samples and positive control refers to polished titanium samples with and addition of chlorhexidine. (A) and (B) represent the concentration of *P. gingivalis* (Pg) and *P. intermedia* (Pi) after 24h and 72h of culture in anaerobic conditions in contact with titanium samples. Data are expressed as $\text{Log}_{10}\text{Geq/mL}$.

2.2. Effect of titanium discs on bacterial proliferation

In order to verify the behavior of the attached bacteria on the surfaces, these were observed by SEM after 24h and 72h of incubation. Samples coated with silver showed some bacterial attachment in areas with titanium and in areas covered with silver as well, as observed in Figure 4.17 and Figure 4.18, (A). Nevertheless, no stable biofilm is visible on those surfaces in contrast to the

samples with a thicker oxide pattern and the polished surfaces, observed in Figure 4.17 and Figure 4.18, (B) and (C). On the positive control few bacteria are observed and, consequently, no dense biofilm is also observed in Figure 4.17 and Figure 4.18, (D)). However, some cracks are visible along the surface indicating some degree of corrosion. The silver samples show, therefore, more promising results than the positive control.

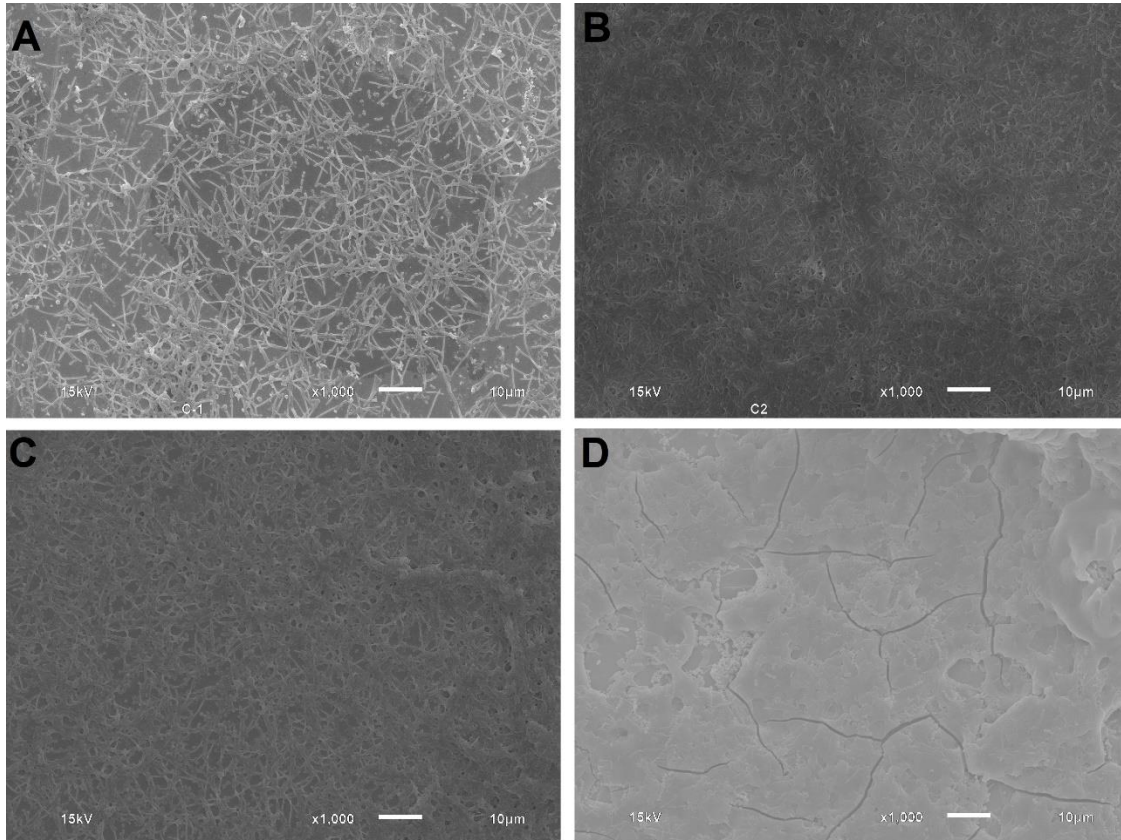


Figure 4.17 – Sample surface by SEM after being incubated with bacteria in anaerobic conditions for 24 hours. **A)** Titanium samples with sintered silver; **B)** Titanium samples with thick oxide pattern; **C)** Polished titanium samples; **D)** Polished titanium samples with chlorhexidine solution.

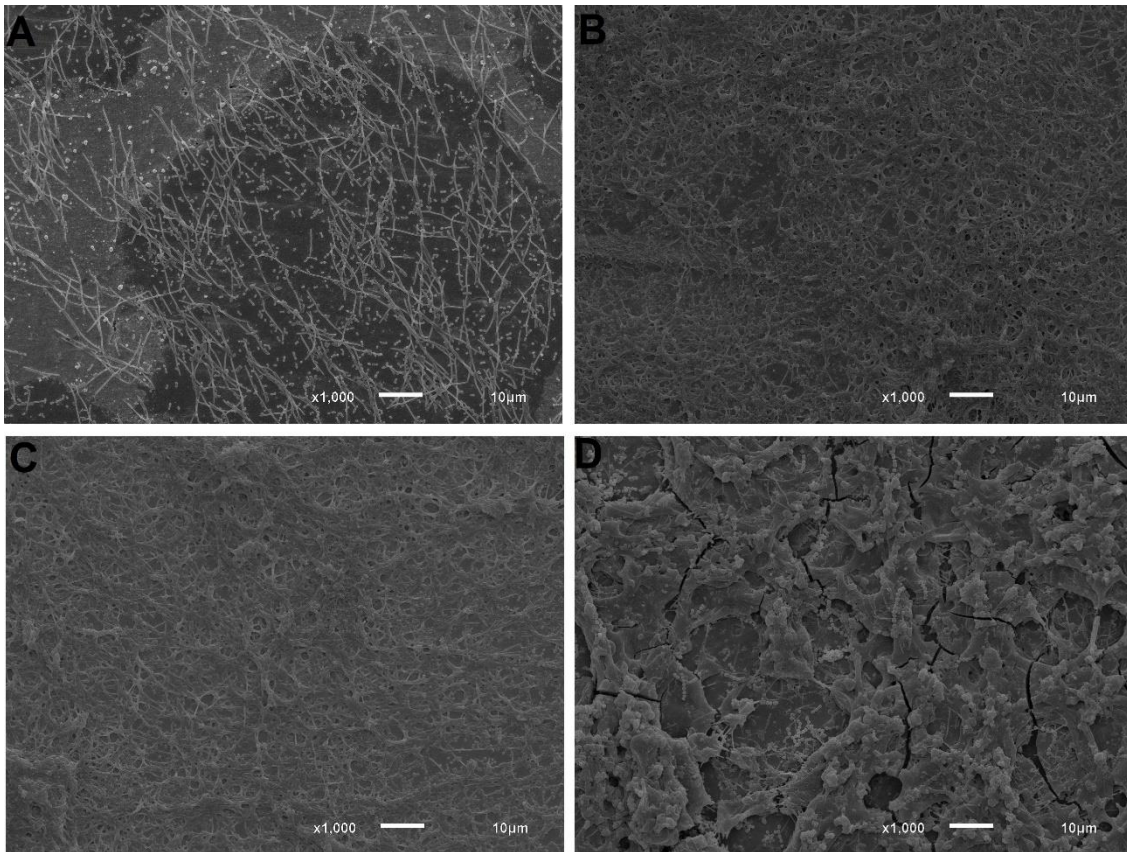


Figure 4.18 – Sample surface by SEM after being incubated with bacteria in anaerobic conditions for 72 hours. **A)** Titanium samples with sintered silver; **B)** Titanium samples with thick oxide pattern; **C)** Polished titanium samples; **D)** Polished titanium samples with chlorhexidine solution.

3. Discussion

In the present study, two different titanium surfaces were developed, and the respective antibacterial properties were tested. Titanium samples were patterned by laser technology and silver was incorporated on the surface of other samples. As expected, the microbial assays revealed an improvement of the antibacterial properties of the samples with silver relatively to the control samples. The patterned samples, in turn, did not showed improvements regarding the reduction of biofilms. Only one of the two surface treatments proposed in this study achieved the intended antibacterial properties.

Modifications of the titanium dioxide layer in dental implants have been studied and include mostly the modification of the crystalline structure, to produce micro or nanostructures over the surface. The use of laser technology

allowed for a better control of the portion of the surface to modify. The second pattern drawn revealed a more uniform and crystalline form than the first pattern. Therefore, it was the one used for the microbiological assays.

The incorporation of silver on titanium surfaces was already studied with a variety of techniques, the most common being plasma immersion ion implantation (PIII), pulsed filtered cathodic vacuum arc deposition, physical vapor deposition (PVD), magnetron sputtering [129,130]. Sintering with both laser and hot-pressing generated surfaces of titanium dioxide interleaved with silver. The results for both techniques were quite similar. Using the hot-pressing method, pressure and temperature were applied at the same time to the sample. Hence, less steps were involved in the process, decreasing the risk of surface contamination. Consequently, it was selected to prepare the samples for the biological assays.

Roughness and wettability are important characteristics regarding cell and bacterial adhesion. Studies verified that a certain degree of roughness stimulated the osteoblast adhesion since the contact area increases. Likewise, the bacterial adherence could also increase.[131–133] Surfaces with roughness (Ra) inferior to 0.2 μm showed no influence on the biofilm formation. The oxide samples were minimally rough [134] due to the grooves made by the laser. The samples with silver were smooth [134], similarly to the roughness of the control samples since the first were polished in order to remove the exceeding amount of silver. Moderately rough surfaces (1 – 2 μm) were indicated as the most advantageous for dental implants [4,135].

The wettability of a surface influences the interaction of proteins with the surface. Hydrophobic surfaces seemingly slow down protein adsorption while hydrophilic surfaces promote the adsorption. Consequently, hydrophilic surfaces are reported as better to improve cell adhesion and proliferation. [130,135–137] All the tested surfaces revealed a hydrophilic behavior since the water contact angle formed was around 20°. After 15 s the contact angle diminished greatly for the oxide and polished samples reaching values bellow 5°. The superhydrophilic behavior was reported as a disadvantage regarding the protein adsorption [43]. The water contact angle of most studies with cpTi varies between 50° to 85° [135,137,138].

Titanium oxide can acquire three different forms, brookite, rutile and anatase, being the last two the most common forms [139,140]. The samples with the titanium dioxide pattern present a greater percentage of rutile than of anatase. The later was reported as an enhancer for osteoblast proliferation [141]. The rutile form is also more chemically stable [142] which could have diminished the electronic shifts expected for antibacterial activity.

The attachment and growth of bacteria present in the oral cavity and bacteria associated with peri-implantitis on two novel titanium surfaces was evaluated on the present study. A significant reduction of the species *P. gingivalis* and *P. intermedia* was verified on the Ti surfaces with silver, as well as a general reduction of the biofilm. Silver ions can interact with thiol groups (-SH) of bacterial respiratory and transport proteins, disrupting their functioning and, consequently, the ATP production [41,143,144]. Silver ions can also induce morphological and physiological alteration in bacterial cells, that lead to cytoplasm leakage and DNA condensation [4,41,86].

Another bactericidal mechanism of silver particles is the generation of reactive oxygen species (ROS), as OH^- , O_2^- and H_2O_2 , in the presence of oxygen, which can also result from the interaction with membrane proteins [143,144]. ROS are usually a subproduct of cellular respiration and, consequently, properly eliminated by cellular mechanisms. Interactions with silver lead to a shift in the electron flux, subsequently increasing the ROS production. In high amount, ROS can affect bacterial cells by inducing extracellular oxidation, membrane potential variation and the release of the cellular contents.[72] Since the experiments were conducted in an anaerobic environment, the bactericidal effect of silver could be less prominent and therefore only significantly affecting the adhesion of *P. gingivalis* and *P. intermedia*.

The disruptions caused on the bacteria can also be due to the micro-galvanic couple that is formed between titanium and silver. In an aquatic environment, silver acts as a cathode and titanium as an anode, interacting through proton consuming reactions. Consequently, proton depleted regions accumulate on the titanium oxide, disrupting the electrochemical gradient amid the intermembrane space of the bacteria and the external medium. Electron

transference is the basis for the cellular respiration, therefore disruptions on the electrochemical balance can cause the impairment of ATP production.[73,80]

P. gingivalis and *P. intermedia* are two of the most common species found in reports associated with periodontal infections [39,41,132,143,145–147]. The first bacteria colonizing the implant surface are called early colonizers and includes species like *S. gordonii*, *S. oralis*, *S. sanguinis* and *S. mitis* [32,33]. These commensal bacteria interact with each other and coaggregate but not with other bacteria. *P. gingivalis* is one of the secondary colonizers that can coaggregate with primary colonizers, allowing other pathogenic bacteria to also coaggregate and contribute to the biofilm formation [32]. Consequently, the reduction of the biofilm observed by microscopy between the silver samples and the negative control might also be due to the reduction of *P. gingivalis*, which in turn leads to the diminish of interactions between early and secondary colonizers.

The different thickness of titanium dioxide was expected to promote electron transference between the two oxides, which would lead to the disturbance of the electronic pathway of the bacterial cells. Nevertheless, most of the formed oxide was in the rutile form and the antibacterial effect of titanium is associated with the anatase form [4,140,148]. The amount of bacteria present in the oxide samples was similar to that of the negative control and a well-developed biofilm was also present on the surface. Consequently, these results show that the rutile phase is not enough to provoke changes in the electronic gradient that could affect bacteria from the oral cavity.

Chlorhexidine (CHX) was used as a positive control since it is a wide used antiseptic in odontology, being present even in mouthwashes [149,150]. Though the total of bacteria was in fact reduced by CHX, some cracks were visible on the surface of the samples. Subsequently, the usage of CHX in high amounts can lead to a faster corrosion and wear of the titanium implants.

To complement the obtained results, upcoming studies should assess the biocompatibility and osteoblast adhesion and proliferation on the tested surfaces. The ion release of the samples with silver should also be investigated, for a better understanding of the antibacterial mechanism.

Chapter 5 – FINAL REMARKS

Chapter V presents the main conclusions of the present work and suggestions for posterior works.

1. Conclusions

In the present work novel ways of treat the titanium surface of dental implants using nanosecond Q-Switching lasers Nd:YAG were explored. The main purpose was to create surfaces with some degree of antibacterial activity to prevent peri-implantitis. After the processing, characterization and analysis of the proposed surfaces, the following conclusions were obtained.

- ⇒ The incorporation of silver particles on a titanium surface can be successfully achieved by laser and hot-pressing techniques. The surfaces presented a consistent layer of titanium and silver interleaved, without fractures nor gaps.
- ⇒ Even though the silver was sintered, the samples exhibited antibacterial properties, reducing the biofilm formation and the adhesion of two pathogenic bacteria, *Porphyromonas gingivalis* and *Prevotella intermedia*. Consequently, the antibacterial effects are possibly due to the shift of electrons between titanium and silver or from the release of silver ions.
- ⇒ The different thickness of titanium dioxide did not show any improvement of the antibacterial properties of the titanium surface, possibly due to the chemical stability of the titanium dioxide in rutile phase.
- ⇒ The roughness of the silver samples was similar to the polished samples, while the oxide samples were rougher. This could have contributed to the differences in the antibacterial properties.
- ⇒ All the samples showed hydrophilic characteristics. Consequently, those characteristics did not seem have a greater influence on the antibacterial properties noticed on the samples.

2. Future Work

Considering the results and conclusions obtained in the course of the present work, the following studies are proposed.

- Some characteristics of the samples with silver need to be optimized. For instance, different titanium patterns could be tested to obtain better properties using the minimal amount of silver
- The release of silver ions could also be tested to verify if the values are below the cytotoxic values. Cytocompatibility assays could also be performed as well as the co-culture of osteoblasts and bacteria on the surfaces with sintered silver.
- The titanium dioxide of the samples was mainly in the rutile phase. Further studies should be made to obtain a greater percentage of anatase phase on the surface. Different degrees of oxide thickness and phase might be needed to achieve antibacterial effects similar to the samples with sintered silver.
- Considering the concerns of silver accumulation in other locations of the body, the incorporation of other antibacterial substances using the same laser or hot-pressing techniques could also be of interest.

BIBLIOGRAPHY

- [1] R.G. Rozier, A. White, G. Slade, Trends in Oral Diseases in the U.S. Population, *J. Dent. Educ.* 81 (2017) e97–e109. doi:10.21815/JDE.017.016.
- [2] N.J. Kassebaum, E. Bernabé, M. Dahiya, B. Bhandari, C.J.L. Murray, W. Marcenes, Global Burden of Severe Tooth Loss : A Systematic Review and Meta-analysis, *JDR Clinical Res. Suppl.* 93 (2014) 20s–28s. doi:10.1177/0022034514537828.
- [3] A.D. Pye, D.E.A. Lockhart, M.P. Dawson, C.A. Murray, A.J. Smith, A review of dental implants and infection, *J. Hosp. Infect.* 72 (2009) 104–110. doi:10.1016/j.jhin.2009.02.010.
- [4] A. Han, J.K.H. Tsoi, F.P. Rodrigues, J.G. Leprince, W.M. Palin, Bacterial adhesion mechanisms on dental implant surfaces and the influencing factors, *Int. J. Adhes. Adhes.* 69 (2016) 58–71. doi:10.1016/j.ijadhadh.2016.03.022.
- [5] P.A. Norowski, J.D. Bumgardner, Biomaterial and antibiotic strategies for peri-implantitis, *J. Biomed. Mater. Res. - Part B Appl. Biomater.* 88 (2009) 530–543. doi:10.1002/jbm.b.31152.
- [6] C.T. Lee, Y.W. Huang, L. Zhu, R. Weltman, Prevalences of peri-implantitis and peri-implant mucositis: systematic review and meta-analysis, *J. Dent.* 62 (2017) 1–12. doi:10.1016/j.jdent.2017.04.011.
- [7] D. Mayrand, D. Grenier, Bacterial interactions in periodontal diseases, *Bull. Inst. Pasteur.* 96 (1998) 125–133. doi:10.1016/S0020-2452(98)80006-7.
- [8] J. Derks, C. Tomasi, Peri-implant health and disease. A systematic review of current epidemiology, *J. Clin. Periodontol.* 42 (2015) S158–S171. doi:10.1111/jcpe.12334.
- [9] L.J.A. Heitz-Mayfield, N.P. Lang, Comparative biology of chronic and aggressive periodontitis vs. peri-implantitis, *Int. J. Genomic Med.* 02 (2014) 1–4. doi:10.4172/2332-0672.1000116.
- [10] S. Ferraris, S. Spriano, Antibacterial titanium surfaces for medical implants, *Mater. Sci. Eng. C.* 61 (2016) 965–978. doi:10.1016/j.msec.2015.12.062.
- [11] A. Jemat, M.J. Ghazali, M. Razali, Y. Otsuka, Surface modifications and their effects on titanium dental implants, *Biomed Res. Int.* 2015 (2015). doi:10.1155/2015/791725.
- [12] R. Vilar, A. Almeida, Laser surface treatment of biomedical alloys, Elsevier Ltd, 2016. doi:10.1016/B978-0-08-100883-6.00002-2.
- [13] B. Del Curto, M.F. Brunella, C. Giordano, M.P. Pedefferri, V. Valtulina, L. Visai, A. Cigada, Decreased bacterial adhesion to surface-treated titanium, *Int. J. Artif. Organs.* 28 (2005) 718–730. doi:10.1177/039139880502800711.
- [14] G. Byrne, *Fundamentals of Implant Dentistry*, 2014. doi:10.1017/CBO9781107415324.004.
- [15] L. Le Guéhennec, A. Soueidan, P. Layrolle, Y. Amouriq, Surface treatments of titanium dental implants for rapid osseointegration, *Dent. Mater.* 23 (2007) 844–854. doi:10.1016/j.dental.2006.06.025.
- [16] J. Hasan, R.J. Crawford, E.P. Ivanova, Antibacterial surfaces : the quest for a new generation of biomaterials, *Trends Biotechnol.* (2012) 1–10.

doi:10.1016/j.tibtech.2013.01.017.

- [17] S. Prasad, M. Ehrensberger, M.P. Gibson, H. Kim, E.A. Monaco, Biomaterial properties of titanium in dentistry, *J. Oral Biosci.* 57 (2015) 192–199. doi:10.1016/j.job.2015.08.001.
- [18] M. Andrei, A. Dinischiotu, A.C. Didilescu, D. Ionita, I. Demetrescu, Periodontal materials and cell biology for guided tissue and bone regeneration, *Ann. Anat.* 216 (2018) 164–169. doi:10.1016/j.aanat.2017.11.007.
- [19] M. McCracken, Dental Implant Materials : Commercially Pure Titanium and Titanium Alloys, *Ann. Biomed. Eng.* 8 (1999) 40–43.
- [20] A.L. Stepanov, X. Xiao, F. Ren, Implantation of titanium dioxide with transition metal ions, *Titan. Dioxide Appl. Synth. Toxic.* (2013).
- [21] U. Diebold, The surface science of titanium dioxide, *Surf. Sci. Rep.* 48 (2003) 53–229. doi:10.1016/S0167-5729(02)00100-0.
- [22] E. Britannica, Hexagonal close-packed structure, (n.d.). <https://www.britannica.com/science/hexagonal-close-packed-structure>.
- [23] The Editors of Encyclopaedia Britannica, Optical crystallography, (n.d.). <https://www.britannica.com/science/optical-crystallography>.
- [24] Z. Liu, Y.G. Andreev, A. Robert Armstrong, S. Brutti, Y. Ren, P.G. Bruce, Nanostructured TiO₂(B): the effect of size and shape on anode properties for Li-ion batteries, *Prog. Nat. Sci. Mater. Int.* 23 (2013) 235–244. doi:10.1016/j.pnsc.2013.05.001.
- [25] D. Brown, J.F. McCabe, R.L. Clarke, J. Nicholson, R. Curtis, M. Sherriff, P. V Hatton, R. Strang, A.J. Ireland, D.C. Watts, Dental materials: 1997 literature review., *J. Dent.* 23 (1995) 67–93.
- [26] A.E.S. El Askary, *Fundamentals of Esthetic Implant Dentistry*, 2008. doi:10.1002/9780470376423.
- [27] What Are Dental Implants, (n.d.). http://www.1888implant.com/mobile/dental_implants.html.
- [28] Dental Implants: How They Work & What They Are Made Of, (n.d.). <https://www.toothwisdom.org/a-z/article/dental-implants-are-not-created-equal/>.
- [29] O. Habimana, A.J.C. Semião, E. Casey, The role of cell-surface interactions in bacterial initial adhesion and consequent biofilm formation on nanofiltration/reverse osmosis membranes, *J. Memb. Sci.* 454 (2014) 82–96. doi:10.1016/j.memsci.2013.11.043.
- [30] W. Teughels, N. Assche, I. Sliepen, M. Quirynen, Effect of Material Characteristics and/or Surface Topography on Biofilm Development, *Clin. Oral Implants Res.* 17 Suppl 2 (2006) 68–81. doi:10.1111/j.1600-0501.2006.01353.x.
- [31] L.L. B. Derjaguin, Theory of the stability of strongly charged lyophobic sols and of the adhesion of strongly charged particles in solutions of electrolytes, *Acta Phys. Chim.* (n.d.) 633–662. doi:10.1016/0079-6816(93)90013-L.
- [32] A.H. Rickard, P. Gilbert, N.J. High, P.E. Kolenbrander, P.S. Handley, Bacterial coaggregation: An integral process in the development of multi-species biofilms, *Trends Microbiol.* 11 (2003) 94–100. doi:10.1016/S0966-842X(02)00034-3.
- [33] R.S. Preethanath, N.W. AlNahas, S.M. Bin Huraib, H.O. Al-Balbeesi, N.K. Almalik, M.H.N.

- Dalati, D.D. Divakar, Microbiome of dental implants and its clinical aspect, *Microb. Pathog.* 106 (2017) 20–24. doi:10.1016/j.micpath.2017.02.009.
- [34] P.E. Kolenbrander, R.J. Palmer, S. Periasamy, N.S. Jakubovics, Oral multispecies biofilm development and the key role of cell-cell distance, *Nat. Rev. Microbiol.* 8 (2010) 471–480. doi:10.1038/nrmicro2381.
- [35] J. Neilands, C. Wickström, B. Kinnby, J.R. Davies, J. Hall, B. Friberg, G. Svensäter, Bacterial profiles and proteolytic activity in peri-implantitis versus healthy sites, *Anaerobe.* 35 (2015) 28–34. doi:10.1016/j.anaerobe.2015.04.004.
- [36] E.S. Ogawa, A.O. Matos, T. Beline, I.S.V. Marques, C. Sukotjo, M.T. Mathew, E.C. Rangel, N.C. Cruz, M.F. Mesquita, R.X. Consani, V.A.R. Barão, Surface-treated commercially pure titanium for biomedical applications: Electrochemical, structural, mechanical and chemical characterizations, *Mater. Sci. Eng. C.* 65 (2016) 251–261. doi:10.1016/j.msec.2016.04.036.
- [37] L. Sbordone, C. Bortolaia, Oral microbial biofilms and plaque-related diseases: microbial communities and their role in the shift from oral health to disease., *Clin. Oral Investig.* 7 (2003) 181–188. doi:10.1007/s00784-003-0236-1.
- [38] M. Costalonga, M.C. Herzberg, The oral microbiome and the immunobiology of periodontal disease and caries, *Immunol. Lett.* 162 (2014) 22–38. doi:10.1016/j.imlet.2014.08.017.
- [39] M. Hultin, A. Gustafsson, H. Hallström, L.Å. Johansson, A. Ekfeldt, B. Klinge, Microbiological findings and host response in patients with periimplantitis, *Clin. Oral Implants Res.* 13 (2002) 349–358. doi:10.1034/j.1600-0501.2002.130402.x.
- [40] S. Sridhar, F. Wang, T.G. Wilson, P. Valderrama, K. Palmer, D.C. Rodrigues, Multifaceted roles of environmental factors toward dental implant performance: Observations from clinical retrievals and in vitro testing, *Dent. Mater.* (2018) 1–15. doi:10.1016/j.dental.2018.08.299.
- [41] O.M. Goudouri, E. Kontonasaki, U. Lohbauer, A.R. Boccaccini, Antibacterial properties of metal and metalloid ions in chronic periodontitis and peri-implantitis therapy, *Acta Biomater.* 10 (2014) 3795–3810. doi:10.1016/j.actbio.2014.03.028.
- [42] M.A. Atieh, N.H.M. Alsabeeha, C.M. Faggion, W.J. Duncan, The Frequency of Peri-Implant Diseases: A Systematic Review and Meta-Analysis, *J. Periodontol.* 84 (2012) 1–15. doi:10.1902/jop.2012.120592.
- [43] F. Rupp, L. Liang, J. Geis-Gerstorfer, L. Scheideler, F. Hüttig, Surface characteristics of dental implants: A review, *Dent. Mater.* 34 (2018) 40–57. doi:10.1016/j.dental.2017.09.007.
- [44] A. Simchi, E. Tamjid, F. Pishbin, A.R. Boccaccini, Recent progress in inorganic and composite coatings with bactericidal capability for orthopaedic applications, *Nanomedicine Nanotechnology, Biol. Med.* 7 (2011) 22–39. doi:10.1016/j.nano.2010.10.005.
- [45] Lasers in minimally invasive periodontal and peri-implant therapy, *71* (2016) 185–212.
- [46] R.A. Valério, V.S. Cunha, R. Galo, F.A. De Lima, L. Bachmann, S.A.M. Corona, M.C. Borsatto, Influence of the Nd : YAG Laser Pulse Duration on the Temperature of Primary Enamel, 2015 (2015).

- [47] M. Vassalli, L. Polidori, Neodymium : yttrium aluminum garnet laser irradiation with low pulse energy : a potential tool for the treatment of peri-implant disease, (2002) 638–643. doi:10.1111/j.1600-0501.2006.01278.x.
- [48] C.M. Abraham, A Brief Historical Perspective on Dental Implants , Their Surface Coatings and Treatments, (2014) 50–55.
- [49] T. Min, Design and Fabrication of Super-Hydrophobic Surfaces By Laser Micro/Nano-Processing, (2012) 142.
- [50] D. Quéré, Wetting and Roughness, *Annu. Rev. Mater. Res.* 38 (2008) 71–99. doi:10.1146/annurev.matsci.38.060407.132434.
- [51] K.L. Mittal, T. Bahners, eds., *Laser Surface Modification and Adhesion*, wiley, 2015.
- [52] G. Chryssolouris, *Mechanical Engineering Series - Laser Machining Theory and Practice*, Springer Science + Business Media, LLC, 1985.
- [53] R. Paschotta, YAG laser, *RP Photonics Encycl.* (2015). https://www.rp-photonics.com/q_switching.html (accessed October 15, 2018).
- [54] J.C. Ion, *Laser Processing of Engineering Materials - principles, procedure and industrial application*, Elsevier, 2005.
- [55] R. Paschotta, Q Switching, *RP Photonics Encycl.* (2015). https://www.rp-photonics.com/q_switching.html (accessed October 15, 2018).
- [56] L.M. Vilhena, M. Sedlaček, B. Podgornik, J. Vižintin, A. Babnik, J. Možina, Surface texturing by pulsed Nd:YAG laser, *Tribol. Int.* 42 (2009) 1496–1504. doi:10.1016/j.triboint.2009.06.003.
- [57] P. Maressa, L. Anodio, A. Bernasconi, A.G. Demir, B. Previtali, Effect of surface texture on the adhesion performance of laser treated Ti6Al4V alloy, *J. Adhes.* 91 (2014) 518–537. doi:10.1080/00218464.2014.933809.
- [58] R.S. Faeda, H.S. Tavares, R. Sartori, A.C. Guastaldi, E. Marcantonio Jr., Evaluation of titanium implants with surface modification by laser beam: biomechanical study in rabbit tibias, *Braz. Oral Res.* 23 (2009) 137–143. doi:10.1590/S1806-83242009000200008.
- [59] C.N. Elias, L. Meirelles, Improving osseointegration of dental implants, 7 (2010) 241–256. doi:10.1586/erd.09.74.
- [60] N. Ohtsu, T. Kozuka, M. Yamane, H. Arai, Surface chemistry and osteoblast-like cell response on a titanium surface modified by a focused Nd:YAG laser, *Surf. Coatings Technol.* 309 (2017) 220–226. doi:10.1016/j.surfcoat.2016.10.024.
- [61] J. Lawrence, L. Hao, H.R. Chew, On the correlation between Nd : YAG laser-induced wettability characteristics modification and osteoblast cell bioactivity on a titanium alloy, 200 (2006) 5581–5589. doi:10.1016/j.surfcoat.2005.07.107.
- [62] C. Hallgren, H. Reimers, D. Chakarov, J. Gold, A. Wennerberg, An in vivo study of bone response to implants topographically modified by laser micromachining, *Biomaterials.* 24 (2003) 701–710. doi:10.1016/S0142-9612(02)00266-1.
- [63] R. Brånemark, L. Emanuelsson, A. Palmquist, P. Thomsen, Bone response to laser-induced micro- and nano-size titanium surface features, *Nanomedicine Nanotechnology, Biol. Med.* 7 (2011) 220–227. doi:10.1016/j.nano.2010.10.006.

- [64] M.D. Paz, J.I. Álava, L. Goikoetxea, S. Chiussi, I. Díaz-Güemes, J. Usón, F. Sánchez, B. León, Biological response of laser macrostructured and oxidized titanium alloy: An in vitro and in vivo study, *J. Appl. Biomater. Biomech.* 9 (2011) 214–222. doi:10.5301/JABB.2011.8923.
- [65] M. Di Giulio, A. Nostro, *Porphyromonas gingivalis* biofilm formation in different titanium surfaces, an in vitro study, (2015) 1–8. doi:10.1111/clr.12659.
- [66] L. Drago, M. Bortolin, E. De Vecchi, S. Agrappi, L. Roberto, R. Mattina, L. Francetti, L. Drago, M. Bortolin, E. De Vecchi, S. Agrappi, L. Drago, M. Bortolin, E. De Vecchi, S. Agrappi, R.L. Weinstein, R. Mattina, L. Francetti, Antibiofilm activity of sandblasted and laser- isolated from peri-implantitis lesions Antibiofilm activity of sandblasted and laser-modified titanium against microorganisms isolated from peri-implantitis lesions, 9478 (2016). doi:10.1080/1120009X.2016.1158489.
- [67] B. Grossner-Schreiber, M. Griepentrog, I. Haustein, W.D. Muller, K.P. Lange, H. Briedigkeit, U.B. Gobel, Plaque formation on surface modified dental implants. An in vitro study., *Clin. Oral Implants Res.* 12 (2001) 543–551.
- [68] A.C. Chan, L. Carson, G.C. Smith, A. Morelli, S. Lee, Enhancing the antibacterial performance of orthopaedic implant materials by fibre laser surface engineering, *Appl. Surf. Sci.* (2017). doi:10.1016/j.apsusc.2017.01.233.
- [69] R.S. Faeda, H.S. Tavares, Biological Performance of Chemical Hydroxyapatite Coating Associated With Implant Surface Modification by Laser Beam : Biomechanical Study in Rabbit Tibias, *YJOMS.* 67 (2009) 1706–1715. doi:10.1016/j.joms.2009.03.046.
- [70] R.S. Faeda, R. Spin-Neto, E. Marcantonio, A.C. Guastaldi, E. Marcantonio, Laser ablation in titanium implants followed by biomimetic hydroxyapatite coating: Histomorphometric study in rabbits, *Microsc. Res. Tech.* 75 (2012) 940–948. doi:10.1002/jemt.22018.
- [71] M. Boutinguiza, M. Fernández-arias, J. Val, J. Buxadera-palomero, D. Rodríguez, F. Lusquiños, F.J. Gil, J. Pou, Synthesis and deposition of silver nanoparticles on cp Ti by laser ablation in open air for antibacterial effect in dental implants, *Mater. Lett.* 231 (2018) 126–129. doi:10.1016/j.matlet.2018.07.134.
- [72] G. Wang, W. Jin, A.M. Qasim, A. Gao, X. Peng, W. Li, H. Feng, P.K. Chu, Antibacterial effects of titanium embedded with silver nanoparticles based on electron-transfer-induced reactive oxygen species, *Biomaterials.* 124 (2017) 25–34. doi:10.1016/j.biomaterials.2017.01.028.
- [73] H. Cao, X. Liu, F. Meng, P.K. Chu, Biological actions of silver nanoparticles embedded in titanium controlled by micro-galvanic effects, *Biomaterials.* 32 (2011) 693–705. doi:10.1016/j.biomaterials.2010.09.066.
- [74] Y. Yu, G. Jin, Y. Xue, D. Wang, X. Liu, J. Sun, Multifunctions of dual Zn/Mg ion co-implanted titanium on osteogenesis, angiogenesis and bacteria inhibition for dental implants, *Acta Biomater.* 49 (2017) 590–603. doi:10.1016/j.actbio.2016.11.067.
- [75] E. Zhang, J. Ren, S. Li, L. Yang, G. Qin, Optimization of mechanical properties, biocorrosion properties and antibacterial properties of as-cast Ti-Cu alloys, *Biomed. Mater.* 11 (2016) 65001. doi:10.1088/1748-6041/11/6/065001.
- [76] G. Jin, H. Cao, Y. Qiao, F. Meng, H. Zhu, X. Liu, Osteogenic activity and antibacterial effect of zinc ion implanted titanium, *Colloids Surfaces B Biointerfaces.* 117 (2014) 158–

165. doi:10.1016/j.colsurfb.2014.02.025.
- [77] G. Jin, H. Qin, H. Cao, S. Qian, Y. Zhao, X. Peng, X. Zhang, X. Liu, P.K. Chu, Synergistic effects of dual Zn/Ag ion implantation in osteogenic activity and antibacterial ability of titanium, *Biomaterials*. 35 (2014) 7699–7713. doi:10.1016/j.biomaterials.2014.05.074.
- [78] G. Jin, H. Qin, H. Cao, Y. Qiao, Y. Zhao, X. Peng, X. Zhang, X. Liu, P.K. Chu, Zn/Ag micro-galvanic couples formed on titanium and osseointegration effects in the presence of *S.aureus*, *Biomaterials*. 65 (2015) 22–31. doi:10.1016/j.biomaterials.2015.06.040.
- [79] T. Yang, S. Qian, Y. Qiao, X. Liu, Cytocompatibility and antibacterial activity of titania nanotubes incorporated with gold nanoparticles, *Colloids Surfaces B Biointerfaces*. 145 (2016) 597–606. doi:10.1016/j.colsurfb.2016.05.073.
- [80] H. Cao, Y. Qiao, X. Liu, T. Lu, T. Cui, F. Meng, P.K. Chu, Electron storage mediated dark antibacterial action of bound silver nanoparticles: Smaller is not always better, *Acta Biomater*. 9 (2013) 5100–5110. doi:10.1016/j.actbio.2012.10.017.
- [81] J. Li, Y. Qiao, Z. Ding, X. Liu, Microstructure and properties of Ag/N dual ions implanted titanium, *Surf. Coatings Technol*. 205 (2011) 5430–5436. doi:10.1016/j.surfcoat.2011.06.006.
- [82] J. Li, H. Zhou, S. Qian, Z. Liu, J. Feng, P. Jin, X. Liu, Plasmonic gold nanoparticles modified titania nanotubes for antibacterial application, *Appl. Phys. Lett*. 104 (2014). doi:10.1063/1.4885401.
- [83] C.N. Lok, C.M. Ho, R. Chen, Q.Y. He, W.Y. Yu, H. Sun, P.K.H. Tam, J.F. Chiu, C.M. Che, Proteomic analysis of the mode of antibacterial action of silver nanoparticles, *J. Proteome Res*. 5 (2006) 916–924. doi:10.1021/pr0504079.
- [84] A. Ivask, A. Elbadawy, C. Kaweeteerawat, D. Boren, H. Fischer, Z. Ji, C.H. Chang, R. Liu, T. Tolaymat, D. Telesca, J.I. Zink, Y. Cohen, P.A. Holden, H.A. Godwin, Toxicity mechanisms in *Escherichia coli* vary for silver nanoparticles and differ from ionic silver, *ACS Nano*. 8 (2014) 374–386. doi:10.1021/nn4044047.
- [85] H. Hu, W. Zhang, Y. Qiao, X. Jiang, X. Liu, C. Ding, Antibacterial activity and increased bone marrow stem cell functions of Zn-incorporated TiO₂ coatings on titanium, *Acta Biomater*. 8 (2012) 904–915. doi:10.1016/j.actbio.2011.09.031.
- [86] M. Chen, E. Zhang, L. Zhang, Microstructure, mechanical properties, bio-corrosion properties and antibacterial properties of Ti-Ag sintered alloys, *Mater. Sci. Eng. C*. 62 (2016) 350–360. doi:10.1016/j.msec.2016.01.081.
- [87] J.S. Möhler, W. Sim, M.A.T. Blaskovich, M.A. Cooper, Z.M. Ziora, Silver bullets: A new lustre on an old antimicrobial agent, *Biotechnol. Adv*. 36 (2018) 1391–1411. doi:10.1016/j.biotechadv.2018.05.004.
- [88] M.J.W. Charles W. Berry, Tera J. Moore, John A. Safar, Clay A. Henry, Antibacterial activity of dental implant metals.pdf, *Implant Dent*. 1 (1992).
- [89] A. Besinis, S.D. Hadi, H.R. Le, C. Tredwin, R.D. Handy, Antibacterial activity and biofilm inhibition by surface modified titanium alloy medical implants following application of silver, titanium dioxide and hydroxyapatite nanocoatings, *Nanotoxicology*. 11 (2017) 327–338. doi:10.1080/17435390.2017.1299890.
- [90] R.A. Bapat, T. V. Chaubal, C.P. Joshi, P.R. Bapat, H. Choudhury, M. Pandey, B. Gorain, P. Kesharwani, An overview of application of silver nanoparticles for biomaterials in

- dentistry, *Mater. Sci. Eng. C*. 91 (2018) 881–898. doi:10.1016/j.msec.2018.05.069.
- [91] S. Spriano, S. Yamaguchi, F. Baines, S. Ferraris, A critical review of multifunctional titanium surfaces: New frontiers for improving osseointegration and host response, avoiding bacteria contamination, *Acta Biomater.* 79 (2018) 1–22. doi:10.1016/j.actbio.2018.08.013.
- [92] J.A. Lemire, J.J. Harrison, R.J. Turner, Antimicrobial activity of metals mechanisms, molecular targets and applications, *Nat. Publ. Gr.* 11 (2013) 371–384. doi:10.1038/nrmicro3028.
- [93] B. Henriques, D. Soares, J.C. Teixeira, F.. Silva, Effect of hot pressing variables on the microstructure, relative density and hardness of sterling silver (Ag-Cu alloy) powder compacts, *Mater. Res.* 17 (2014) 664–671. doi:10.1590/S1516-14392014005000022.
- [94] P.W. Lee, *Powder Metal Technologies and Applications*, ASM International, 1998.
- [95] S.T. Mileiko, ed., *Hot Pressing*, in: *Met. Ceram. Based Compos.*, Elsevier, 1997: pp. 475–515.
- [96] M. Qian, F.H. Sam Froes, *Titanium powder metallurgy: Science, technology and applications*, 2015. doi:10.1016/C2013-0-13619-7.
- [97] H.H.. K.H.R.P.K.J. Hausner, ed., *New Methods for the Consolidation of Metal Powders – Volume 1*, Springer Science+Business Media, 1967. doi:10.1007/978-1-4899-6423-6.
- [98] V. Sarin, *Development of Hot Pressing as a Low Cost Processing Technique for Fuel Cell Fabrication*, (2003) 40. http://www.osti.gov/bridge/product.biblio.jsp?osti_id=885896.
- [99] H.H. Hausner, ed., *Modern Developments in Powder Metallurgy – Volume 3: Development and Future Prospects*, PLENUM PRESS, 1966.
- [100] J.M. Torralba, *Improvement of Mechanical and Physical Properties in Powder Metallurgy*, Elsevier, 2014. doi:10.1016/B978-0-08-096532-1.00316-2.
- [101] L.F. Francis, B.J.H. Stadler, C.C. Roberts, *Materials Processing – A Unified Approach to Processing of Metals, Ceramics and Polymers*, 1st ed., Elsevier, 2016.
- [102] R. German, *Sintering: From Empirical Observations to Scientific Principles*, 2014. doi:10.1016/C2012-0-00717-X.
- [103] W.B. James, H. Corporation, *Powder Metallurgy Methods and Applications*, ASM Handb. Vol. 7 *Powder Metall.* 7 (2015) 9–19(11). doi:10.1017/CBO9781107415324.004.
- [104] T. Leonhardt, N. Moore, J. Downs, M. Hamister, *Advances in powder metallurgy - Properties, processing and applications*, Woodhead Publishing Limited, 2001. doi:10.1016/0026-0657(92)91807-V.
- [105] Howard A. Kuhn, *Forging and Hot Pressing*, ASM Handbook, Vol. 7 *Powder Met. Technol. Appl.* (1998) 632–637. doi:10.1361/asmhba00015.
- [106] G.S. Upadhyaya, *Powder Metallurgy Technology*, 1st ed., Cambridge International Science Publishing, 2002.
- [107] B. Bai, E. Zhang, H. Dong, J. Liu, Biocompatibility of antibacterial Ti–Cu sintered alloy: in vivo bone response, *J. Mater. Sci. Mater. Med.* 26 (2015) 1–12. doi:10.1007/s10856-015-5600-6.
- [108] J. Liu, F. Li, C. Liu, H. Wang, B. Ren, K. Yang, E. Zhang, Effect of Cu content on the

- antibacterial activity of titanium-copper sintered alloys, *Mater. Sci. Eng. C.* 35 (2014) 392–400. doi:10.1016/j.msec.2013.11.028.
- [109] M. Chen, L. Yang, L. Zhang, Y. Han, Z. Lu, G. Qin, E. Zhang, Effect of nano/micro-Ag compound particles on the bio-corrosion, antibacterial properties and cell biocompatibility of Ti-Ag alloys, *Mater. Sci. Eng. C.* 75 (2017) 906–917. doi:10.1016/j.msec.2017.02.142.
- [110] B. Guan, H. Wang, R. Xu, G. Zheng, J. Yang, Z. Liu, M. Cao, M. Wu, J. Song, N. Li, T. Li, Q. Cai, X. Yang, Y. Li, X. Zhang, Establishing Antibacterial Multilayer Films on the Surface of Direct Metal Laser Sintered Titanium Primed with Phase-Transited Lysozyme, *Sci. Rep.* 6 (2016) 36408. doi:10.1038/srep36408.
- [111] M. Brama, N. Rhodes, J. Hunt, A. Ricci, R. Teghil, S. Migliaccio, C. Della Rocca, S. Leccisotti, A. Lioi, M. Scandurra, G. De Maria, D. Ferro, F. Pu, G. Panzini, L. Politi, R. Scandurra, Effect of titanium carbide coating on the osseointegration response in vitro and in vivo, *Biomaterials.* 28 (2007) 595–608. doi:10.1016/j.biomaterials.2006.08.018.
- [112] S.R. Paital, N.B. Dahotre, Calcium phosphate coatings for bio-implant applications: Materials, performance factors, and methodologies, *Mater. Sci. Eng. R Reports.* 66 (2009) 1–70. doi:10.1016/j.mser.2009.05.001.
- [113] T.P. Queiroz, R.S. de Molon, F.Á. Souza, R. Margonar, A.H.A. Thomazini, A.C. Guastaldi, E. Hochuli-Vieira, In vivo evaluation of cp Ti implants with modified surfaces by laser beam with and without hydroxyapatite chemical deposition and without and with thermal treatment: topographic characterization and histomorphometric analysis in rabbits, *Clin. Oral Investig.* 21 (2017) 685–699. doi:10.1007/s00784-016-1936-7.
- [114] M. Tlotleng, E. Akinlabi, M. Shukla, S. Pityana, Microstructures, hardness and bioactivity of hydroxyapatite coatings deposited by direct laser melting process, *Mater. Sci. Eng. C.* 43 (2014) 189–198. doi:10.1016/j.msec.2014.06.032.
- [115] C.-S. Chien, Y.-S. Ko, T.-Y. Kuo, T.-Y. Liao, T.-M. Lee, T.-F. Hong, Effect of TiO₂ addition on surface microstructure and bioactivity of fluorapatite coatings deposited using Nd:YAG laser, *Proc. Inst. Mech. Eng. Part H J. Eng. Med.* 228 (2014) 379–387. doi:10.1177/0954411914528307.
- [116] A. Hindy, F. Farahmand, F. sadat Tabatabaei, In vitro biological outcome of laser application for modification or processing of titanium dental implants, *Lasers Med. Sci.* 32 (2017) 1197–1206. doi:10.1007/s10103-017-2217-7.
- [117] X. Xu, Y. Lu, S. Li, S. Guo, M. He, K. Luo, J. Lin, Copper-modified Ti6Al4V alloy fabricated by selective laser melting with pro-angiogenic and anti-inflammatory properties for potential guided bone regeneration applications, *Mater. Sci. Eng. C.* 90 (2018) 198–210. doi:10.1016/j.msec.2018.04.046.
- [118] J. Luo, S. Guo, Y. Lu, X. Xu, C. Zhao, S. Wu, J. Lin, Materials Characterization Cytocompatibility of Cu-bearing Ti6Al4V alloys manufactured by selective laser melting, *Mater. Charact.* 143 (2018) 127–136. doi:10.1016/j.matchar.2017.12.003.
- [119] L. Liu, M. He, X. Xu, C. Zhao, Y. Gan, J. Lin, J. Luo, J. Lin, Preliminary study on the corrosion resistance, antibacterial activity and cytotoxicity of selective-laser-melted Ti6Al4V-xCu alloys, *Mater. Sci. Eng. C.* 72 (2017) 631–640. doi:10.1016/j.msec.2016.11.126.
- [120] X. Liu, H.C. Man, Laser fabrication of Ag-HA nanocomposites on Ti6Al4V implant for

- enhancing bioactivity and antibacterial capability, *Mater. Sci. Eng. C*. 70 (2017) 1–8. doi:10.1016/j.msec.2016.08.059.
- [121] B. Henriques, P. Ferreira, M. Buciumeanu, M. Fredel, A. Cabral, F.S. Silva, G. Miranda, Copper–nickel-based diamond cutting tools: stone cutting evaluation, *Int. J. Adv. Manuf. Technol.* 92 (2017) 1339–1348. doi:10.1007/s00170-017-0220-6.
- [122] M.E. Galarraga-Vinueza, B. Passoni, C.A.M. Benfatti, J. Mesquita-Guimarães, B. Henriques, R.S. Magini, M.C. Fredel, B. V. Meerbeek, W. Teughels, J.C.M. Souza, Inhibition of multi-species oral biofilm by bromide doped bioactive glass, *J. Biomed. Mater. Res. - Part A*. 105 (2017) 1994–2003. doi:10.1002/jbm.a.36056.
- [123] Z. Bai, M.J. Filiaggi, J.R. Dahn, Surface Science Fibrinogen adsorption onto 316L stainless steel, Nitinol and titanium, *Surf. Sci.* 603 (2009) 839–846. doi:10.1016/j.susc.2009.01.040.
- [124] E.R. Herrero, S. Fernandes, T. Verspecht, E. Ugarte-Berzal, N. Boon, P. Proost, K. Bernaerts, M. Quirynen, W. Teughels, Dysbiotic Biofilms Deregulate the Periodontal Inflammatory Response, *J. Dent. Res.* 97 (2018) 547–555. doi:10.1177/0022034517752675.
- [125] E.R. Herrero, V. Slomka, N. Boon, K. Bernaerts, E. Hernandez-Sanabria, M. Quirynen, W. Teughels, Dysbiosis by neutralizing commensal mediated inhibition of pathobionts, *Sci. Rep.* 6 (2016) 1–10. doi:10.1038/srep38179.
- [126] E.R. Herrero, V. Slomka, K. Bernaerts, N. Boon, E. Hernandez-Sanabria, B.B. Passoni, M. Quirynen, W. Teughels, Antimicrobial effects of commensal oral species are regulated by environmental factors, *J. Dent.* 47 (2016) 23–33. doi:10.1016/j.jdent.2016.02.007.
- [127] E.R. Herrero, N. Boon, K. Bernaerts, V. Slomka, T. Verspecht, M. Quirynen, W. Teughels, Clinical concentrations of peroxidases cause dysbiosis in in vitro oral biofilms, *J. Periodontol.* 53 (2018) 457–466. doi:10.1111/jre.12534.
- [128] E. Rodriguez Herrero, N. Boon, M. Pauwels, K. Bernaerts, V. Slomka, M. Quirynen, W. Teughels, Necrotrophic growth of periodontopathogens is a novel virulence factor in oral biofilms, *Sci. Rep.* 7 (2017) 1–10. doi:10.1038/s41598-017-01239-9.
- [129] L. Zhao, P.K. Chu, Y. Zhang, Z. Wu, Review Antibacterial Coatings on Titanium Implants, (2009) 470–480. doi:10.1002/jbm.b.31463.
- [130] H. Cao, X. Liu, Activating titanium oxide coatings for orthopedic implants, *Surf. Coatings Technol.* 233 (2013) 57–64. doi:10.1016/j.surfcoat.2013.01.043.
- [131] T. Albrektsson, A. Wennerberg, Oral implant surfaces: Part 1-review focusing on topographic and chemical properties of different surfaces and in vivo responses to them, *Int. J. Prosthodont.* 17 (2004) 536–543.
- [132] C. Giordano, E. Saino, L. Rimondini, M.P. Pedefferri, L. Visai, A. Cigada, R. Chiesa, Electrochemically induced anatase inhibits bacterial colonization on Titanium Grade 2 and Ti6Al4V alloy for dental and orthopedic devices, *Colloids Surfaces B Biointerfaces.* 88 (2011) 648–655. doi:10.1016/j.colsurfb.2011.07.054.
- [133] V. Christiaens, W. Jacquet, M. Jacobsson, J. Cosyn, R. Doornewaard, H. De Bruyn, S. Vervaeke, Implant surface roughness and patient factors on long-term peri-implant bone loss, *Periodontol.* 2000. 73 (2016) 218–227. doi:10.1111/prd.12177.
- [134] C. Ferreira Ribeiro, K. Cogo-Müller, G.C. Franco, L.R. Silva-Concílio, M. Sampaio Campos,

- S. De Mello Rode, A.C. Claro Neves, Initial oral biofilm formation on titanium implants with different surface treatments: An in vivo study, *Arch. Oral Biol.* 69 (2016) 33–39. doi:10.1016/j.archoralbio.2016.05.006.
- [135] C.N. Elias, Y. Oshida, J.H.C. Lima, C.A. Muller, Relationship between surface properties (roughness, wettability and morphology) of titanium and dental implant removal torque, *J. Mech. Behav. Biomed. Mater.* 1 (2008) 234–242. doi:10.1016/j.jmbbm.2007.12.002.
- [136] Y.G. Ko, D.-H. Lee, C.S. Lee, J.-H. Jang, C.H. Park, Y.-J. Kim, J.-W. Park, Enhanced osteoblast response to an equal channel angular pressing-processed pure titanium substrate with microrough surface topography, *Acta Biomater.* 5 (2009) 3272–3280. doi:10.1016/j.actbio.2009.04.038.
- [137] C. Ruiz, G. Mazzaglia, J.I. Rosales-Leal, M.A. Cabrerizo-Vílchez, P.J. Ramón-Torregrosa, O. García-Martínez, L. Díaz-Rodríguez, M. Vallecillo-Capilla, M.A. Rodríguez-Valverde, Effect of roughness, wettability and morphology of engineered titanium surfaces on osteoblast-like cell adhesion, *Colloids Surfaces A Physicochem. Eng. Asp.* 365 (2009) 222–229. doi:10.1016/j.colsurfa.2009.12.017.
- [138] L. Ponsonnet, K. Reybier, N. Jaffrezic, V. Comte, C. Lagneau, M. Lissac, C. Martelet, Relationship between surface properties (roughness, wettability) of titanium and titanium alloys and cell behaviour, *Mater. Sci. Eng. C.* 23 (2003) 551–560. doi:10.1016/S0928-4931(03)00033-X.
- [139] I. Zollino, A. Girardi, A. Palmieri, F. Cura, V. Sollazzo, G. Brunelli, F. Carinci, Anatase-based implants nanocoating on stem cells derived from adipose tissue, *Implant Dent.* 21 (2012) 118–123. doi:10.1097/ID.0b013e31824bc948.
- [140] H.N. Pantaroto, A.P. Ricomini-Filho, M.M. Bertolini, J.H. Dias da Silva, N.F. Azevedo Neto, C. Sukotjo, E.C. Rangel, V.A.R. Barão, Antibacterial photocatalytic activity of different crystalline TiO₂ phases in oral multispecies biofilm, *Dent. Mater.* 34 (2018) e182–e195. doi:10.1016/j.dental.2018.03.011.
- [141] S. Bianchi, S. Bernardi, M.A. Continenza, E. Rastelli, M.G. Palmerini, G. Botticelli, G. Macchiarelli, A.R. Tomei, Scanning electron microscopy and microbiological approaches for the evaluation of salivary microorganisms behaviour on anatase titanium surfaces: In vitro study, *Morphologie.* 102 (2017) 1–6. doi:10.1016/j.morpho.2017.12.001.
- [142] N. Rahimi, R.A. Pax, E.M.A. Gray, Review of functional titanium oxides. I: TiO₂ and its modifications, *Prog. Solid State Chem.* 44 (2016) 86–105. doi:10.1016/j.progsolidstchem.2016.07.002.
- [143] M.A. Vargas-reus, K. Memarzadeh, J. Huang, G.G. Ren, R.P. Allaker, International Journal of Antimicrobial Agents Antimicrobial activity of nanoparticulate metal oxides against peri-implantitis pathogens, *Int. J. Antimicrob. Agents.* 40 (2012) 135–139. doi:10.1016/j.ijantimicag.2012.04.012.
- [144] S.-H. Uhm, S.-B. Lee, D.-H. Song, J.-S. Kwon, J.-G. Han, K.-N. Kim, Fabrication of Bioactive, Antibacterial TiO₂ Nanotube Surfaces, Coated with Magnetron Sputtered Ag Nanostructures for Dental Applications, *J. Nanosci. Nanotechnol.* 14 (2014) 7847–7854. doi:10.1166/jnn.2014.9412.
- [145] R. Harada, E. Kokubu, H. Kinoshita, M. Yoshinari, K. Ishihara, E. Kawada, S. Takemoto, Corrosion behavior of titanium in response to sulfides produced by *Porphyromonas gingivalis*, *Dent. Mater.* 34 (2017) 183–191. doi:10.1016/j.dental.2017.10.004.

- [146] C. Do Nascimento, M.S. Pita, E.D.S. Santos, N. Monesi, V. Pedrazzi, R.F. De Albuquerque Junior, R.F. Ribeiro, Microbiome of titanium and zirconia dental implants abutments, *Dent. Mater.* 32 (2016) 93–101. doi:10.1016/j.dental.2015.10.014.
- [147] E. Gerits, P. Spincemaille, K. De Cremer, K. De Brucker, S. Beullens, K. Thevissen, B.P.A. Cammue, K. Vandamme, M. Fauvart, N. Verstraeten, J. Michiels, Repurposing AM404 for the treatment of oral infections by *Porphyromonas gingivalis*, *Clin. Exp. Dent. Res.* 3 (2017) 69–76. doi:10.1002/cre2.65.
- [148] B.D.E.L. Curto, M.F. Brunella, C. Giordano, M.P. Pedferri, V. Valtulina, L. Visai, A. Cigada, Decreased bacterial adhesion to surface-treated titanium, 28 (2005) 718–730.
- [149] E. Varoni, M. Tarce, G. Lodi, a Carrassi, Chlorhexidine (CHX) in dentistry: state of the art., *Minerva Stomatol.* 61 (2012) 399–419.
<http://www.ncbi.nlm.nih.gov/pubmed/22976567>.
- [150] A. Kozlovsky, Z. Artzi, O. Moses, N. Kamin-Belsky, R.B.-N. Greenstein, Interaction of Chlorhexidine With Smooth and Rough Types of Titanium Surfaces, *J. Periodontol.* 77 (2006) 1194–1200. doi:10.1902/jop.2006.050401.

APPENDIX

Tested laser parameters for silver sintering on titanium surface

Tested Conditions

Frequency (Hz)	Current (A)	Pulse (ms)
200	1	0.2
		0.4
		0.6
		0.8
		1.0
		1.2
	2	0.2
		0.4
		0.6
		0.8
		1.0
		1.2

Tested Laser Conditions

Frequency (Hz)	Current (A)	Pulse (ms)
200	1	0.2
		0.4
		0.6
		0.8
	2	1.0
		1.2

Tested Conditions

Frequency (Hz)	Current (A)	Pulse (ms)
200	1 and 2	0.1
		0.2
		0.3
		0.4
		0.5
		0.6
		0.7
		0.8
		0.9

Tested Conditions

Frequency (Hz)	Current (A)	Pulse (ms)
<i>200</i>	1	0.8
	2	0.3
	2	0.4
	2	0.5
	2	0.6
	2	0.7
	2	0.8
	2	0.9
	3	0.3
	3	0.4
	3	0.6

Oxide pattern with laser 3

Current (A)	Frequency (Hz)	Pulse (ms)	Point Time (ms)	Point Distance (mm)	Light (mm)	Passes
1	200	0,1	10	0,025	0,1	1
1	200	0,2	10	0,025	0,1	1
1	200	0,3	10	0,025	0,1	1
1	200	0,4	10	0,025	0,1	1
1	200	0,5	10	0,025	0,1	1
1	200	0,6	10	0,025	0,1	1
1	200	0,7	10	0,025	0,1	1
1	200	0,8	10	0,025	0,1	1
1	200	0,9	10	0,025	0,1	1
1	200	1,0	10	0,025	0,1	1
1	200	0,1	10	0,025	0,2	1
1	200	0,2	10	0,025	0,2	1
1	200	0,3	10	0,025	0,2	1
1	200	0,4	10	0,025	0,2	1
1	200	0,5	10	0,025	0,2	1
1	200	0,6	10	0,025	0,2	1
1	200	0,7	10	0,025	0,2	1
1	200	0,8	10	0,025	0,2	1
1	200	0,9	10	0,025	0,2	1
1	200	1,0	10	0,025	0,2	1
1	200	0,1	10	0,025	0,3	1
1	200	0,2	10	0,025	0,3	1
1	200	0,3	10	0,025	0,3	1
1	200	0,4	10	0,025	0,3	1
1	200	0,5	10	0,025	0,3	1
1	200	0,6	10	0,025	0,3	1
1	200	0,7	10	0,025	0,3	1

Implant surface modification by laser treatment to enhance the osseointegration and antibacterial potential of dental implants

Current (A)	Frequency (Hz)	Pulse (ms)	Point Time (ms)	Point Distance (mm)	Light (mm)	Passes
1	200	0,8	10	0,025	0,3	1
1	200	0,9	10	0,025	0,3	1
1	200	1,0	10	0,025	0,3	1
2	200	0,8	10	0,02	0,1	1
2	200	0,8	10	0,04	0,1	1
2	200	0,8	10	0,06	0,1	1
2	200	0,8	10	0,08	0,1	1
2	200	0,8	10	0,10	0,1	1
2	200	0,8	10	0,15	0,1	1
2	200	0,8	10	0,20	0,1	1
2	200	0,8	10	0,25	0,1	1
4	200	0,8	10	0,02	0,1	1
4	200	0,8	10	0,04	0,1	1
4	200	0,8	10	0,06	0,1	1
4	200	0,8	10	0,08	0,1	1
4	200	0,8	10	0,10	0,1	1
4	200	0,8	10	0,15	0,1	1
4	200	0,8	10	0,20	0,1	1
4	200	0,8	10	0,25	0,1	1
6	200	0,8	10	0,02	0,1	1
6	200	0,8	10	0,04	0,1	1
6	200	0,8	10	0,06	0,1	1
6	200	0,8	10	0,08	0,1	1
6	200	0,8	10	0,10	0,1	1
6	200	0,8	10	0,15	0,1	1
6	200	0,8	10	0,20	0,1	1
6	200	0,8	10	0,25	0,1	1
8	200	0,8	10	0,02	0,1	1
8	200	0,8	10	0,04	0,1	1

Implant surface modification by laser treatment to enhance the osseointegration and antibacterial potential of dental implants

Current (A)	Frequency (Hz)	Pulse (ms)	Point Time (ms)	Point Distance (mm)	Light (mm)	Passes
8	200	0,8	10	0,06	0,1	1
8	200	0,8	10	0,08	0,1	1
8	200	0,8	10	0,10	0,1	1
8	200	0,8	10	0,15	0,1	1
8	200	0,8	10	0,20	0,1	1
8	200	0,8	10	0,25	0,1	1
10	200	0,8	10	0,02	0,1	1
10	200	0,8	10	0,04	0,1	1
10	200	0,8	10	0,06	0,1	1
10	200	0,8	10	0,08	0,1	1
10	200	0,8	10	0,10	0,1	1
10	200	0,8	10	0,15	0,1	1
10	200	0,8	10	0,20	0,1	1
10	200	0,8	10	0,25	0,1	1
15	200	0,8	10	0,02	0,1	1
15	200	0,8	10	0,04	0,1	1
15	200	0,8	10	0,06	0,1	1
15	200	0,8	10	0,08	0,1	1
15	200	0,8	10	0,10	0,1	1
15	200	0,8	10	0,15	0,1	1
15	200	0,8	10	0,20	0,1	1
15	200	0,8	10	0,25	0,1	1
20	200	0,8	10	0,02	0,1	1
20	200	0,8	10	0,04	0,1	1
20	200	0,8	10	0,06	0,1	1
20	200	0,8	10	0,08	0,1	1
20	200	0,8	10	0,10	0,1	1
20	200	0,8	10	0,15	0,1	1
20	200	0,8	10	0,20	0,1	1

Implant surface modification by laser treatment to enhance the osseointegration and antibacterial potential of dental implants

Current (A)	Frequency (Hz)	Pulse (ms)	Point Time (ms)	Point Distance (mm)	Light (mm)	Passes
20	200	0,8	10	0,25	0,1	1
2	200	0,7	20	0,02	0,1	1
2	200	0,7	20	0,04	0,1	1
2	200	0,7	20	0,06	0,1	1
2	200	0,7	20	0,08	0,1	1
2	200	0,7	20	0,10	0,1	1
2	200	0,7	20	0,15	0,1	1
2	200	0,7	20	0,20	0,1	1
2	200	0,7	20	0,25	0,1	1
2	200	0,7	40	0,02	0,1	1
2	200	0,7	40	0,04	0,1	1
2	200	0,7	40	0,06	0,1	1
2	200	0,7	40	0,08	0,1	1
2	200	0,7	40	0,10	0,1	1
2	200	0,7	40	0,15	0,1	1
2	200	0,7	40	0,20	0,1	1
2	200	0,7	40	0,25	0,1	1
2	200	0,7	60	0,02	0,1	1
2	200	0,7	60	0,04	0,1	1
2	200	0,7	60	0,06	0,1	1
2	200	0,7	60	0,08	0,1	1
2	200	0,7	60	0,10	0,1	1
2	200	0,7	60	0,15	0,1	1
2	200	0,7	60	0,20	0,1	1
2	200	0,7	60	0,25	0,1	1
2	200	0,7	80	0,02	0,1	1
2	200	0,7	80	0,04	0,1	1
2	200	0,7	80	0,06	0,1	1
2	200	0,7	80	0,08	0,1	1

Implant surface modification by laser treatment to enhance the osseointegration and antibacterial potential of dental implants

Current (A)	Frequency (Hz)	Pulse (ms)	Point Time (ms)	Point Distance (mm)	Light (mm)	Passes
2	200	0,7	80	0,10	0,1	1
2	200	0,7	80	0,15	0,1	1
2	200	0,7	80	0,20	0,1	1
2	200	0,7	80	0,25	0,1	1
2	200	0,7	100	0,02	0,1	1
2	200	0,7	100	0,04	0,1	1
2	200	0,7	100	0,06	0,1	1
2	200	0,7	100	0,08	0,1	1
2	200	0,7	100	0,10	0,1	1
2	200	0,7	100	0,15	0,1	1
2	200	0,7	100	0,20	0,1	1
2	200	0,7	100	0,25	0,1	1
2	200	0,7	150	0,02	0,1	1
2	200	0,7	150	0,04	0,1	1
2	200	0,7	150	0,06	0,1	1
2	200	0,7	150	0,08	0,1	1
2	200	0,7	150	0,10	0,1	1
2	200	0,7	150	0,15	0,1	1
2	200	0,7	150	0,20	0,1	1
2	200	0,7	150	0,25	0,1	1
1	200	0,7	20	0,02	0,1	1
1	200	0,7	20	0,04	0,1	1
1	200	0,7	20	0,06	0,1	1
1	200	0,7	20	0,08	0,1	1
1	200	0,7	20	0,10	0,1	1
1	200	0,7	20	0,15	0,1	1
1	200	0,7	20	0,20	0,1	1
1	200	0,7	20	0,25	0,1	1
1	200	0,7	40	0,02	0,1	1

Implant surface modification by laser treatment to enhance the osseointegration and antibacterial potential of dental implants

Current (A)	Frequency (Hz)	Pulse (ms)	Point Time (ms)	Point Distance (mm)	Light (mm)	Passes
1	200	0,7	40	0,04	0,1	1
1	200	0,7	40	0,06	0,1	1
1	200	0,7	40	0,08	0,1	1
1	200	0,7	40	0,10	0,1	1
1	200	0,7	40	0,15	0,1	1
1	200	0,7	40	0,20	0,1	1
1	200	0,7	40	0,25	0,1	1
1	200	0,7	60	0,02	0,1	1
1	200	0,7	60	0,04	0,1	1
1	200	0,7	60	0,06	0,1	1
1	200	0,7	60	0,08	0,1	1
1	200	0,7	60	0,10	0,1	1
1	200	0,7	60	0,15	0,1	1
1	200	0,7	60	0,20	0,1	1
1	200	0,7	60	0,25	0,1	1
1	200	0,7	80	0,02	0,1	1
1	200	0,7	80	0,04	0,1	1
1	200	0,7	80	0,06	0,1	1
1	200	0,7	80	0,08	0,1	1
1	200	0,7	80	0,10	0,1	1
1	200	0,7	80	0,15	0,1	1
1	200	0,7	80	0,20	0,1	1
1	200	0,7	80	0,25	0,1	1
1	200	0,7	100	0,02	0,1	1
1	200	0,7	100	0,04	0,1	1
1	200	0,7	100	0,06	0,1	1
1	200	0,7	100	0,08	0,1	1
1	200	0,7	100	0,10	0,1	1
1	200	0,7	100	0,15	0,1	1

Implant surface modification by laser treatment to enhance the osseointegration and antibacterial potential of dental implants

Current (A)	Frequency (Hz)	Pulse (ms)	Point Time (ms)	Point Distance (mm)	Light (mm)	Passes
1	200	0,7	100	0,20	0,1	1
1	200	0,7	100	0,25	0,1	1
1	200	0,7	150	0,02	0,1	1
1	200	0,7	150	0,04	0,1	1
1	200	0,7	150	0,06	0,1	1
1	200	0,7	150	0,08	0,1	1
1	200	0,7	150	0,10	0,1	1
1	200	0,7	150	0,15	0,1	1
1	200	0,7	150	0,20	0,1	1
1	200	0,7	150	0,25	0,1	1
1	200	0,7	30	0,20	0,1	1
1	200	0,7	30	0,25	0,1	1
1	200	0,7	30	0,30	0,1	1
1	200	0,7	30	0,40	0,1	1
1	200	0,7	30	0,60	0,1	1
1	200	0,7	40	0,60	0,1	1
1	200	0,7	50	0,60	0,1	1
2	200	0,7	40	0,60	0,1	1
2	200	0,7	50	0,60	0,1	1
2	200	0,7	40	0,50	0,1	1
2	200	0,7	40	0,55	0,1	1
2	200	0,7	80	0,60	0,1	1
2	200	0,7	80	0,70	0,1	1
2	200	0,7	100	0,70	0,1	1
2	200	0,7	80	0,65	0,1	1
2	200	0,7	100	0,65	0,1	1
2	200	0,7	80	0,60	0,1	1
3	200	0,7	80	0,60	0,1	1
4	200	0,7	80	0,60	0,1	1

Implant surface modification by laser treatment to enhance the osseointegration and antibacterial potential of dental implants

Current (A)	Frequency (Hz)	Pulse (ms)	Point Time (ms)	Point Distance (mm)	Light (mm)	Passes
5	200	0,7	80	0,60	0,1	1
3	200	0,7	80	0,60	0,1	1
4	200	0,7	80	0,60	0,1	1
5	200	0,7	80	0,60	0,1	1
6	200	0,7	80	0,60	0,1	1
7	200	0,7	80	0,60	0,1	1
8	200	0,7	80	0,60	0,1	1
9	200	0,7	80	0,60	0,1	1
10	200	0,7	80	0,60	0,1	1
2	200	0,7	100	0,6	0,1	1
2	200	0,7	150	0,6	0,1	1
2	200	0,7	200	0,6	0,1	1
2	200	0,7	250	0,6	0,1	1
2	200	0,7	300	0,6	0,1	1
2	200	0,7	350	0,6	0,1	1
2	200	0,7	400	0,6	0,1	1
2	200	0,7	450	0,6	0,1	1
2	200	0,7	80	0,6	0,1	1
2	200	0,7	85	0,6	0,1	1
2	200	0,7	90	0,6	0,1	1
2	200	0,7	95	0,6	0,1	1
2	200	0,7	100	0,6	0,1	1
3	200	0,7	80	0,6	0,1	1
3	200	0,7	85	0,6	0,1	1
3	200	0,7	90	0,6	0,1	1
3	200	0,7	95	0,6	0,1	1
3	200	0,7	100	0,6	0,1	1
4	200	0,7	80	0,6	0,1	1
4	200	0,7	85	0,6	0,1	1

Implant surface modification by laser treatment to enhance the osseointegration and antibacterial potential of dental implants

Current (A)	Frequency (Hz)	Pulse (ms)	Point Time (ms)	Point Distance (mm)	Light (mm)	Passes
4	200	0,7	90	0,6	0,1	1
4	200	0,7	95	0,6	0,1	1
4	200	0,7	100	0,6	0,1	1
1	200	0,7	90	0,6	0,1	1
1	200	0,7	85	0,6	0,1	1
1	200	0,7	80	0,6	0,1	1
1	200	0,7	75	0,6	0,1	1
1	200	0,7	70	0,6	0,1	1
1	200	0,7	65	0,6	0,1	1
1	200	0,7	60	0,6	0,1	1
1	200	0,7	55	0,6	0,1	1
1	200	0,7	80	0,6	0,1	2
1	200	0,7	75	0,6	0,1	2
1	200	0,7	70	0,6	0,1	2
1	200	0,7	65	0,6	0,1	2
1	200	0,7	60	0,6	0,1	2
1	200	0,7	55	0,6	0,1	2
1	200	0,7	50	0,6	0,1	2
1	200	0,7	45	0,6	0,1	2
1	200	0,7	60	0,6	0,1	3
1	200	0,7	60	0,6	0,1	4
1	200	0,7	55	0,6	0,1	3
1	200	0,7	55	0,6	0,1	4
2	200	0,7	60	0,6	0,1	2
3	200	0,7	60	0,6	0,1	2
2	200	0,7	55	0,6	0,1	2
3	200	0,7	55	0,6	0,1	2
2	200	0,7	60	0,50	0,1	2
3	200	0,7	60	0,50	0,1	2

Implant surface modification by laser treatment to enhance the osseointegration and antibacterial potential of dental implants

Current (A)	Frequency (Hz)	Pulse (ms)	Point Time (ms)	Point Distance (mm)	Light (mm)	Passes
4	200	0,7	60	0,60	0,1	2
5	200	0,7	60	0,60	0,1	2
2	200	0,7	100	0,70	0,1	1
2	200	0,7	150	0,70	0,1	1
2	200	0,7	200	0,70	0,1	1
2	200	0,7	200	0,65	0,1	1
2	200	0,7	200	0,70	0,1	1
2	200	0,7	150	0,70	0,1	1
1	200	0,7	60	0,70	0,1	2
1	200	0,7	55	0,70	0,1	2
1	200	0,7	60	0,65	0,1	2
1	200	0,7	55	0,65	0,1	2
2	200	0,7	60	0,60	0,1	2
2	200	0,7	55	0,60	0,1	2
2	200	0,7	60	0,60	0,1	2
1	200	0,7	65	0,70	0,1	2
2	200	0,7	65	0,70	0,1	1
1	200	0,7	60	0,70	0,1	2

Oxide pattern with laser 2

Power (%)	Point time (ms)	Frequency (Hz)	Diameter (mm)	Passes	Pulse duration (s)	Pulse type
7	0.3	5	0.5	1	–	Single pulse
8	0.3	5	0.5	2	–	Single pulse
10	0.5	5	0.8	3	–	Single pulse
9	0.6	5	0.9	1	–	Single pulse
9	0.7	5	0.9	1	–	Single pulse
10	0.6	5	0.9	1	–	Single pulse
10	0.8	5	0.9	2	–	Single pulse
10	0.7	5	0.9	2	–	Single pulse
10	0.8	6	0.9	5	–	Single pulse
8	0.8	6	0.7	2	–	Single pulse
8	0.9	6	0.5	1	–	Single pulse
8	0.7	5	0.5	3	–	Single pulse
7	0.7	5	0.5	1	–	Single pulse
6	0.7	5	0.5	1	–	Single pulse
5	0.7	5	0.5	1	–	Single pulse
5	0.9	5	0.5	1	–	Single pulse
5	0.7	7	0.5	1	–	Single pulse
5	0.7	10	0.5	1	–	Single pulse
7	0.7	5	0.5	3	–	Single pulse
7	0.7	5	0.5	1	5	Single pulse
6	0.7	5	0.5	1	10	Single pulse
5	0.7	5	0.5	1	5	Single pulse
7	0.5	5	0.5	1	5	Single pulse
7	0.9	5	0.5	1	10	Single pulse
6	0.5	5	0.5	1	5	Single pulse
6	0.9	5	0.5	1	10	Single pulse
5	0.5	5	0.5	1	5	Single pulse

Implant surface modification by laser treatment to enhance the osseointegration and antibacterial potential of dental implants

Power (%)	Point time (ms)	Frequency (Hz)	Diameter (mm)	Passes	Pulse duration (s)	Pulse type
5	0.9	5	0.5	1	10	Single pulse
7	0.7	3.5	0.5	1	5	Single pulse
7	0.7	6.5	0.5	1	10	Single pulse
6	0.7	3.5	0.5	1	5	Single pulse
6	0.7	6.5	0.5	1	10	Single pulse
5	0.7	3.5	0.5	1	5	Single pulse
5	0.7	6.5	0.5	1	10	Single pulse
5	0.7	5	0.5	1	5	Single pulse
5	0.7	5	0.5	1	3	Single pulse
5	0.7	5	0.5	1	2	Single pulse
5	0.7	5	0.5	1	1	Single pulse
4	0.7	5	0.5	1	5	Single pulse
4	0.7	5	0.5	1	3	Single pulse
4	0.7	5	0.5	1	2	Single pulse
4	0.7	5	0.5	1	1	Single pulse
3	0.7	5	0.5	1	5	Single pulse
3	0.7	5	0.5	1	3	Single pulse
3	0.7	5	0.5	1	2	Single pulse
3	0.7	5	0.5	1	1	Single pulse
2	0.7	5	0.5	1	5	Single pulse
2	0.7	5	0.5	1	5	Single pulse
2	0.7	5	0.5	1	6	Single pulse
2	0.7	5	0.5	1	7	Single pulse
2	0.7	5	0.5	1	2	Single pulse
3	0.8	5	0.5	1	2	Single pulse
3	0.8	5	0.5	1	1	Single pulse
3	0.9	5	0.5	1	2	Single pulse
3	0.9	5	0.5	1	1	Single pulse
3	0.6	5	0.5	1	2	Single pulse

Implant surface modification by laser treatment to enhance the osseointegration and antibacterial potential of dental implants

Power (%)	Point time (ms)	Frequency (Hz)	Diameter (mm)	Passes	Pulse duration (s)	Pulse type
3	0.6	5	0.5	1	1	Single pulse
3	0.7	5.5	0.5	1	2	Single pulse
3	0.7	5.5	0.5	1	1	Single pulse
3	0.7	6	0.5	1	2	Single pulse
3	0.7	6	0.5	1	1	Single pulse
3	0.7	7	0.5	1	2	Single pulse
3	0.7	7	0.5	1	1	Single pulse
3	0.7	4.5	0.5	1	2	Single pulse
3	0.7	4.5	0.4	1	1	Single pulse
3	0.7	5	0.4	1	2	Single pulse
3	0.7	5	0.4	1	1	Single pulse
2	0.7	5	0.4	1	2	Single pulse
2	0.7	5	0.4	1	1	Single pulse
2	0.7	5	0.3	1	5	Single pulse
3	0.7	5	0.3	1	2	Single pulse
3	0.7	5	0.5	1	1	Single pulse
3	0.7	5	0.5	1	2	Single pulse
2	0.7	5	0.5	1	2	Single pulse
2	0.7	5	0.5	1	5	Single pulse
1	0.7	5	0.5	1	5	Single pulse
2	0.7	5	0.3	1	2	Single pulse
4	0.9	5	0.5	1	2	3 section mode
3	0.9	7	0.5	1	2	3 section mode
3	0.7	7	0.5	1	2	3 section mode
3	0.9	7	0.5	1	2	3 section mode
3	1.0	5	0.5	1	2	3 section mode
3	0.7	8	0.5	1	2	3 section mode
3	0.7	5	0.5	1	5	Reduced single mode

Implant surface modification by laser treatment to enhance the osseointegration and antibacterial potential of dental implants

Power (%)	Point time (ms)	Frequency (Hz)	Diameter (mm)	Passes	Pulse duration (s)	Pulse type
2	0.7	5	0.5	1	5	Single pulse
2	0.7	5	0.5	1	10	Single pulse
2	0.7	5	0.5	1	15	Single pulse
2	0.7	5	0.4	1	5	Single pulse
2	0.7	5	0.3	1	5	Single pulse
2	0.3	5	0.5	1	2	3 section mode
2	0.4	5	0.5	1	2	3 section mode
2	0.5	5	0.5	1	2	3 section mode
2	0.7	5	0.5	1	2	3 section mode
2	0.9	5	0.5	1	2	3 section mode
2	0.5	3	0.5	1	2	3 section mode
2	0.5	4	0.5	1	2	3 section mode
2	0.5	5	0.5	1	2	3 section mode
2	0.5	6	0.5	1	2	3 section mode
2	0.5	7	0.5	1	2	3 section mode
2	0.5	5	0.3	1	2	3 section mode
2	0.5	5	0.4	1	2	3 section mode
2	0.5	5	0.5	1	2	3 section mode
2	0.5	5	0.6	1	2	3 section mode
3	0.3	5	0.5	1	2	3 section mode
3	0.4	5	0.5	1	2	3 section mode
3	0.5	5	0.5	1	2	3 section mode
3	0.7	5	0.5	1	2	3 section mode
3	0.9	5	0.5	1	2	3 section mode
3	0.7	3	0.5	1	2	3 section mode
3	0.7	4	0.5	1	2	3 section mode
3	0.7	5	0.5	1	2	3 section mode
3	0.7	6	0.5	1	2	3 section mode
3	0.7	7	0.5	1	2	3 section mode

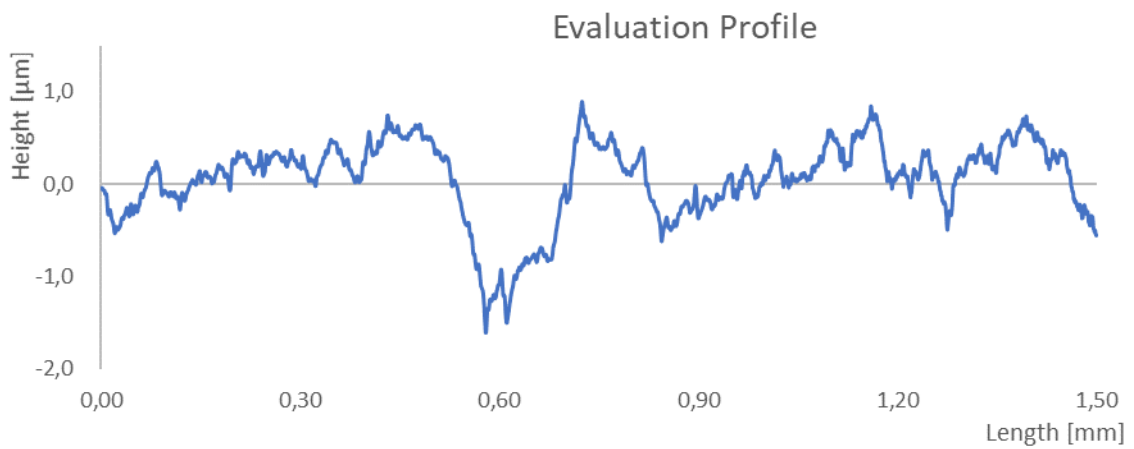
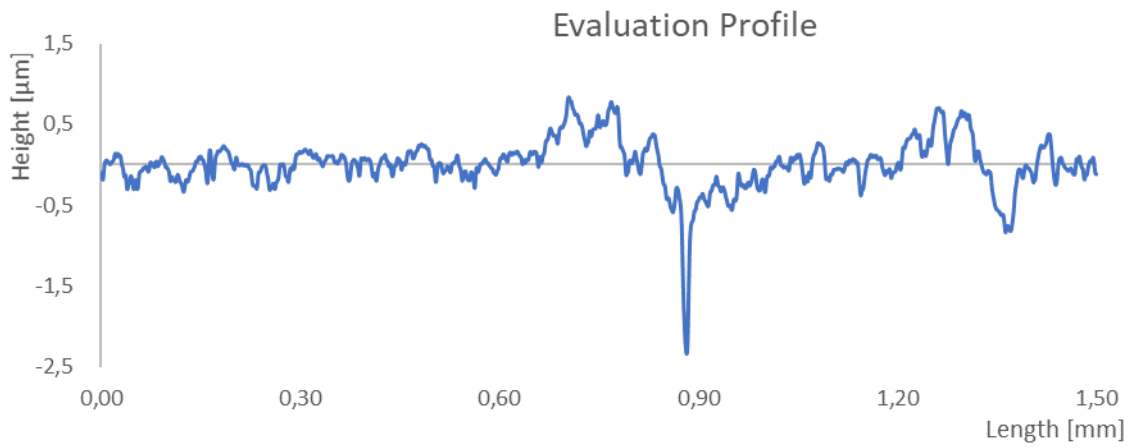
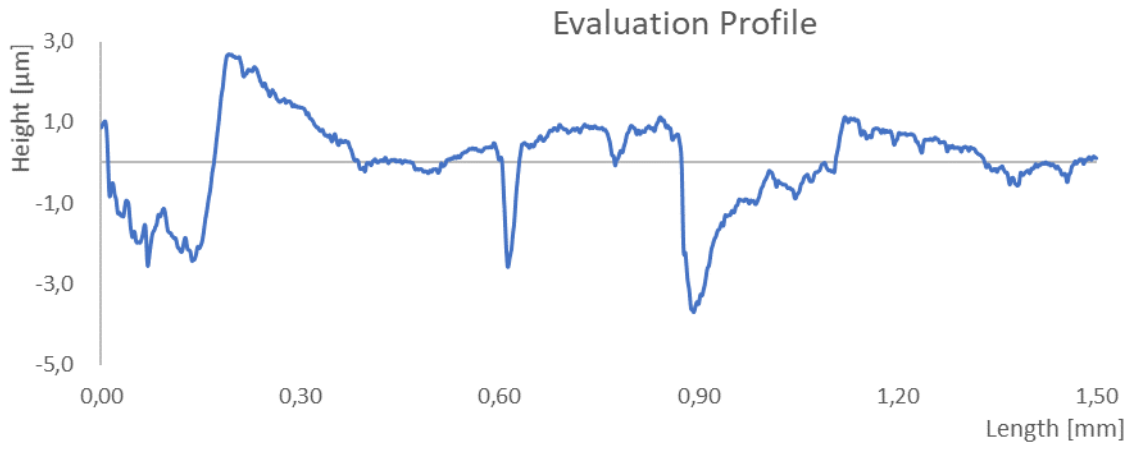
Implant surface modification by laser treatment to enhance the osseointegration and antibacterial potential of dental implants

Power (%)	Point time (ms)	Frequency (Hz)	Diameter (mm)	Passes	Pulse duration (s)	Pulse type
3	0.7	3	0.3	1	2	3 section mode
3	0.7	5	0.4	1	2	3 section mode
3	0.7	5	0.5	1	2	3 section mode
3	0.7	5	0.6	1	2	3 section mode
3	0.7	5	0.3	1	2	3 section mode
3	0.7	2.5	0.3	1	2	3 section mode
3	0.7	2.5	0.3	1	2	3 section mode
3	0.7	5	0.3	1	2	3 section mode
2	0.7	5	0.5	1	2	3 section mode
2	0.7	5	0.3	1	2	3 section mode
3	0.6	5	0.3	1	2	3 section mode
3	0.8	5	0.3	1	2	3 section mode
3	0.9	5	0.3	1	2	3 section mode
3	1.0	5	0.3	1	2	3 section mode
3	0.7	5	0.3	1	20	Single pulse
3	0.7	5	0.3	1	–	3 section mode
3	0.7	5	0.3	1	–	20 section pulse shape mode
3	0.9	5	0.3	1	–	20 section pulse shape mode
3	0.9	5	0.5	1	–	20 section pulse shape mode
3	0.9	5	0.5	1	–	20 section pulse shape mode
3	0.9	5	0.5	1	–	20 section pulse shape mode
3	0.7	5	0.3	1	–	20 section pulse shape mode
3	0.9	5	0.3	1	–	20 section pulse shape mode
3	0.9	5	0.5	1	–	20 section pulse shape mode

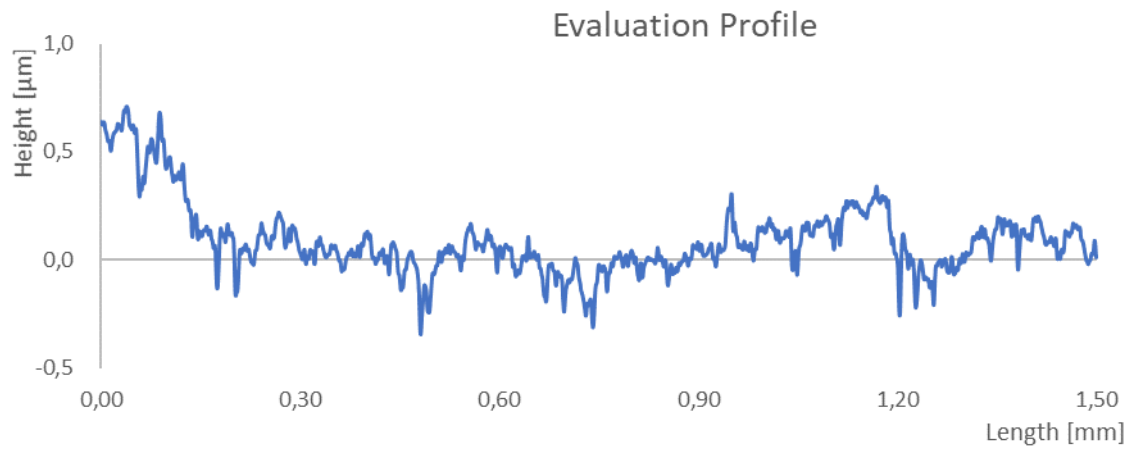
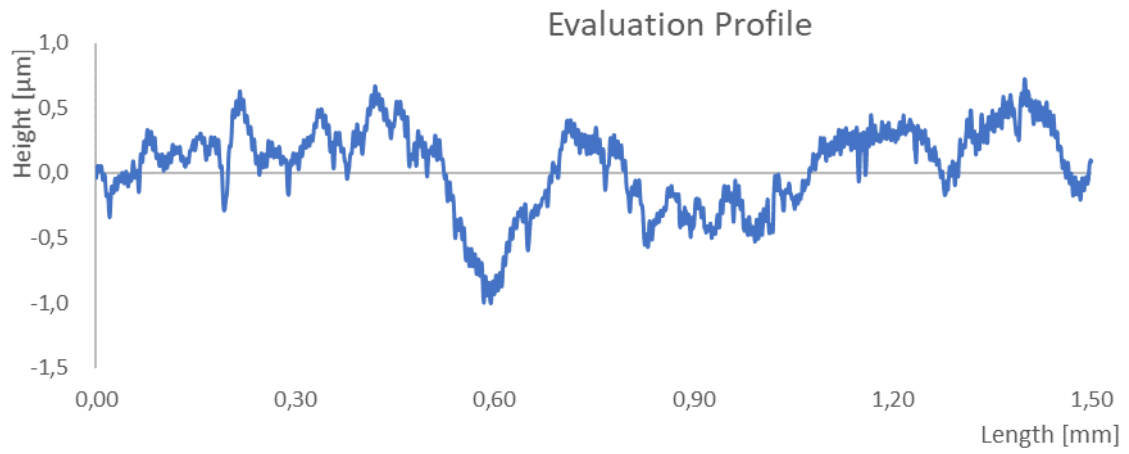
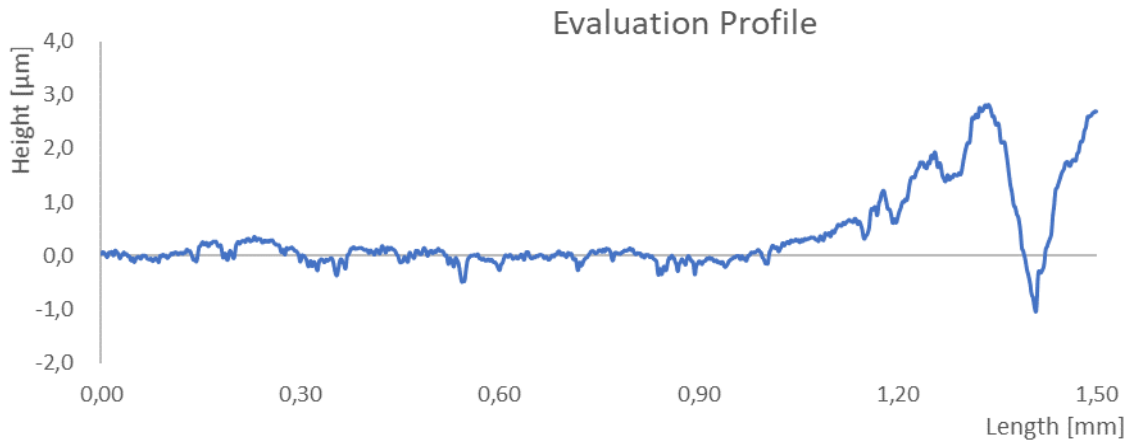
Roughness Measurements

Polished Samples

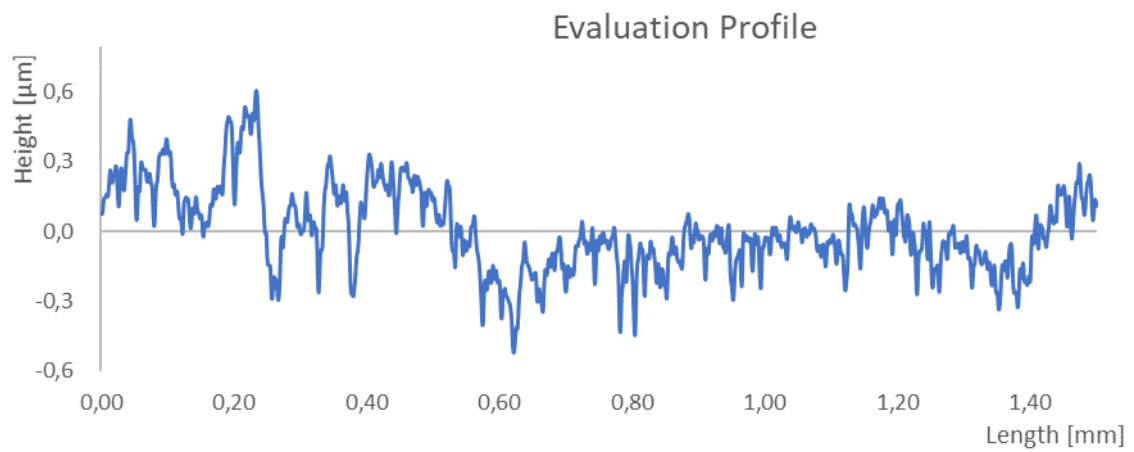
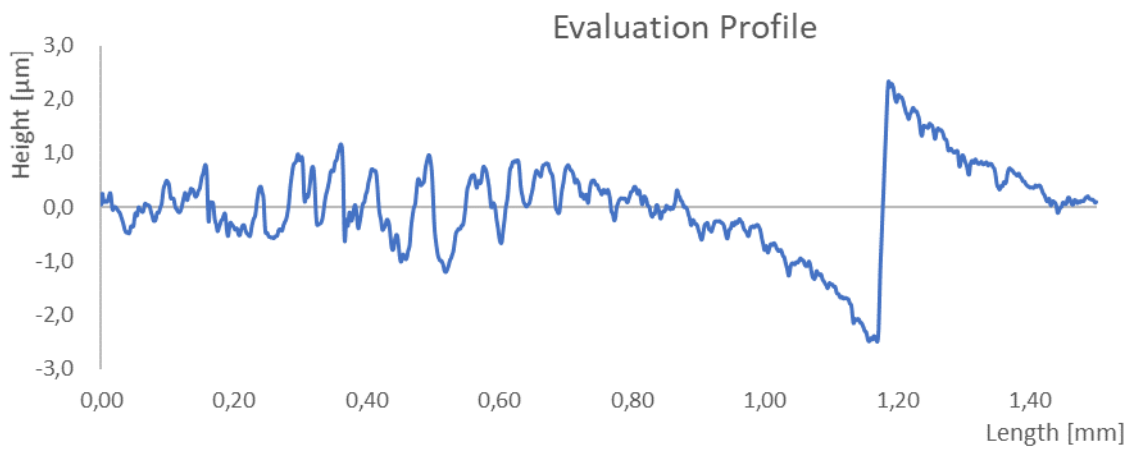
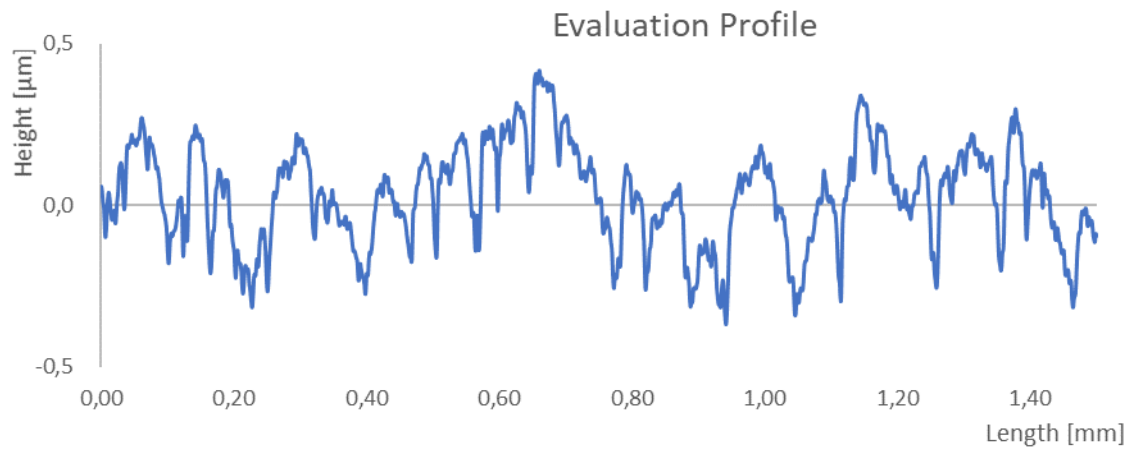
Sample 1



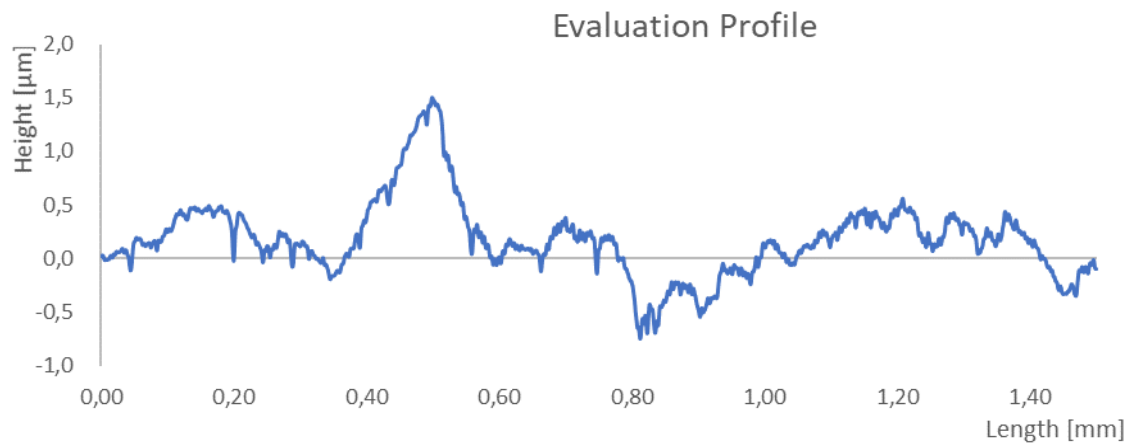
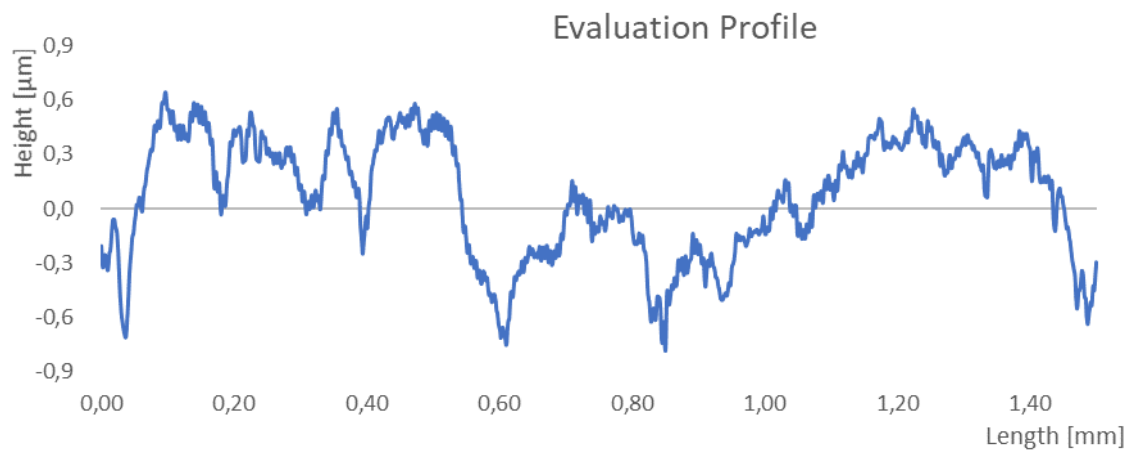
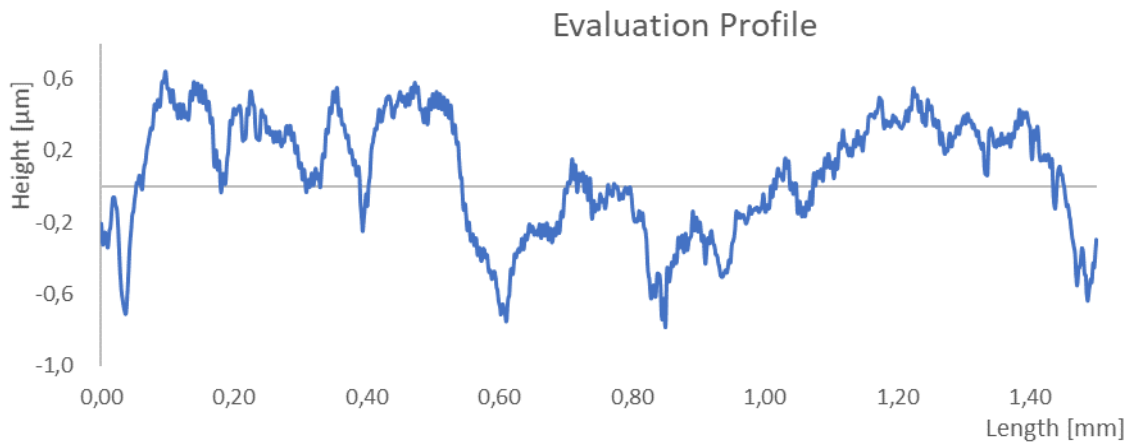
Sample 2



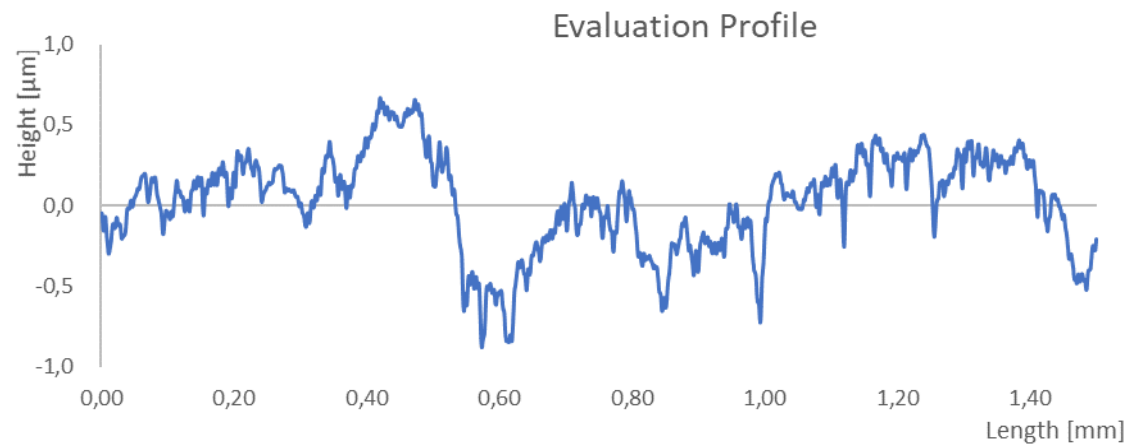
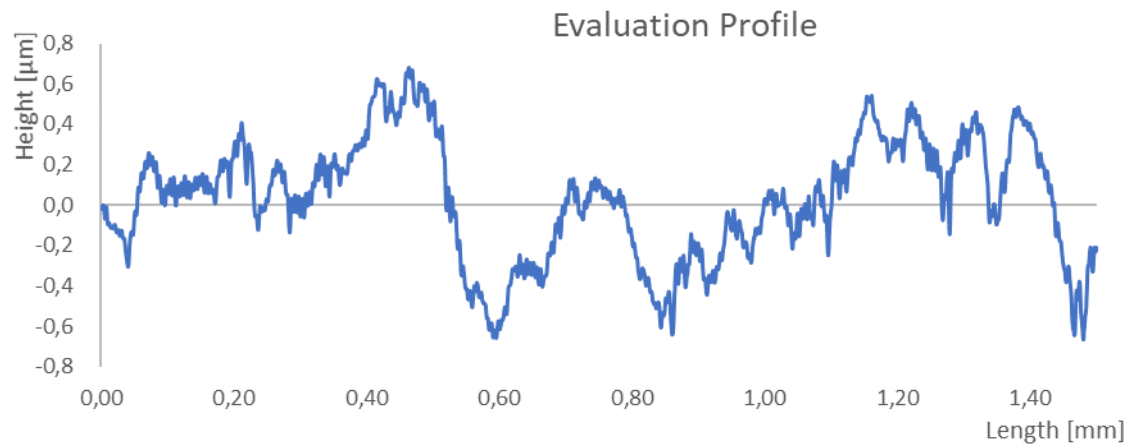
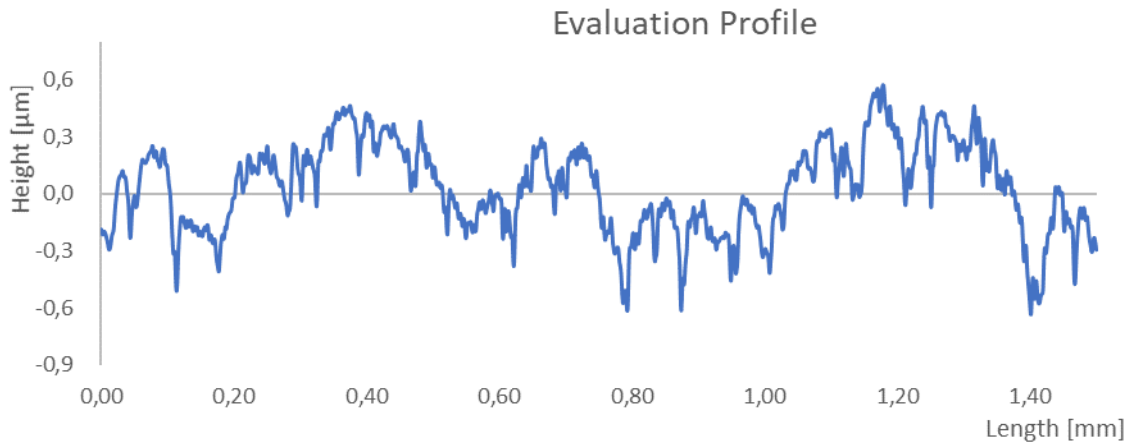
Sample 3



Sample 4

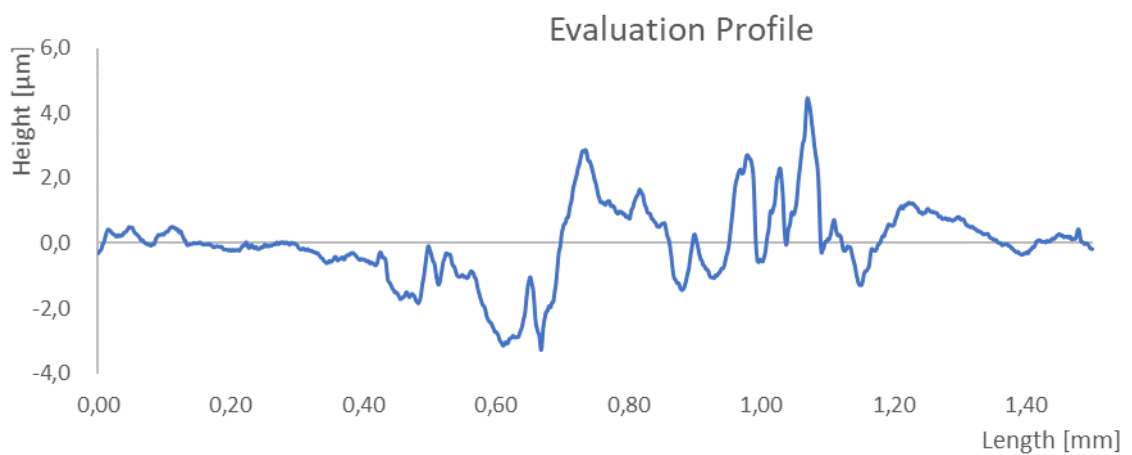
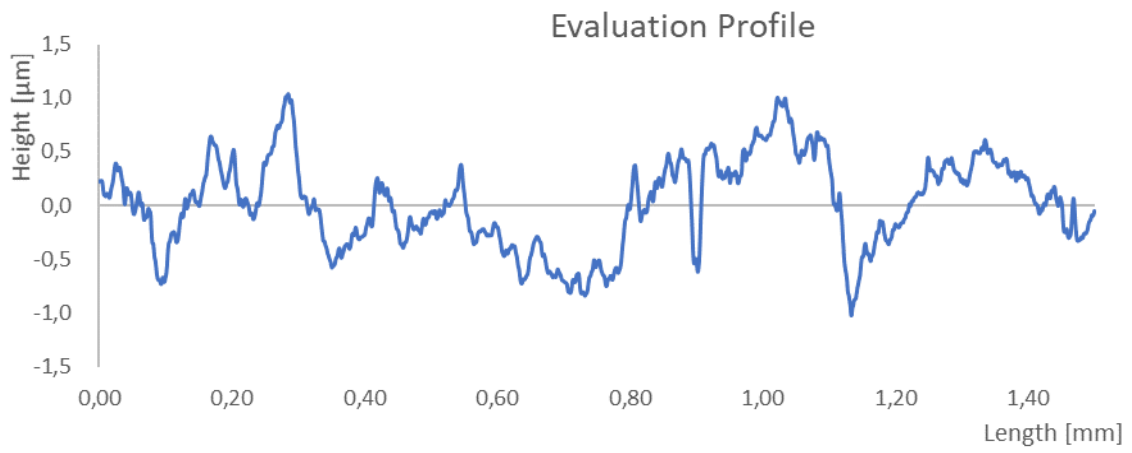
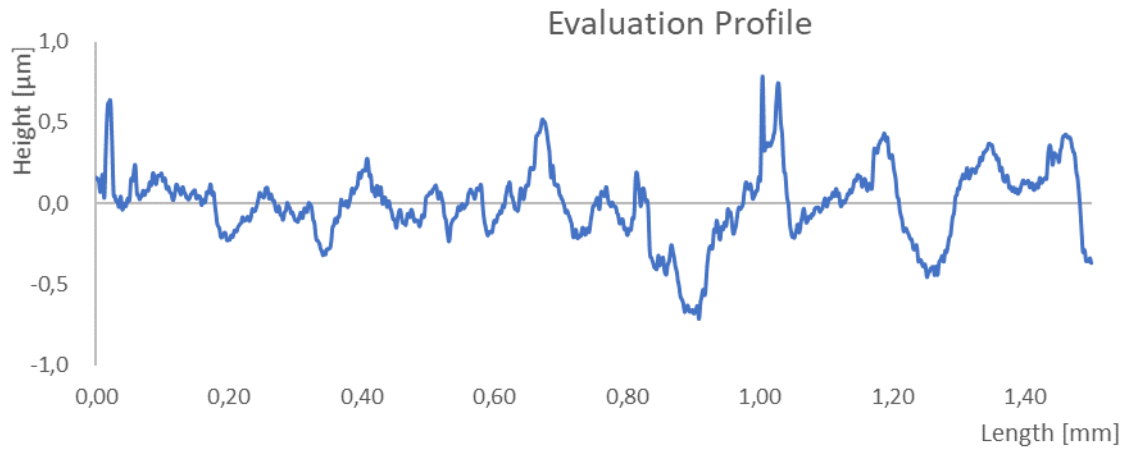


Sample 5

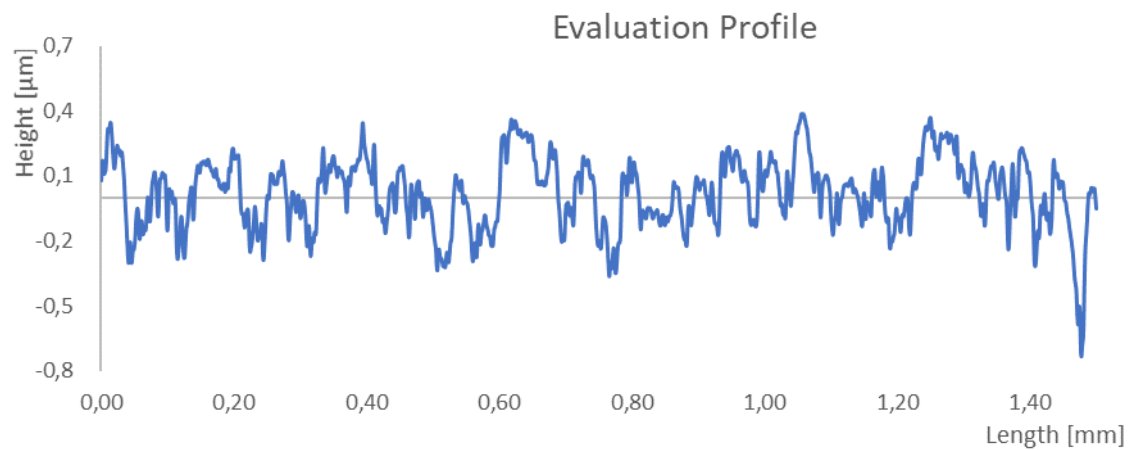
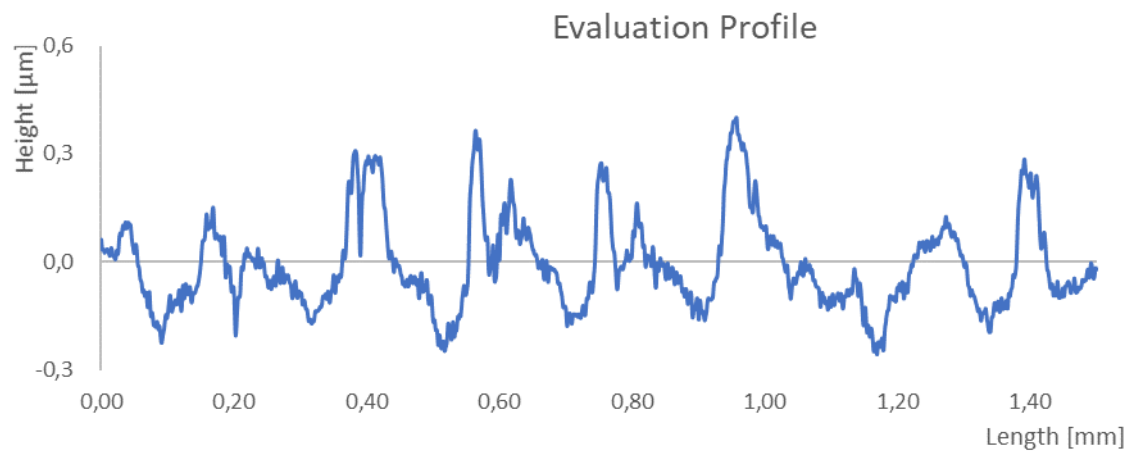
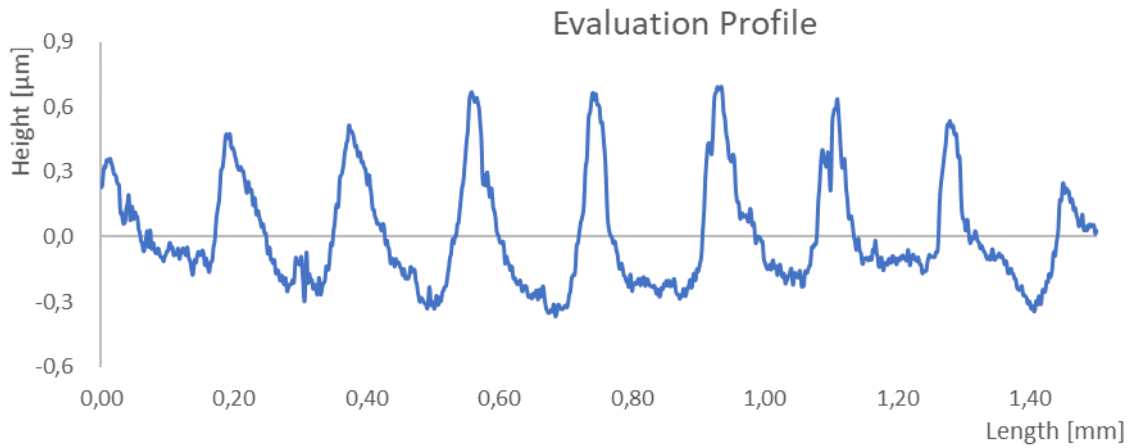


Silver Samples

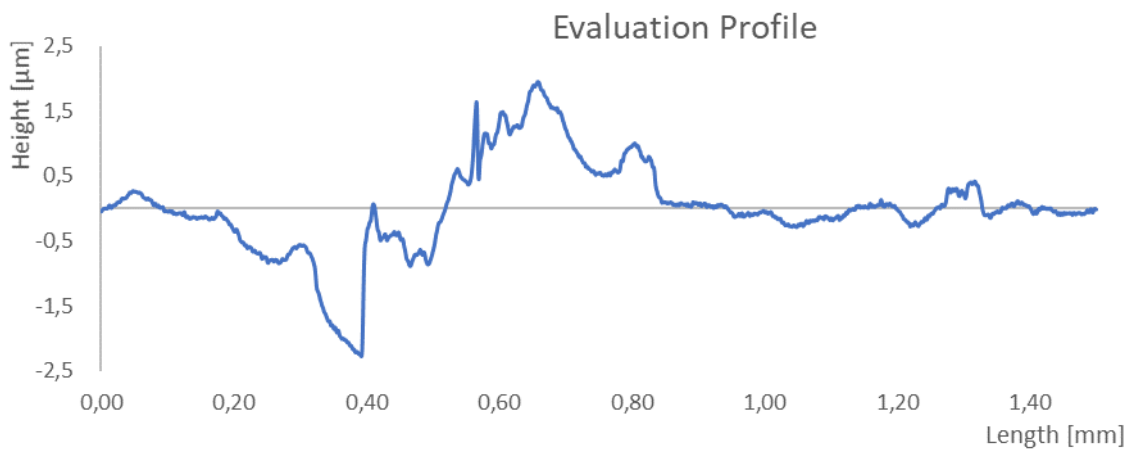
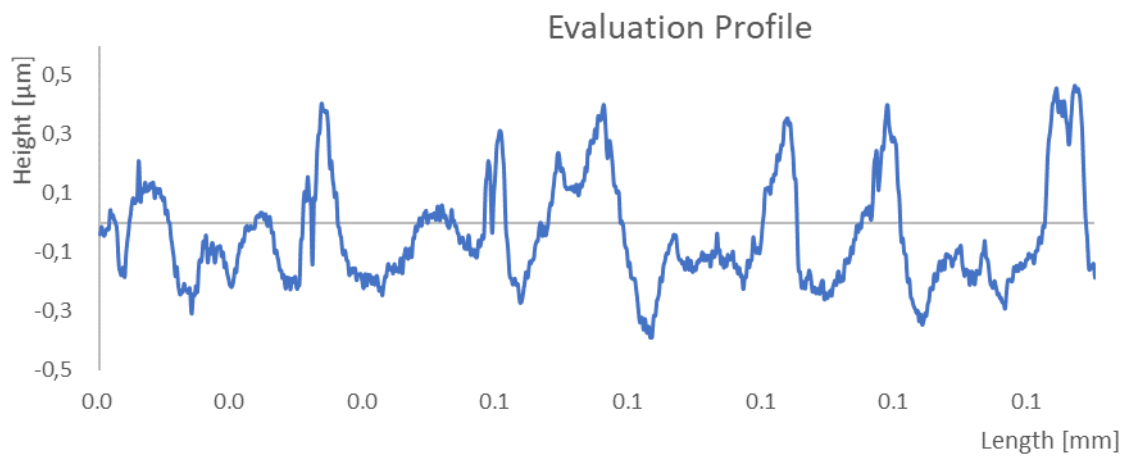
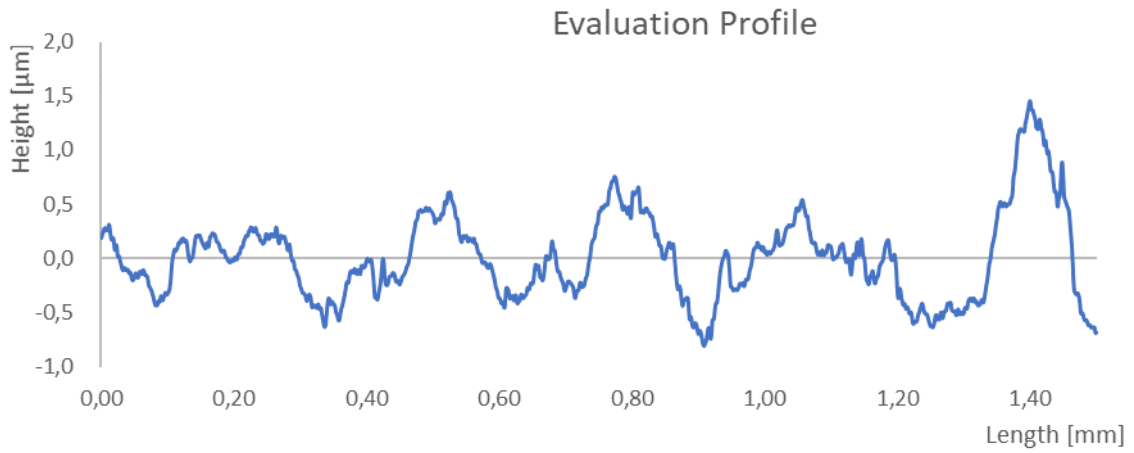
Sample 1



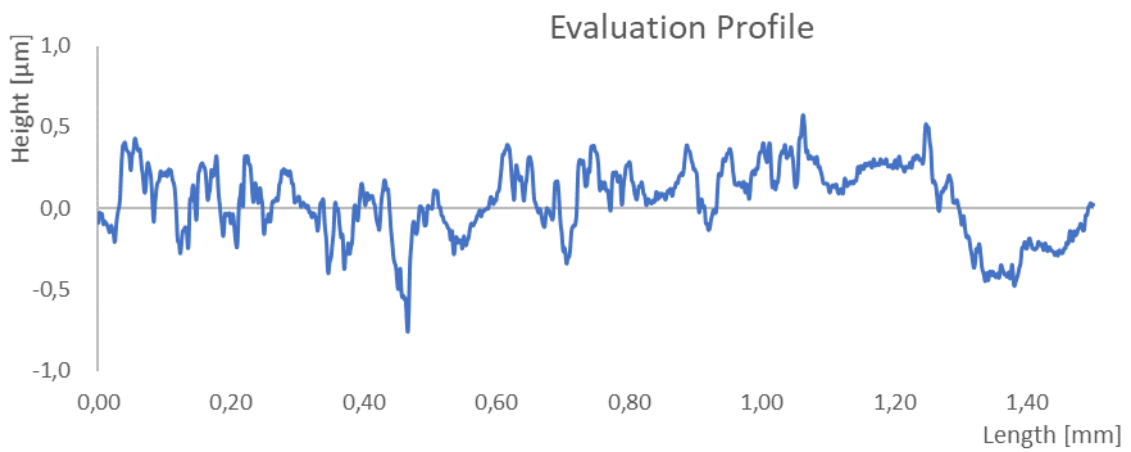
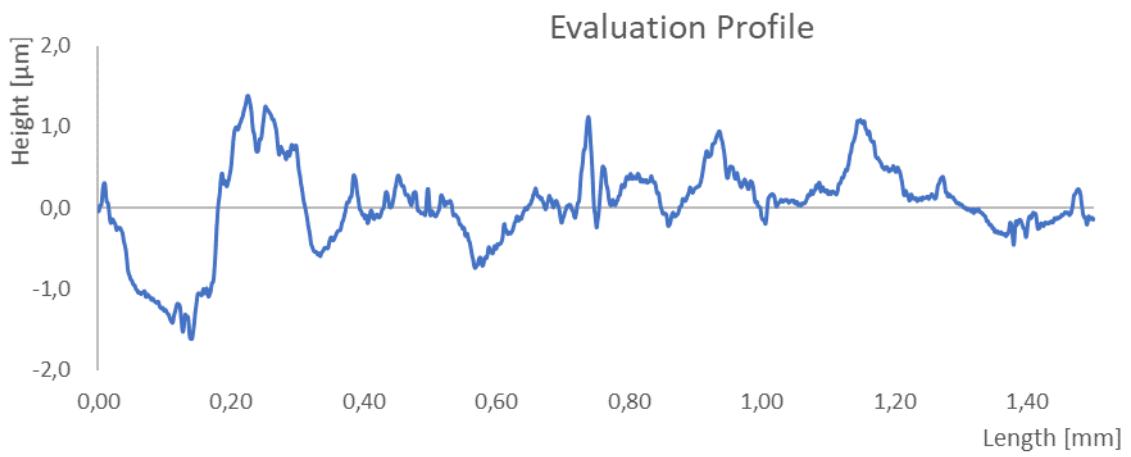
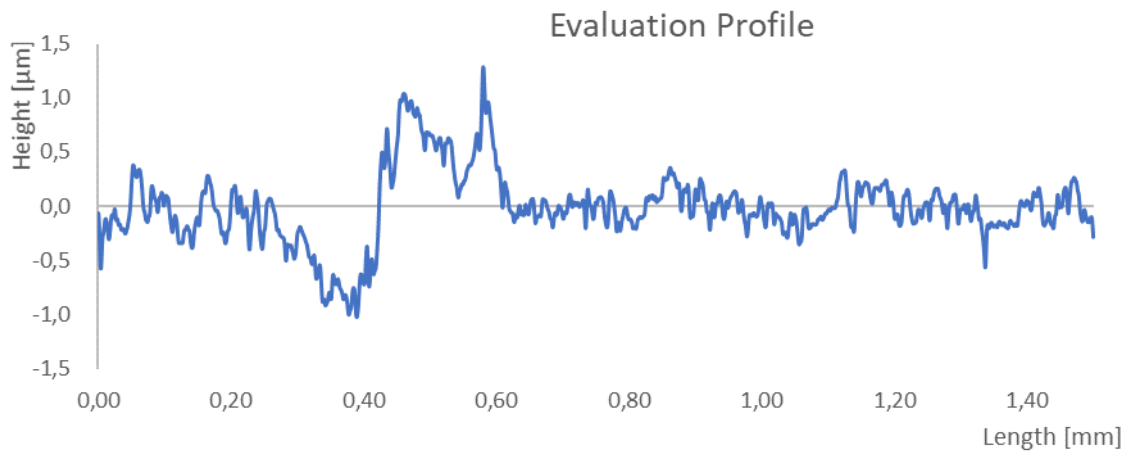
Sample 2



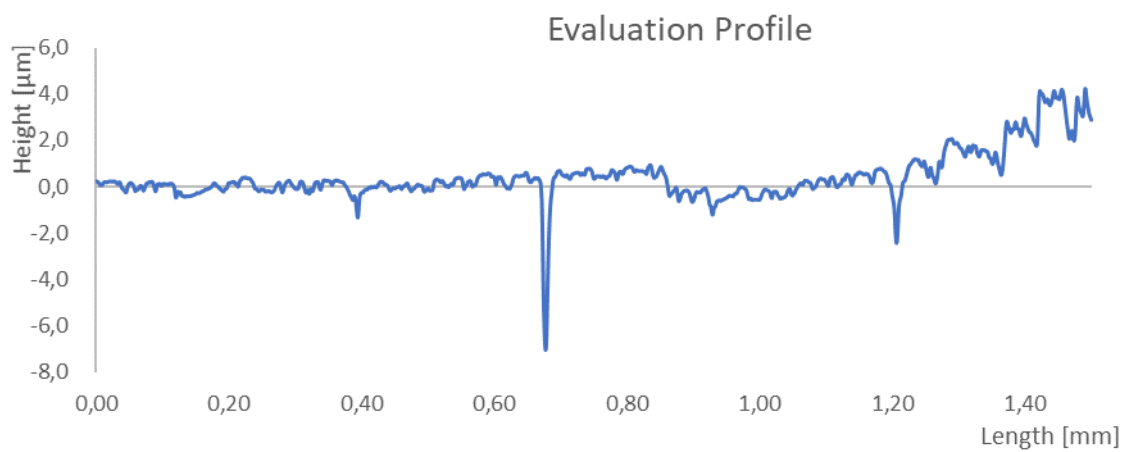
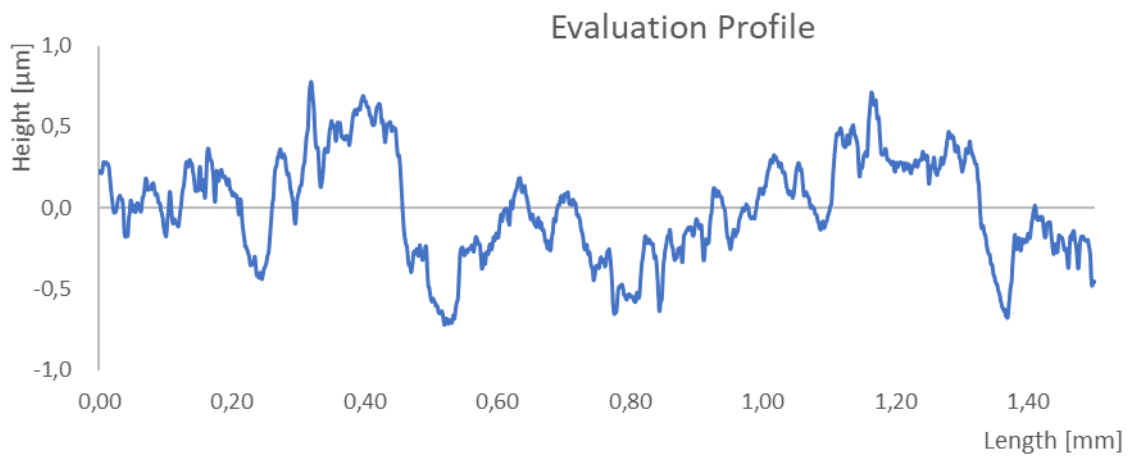
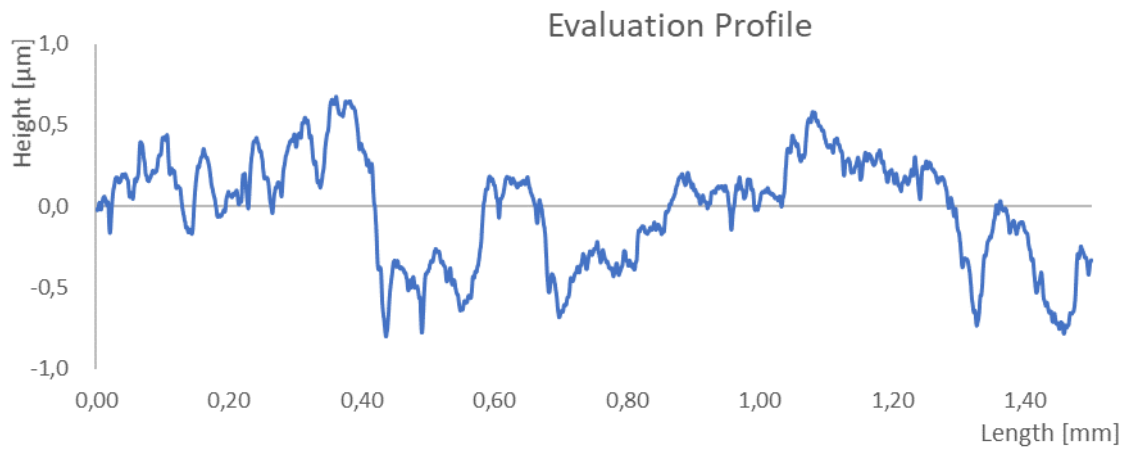
Sample 3



Sample 4

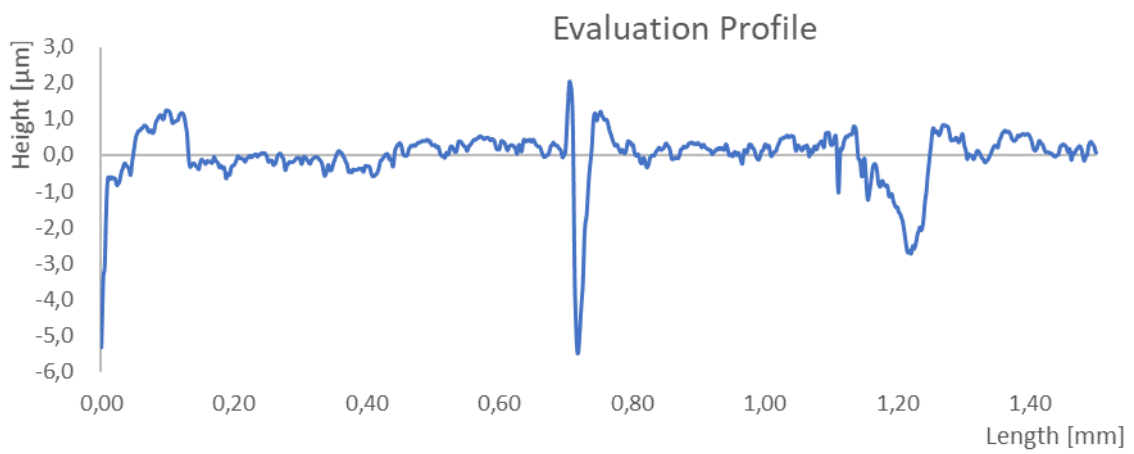
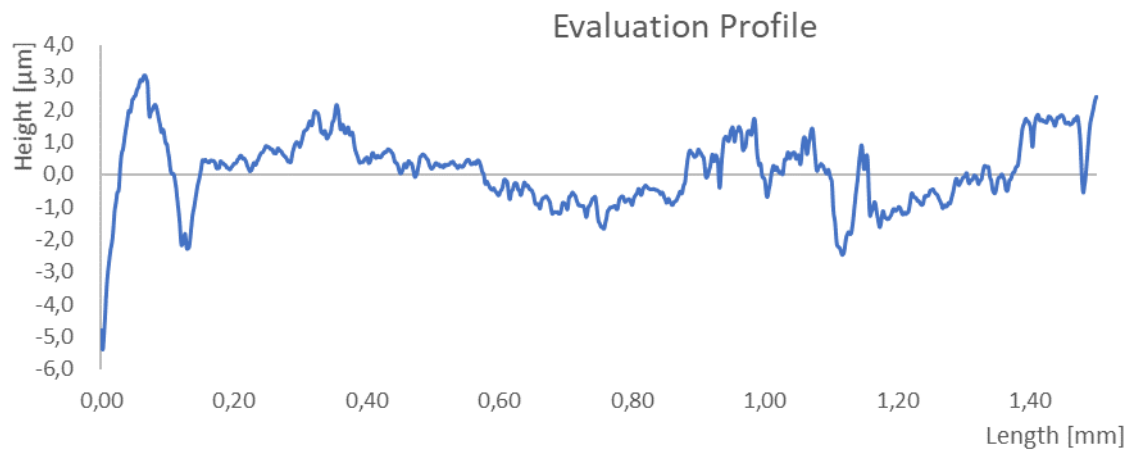
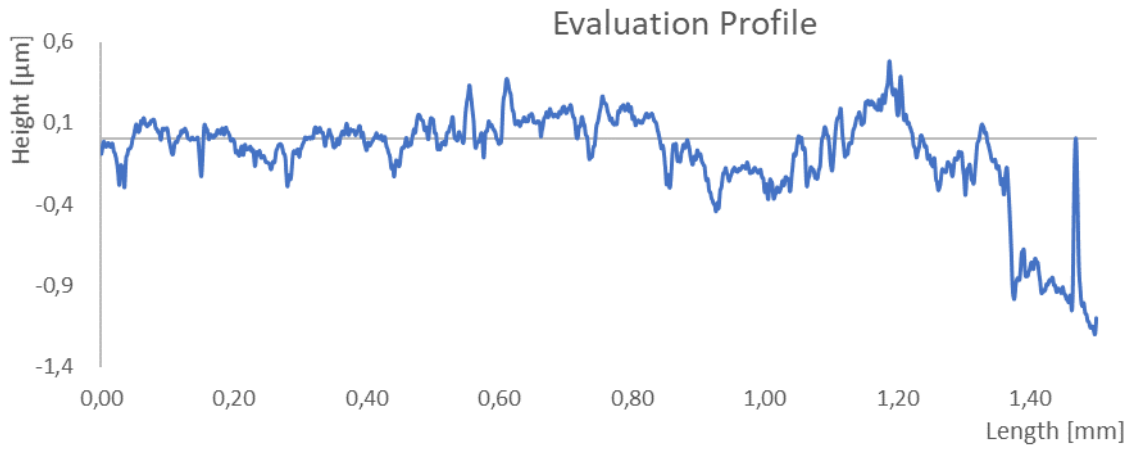


Sample 5

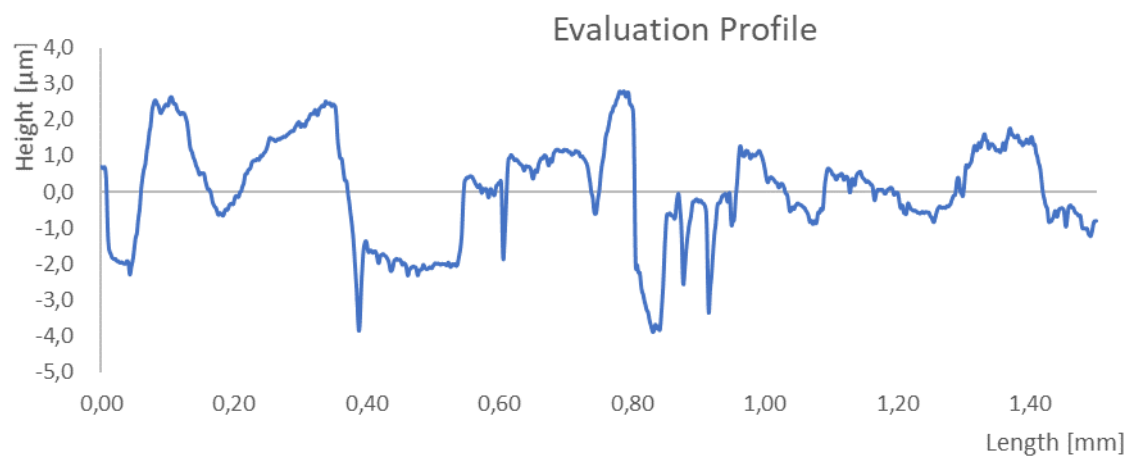
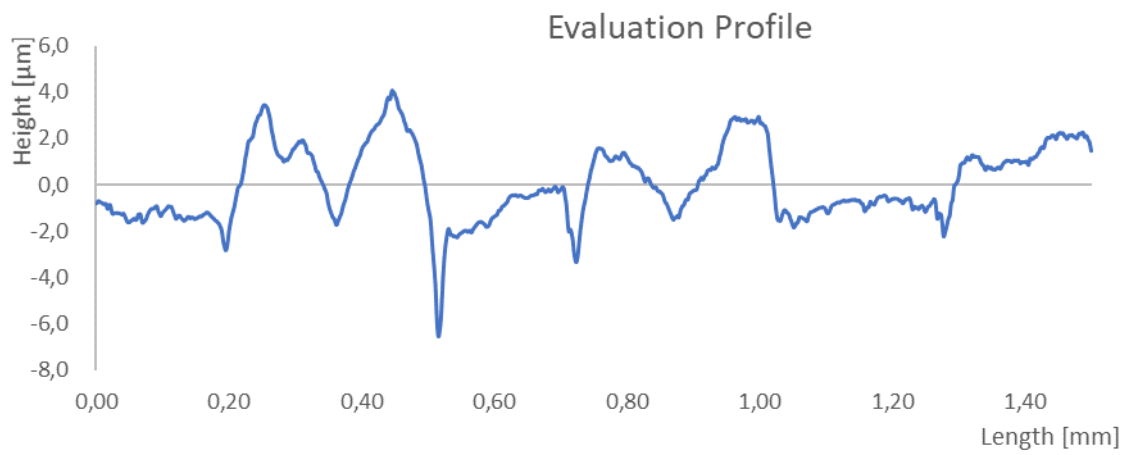
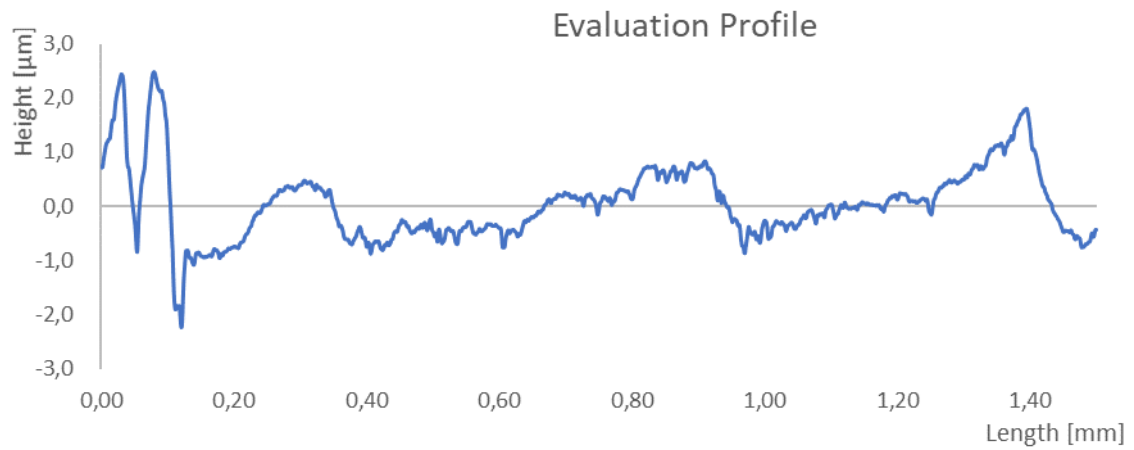


Oxide Samples

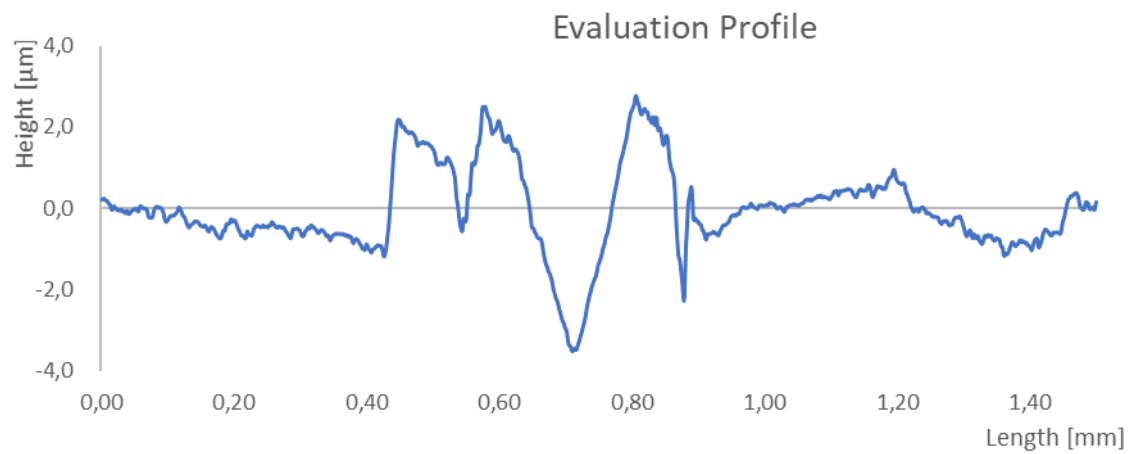
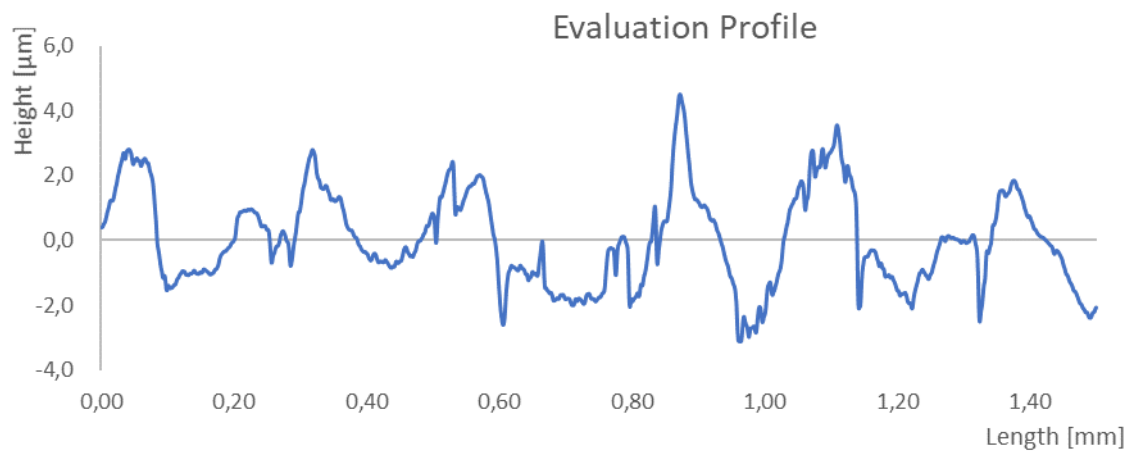
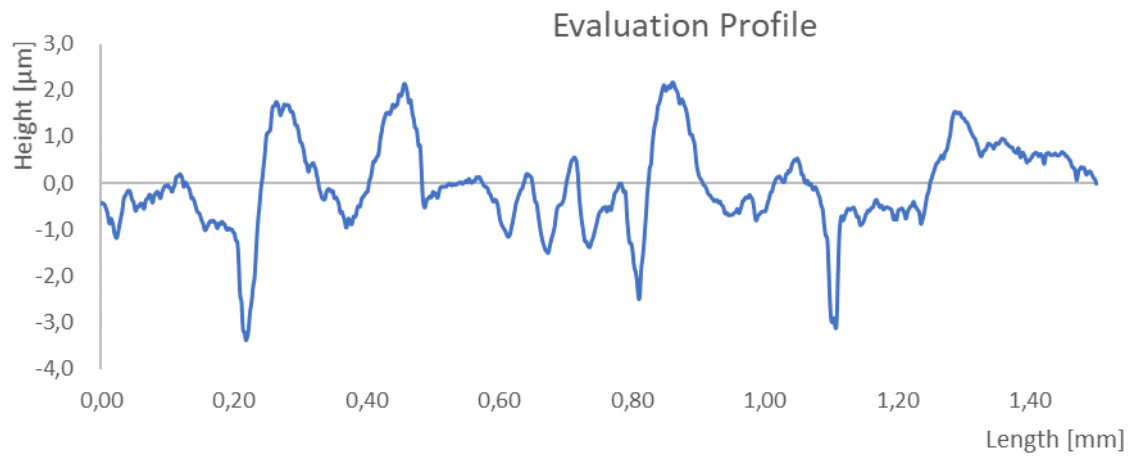
Sample 1



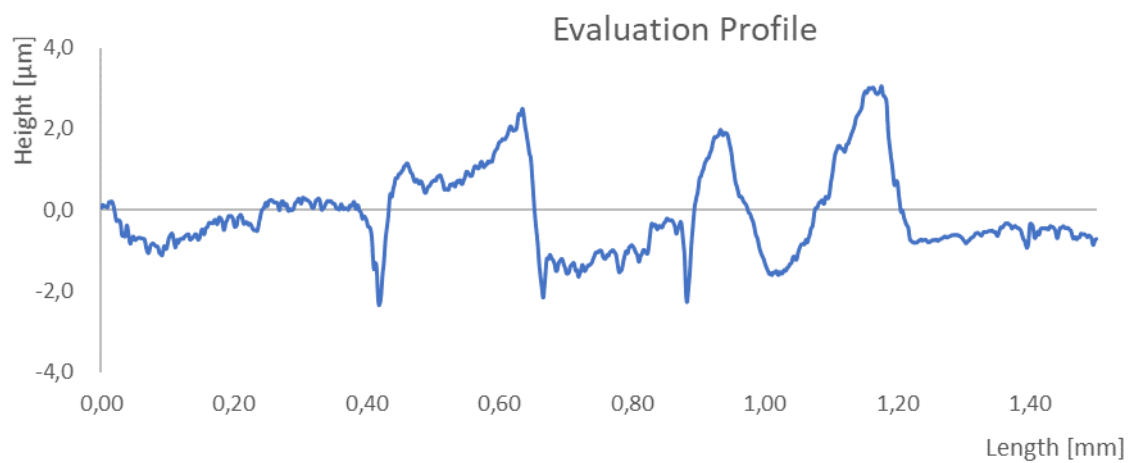
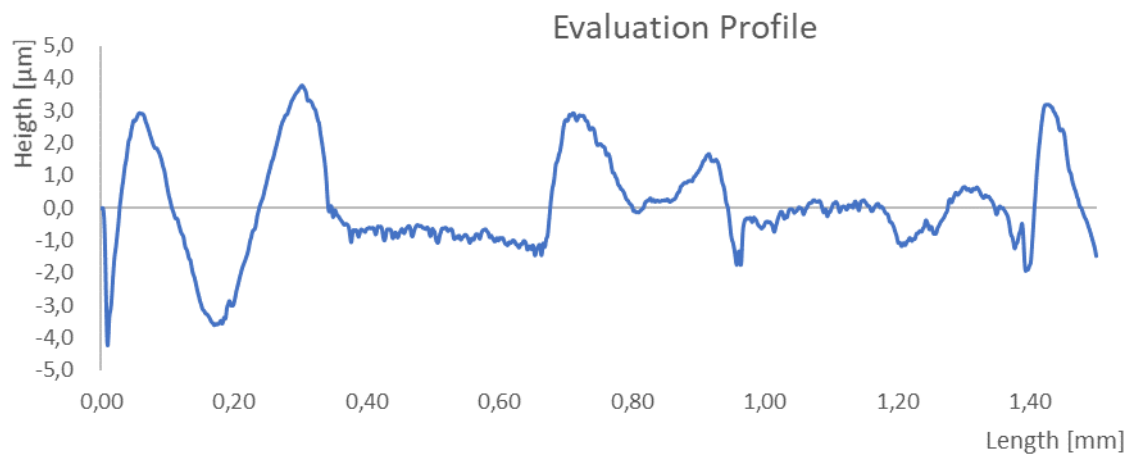
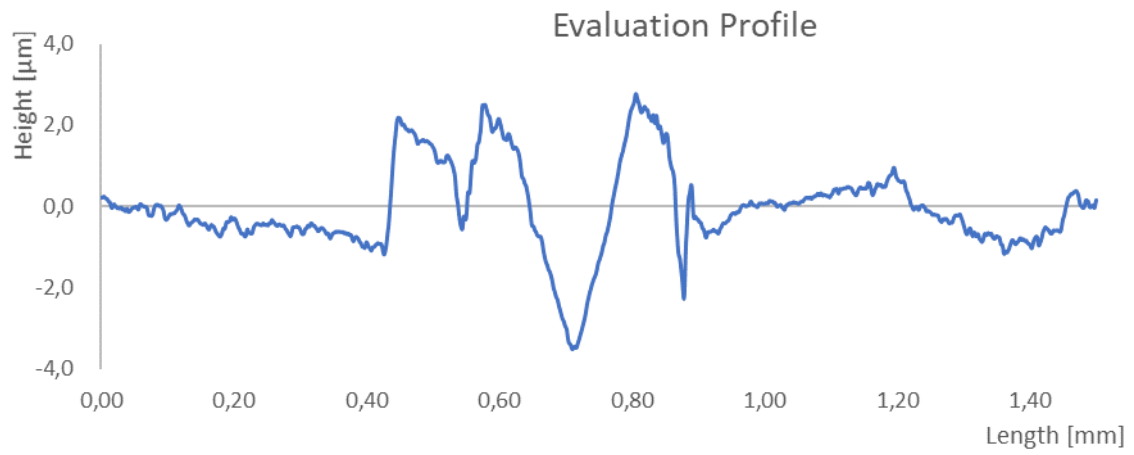
Sample 2



Sample 3



Sample 4



Sample 5

